Measurement of the Mechanical Property of Unicellular Organism Using Microfluidic Chip and Atomic Force Microscopy

Author: Di Chang

Supervisor: Hisataka Maruyama

A thesis submitted in fulfilment of the requirement for the award of the
Doctor of Philosophy

Department of Micro-Nano Systems Engineering
Graduate School of Engineering
Nagoya University

Acknowledgement

It is my great pleasure to acknowledgement all people who concern this work.

First of all, I would like to express great gratitude to Professor Fumihito Arai from the Department of Mechanical Engineering, The University of Tokyo, and for his great support and Associate Professor Hisataka Maruyama from the Department of Micro-Nano Mechanical Science and Engineering for their guidance, instructions and support.

Special thanks to Professor Yasuhisa Hasegawa from the Department of Micro-Nano Mechanical Science and Engineering, Nagoya University and Professor Takeo Matsumoto from the Department of Mechanical Systems Engineering, Nagoya University for their kind agreement with being my doctoral committee member.

I would like to thank Prof. Nobuyuki Uozumi, Dr. Kota Kera, and Miss Chihiro Uehara from Department of Biomolecular Engineering, Tohoku University for their great help in supporting my research.

I would like to thank Dr. Shinya Sakuma, Dr. Taisuke Masuda, Dr. Seiji Omata and Dr. Hirotaka Sugiura for their great and kind advices, help and support.

I would like to thank my wife Yun ZOU for her great patience, love and support in my life. And I feel lucky and happy to share the happiness and hardship together with her. I would like to thank my parents, Mr. Jiangang Chang and Ms. Xiurong Wang for their support and advices. I would like to thank the Chinese Scholarship Council for their finical supporting.

Abstract

This thesis focusses on the measurement of the mechanical property, such as Young's modulus, of unicellular organism.

Unicellular organisms, such as cyanobacterium and yeast, play important roles in the study of biofuel, gen analysis, protein production and so on. The mechanical property of the cell is different according to the environment condition or the cell gene. Thus, it is considered as an important parameter that present the cell living condition. But the diameter of the cell is as small as several micrometers, which makes it difficult to operate the cell. And it is also difficult to measure the cellular deformation and the applied force because of their small size.

Firstly, to overcome the difficulties caused by the small size of the cell, I constructed a measurement system. This system consists of a robot integrated microfluidic chip and an optical tweezers system. The optical tweezers allow us to manipulate the cell. The microfluidic chip integrated with a force sensor and a pushing probe allows us to deform a cell. And then, we can measure the deformation and applied force accurately using the chip. I succeed in measuring the stiffness of single cyanobacterium cell (*Synechocystis* sp. strain PCC6803) whose diameter is less than 2 μm. I also measured the Young's modulus of single cyanobacterium cell in different osmotic environment conditions. Two types of cell are measured, the wild type (WT) and the *ΔmscL*. The wild type is not genetically modified. The *ΔmscL* is genetically modified and lacks a specific kind of ion-channel called mechanosensitive channel (MscL). I confirmed that the *ΔmscL* and WT have different Young's modulus in different osmotic conditions.

Secondly, for the purpose of comparing with conventional research which utilize the atomic force microscopy (AFM) to study cell mechanical property, I studied the measurement of single yeast cell using atomic force microscope and microfluidic chip. There are lots of studies which studied the property of yeast cell using AFM. I measured the Young's modulus of single yeast cell using AFM with a sharp tip and a customized flat tip respectively. The sharp tip indents the cell and measure the local property of the cell, which is a conventional research method. While the flat tip compresses the whole cell and evaluate the Young's modulus of the cell as a whole. I confirmed that the Young's modulus measured by microfluidic chip and AFM with flat tip are similar, which prove the reliability of this method. While the Young's modulus measured by sharp tip (0.72 ± 0.36 MPa) (mean ± standard deviation, n = 10) and flat tip (5.09 ± 1.51 MPa) (mean ± standard deviation, n = 10) are quite different with each other. This might because the sharp tip measures stiffness of the local position on the surface of a cell, while the flat tip evaluates the stiffness of the whole cell. Other researches which studied the Young's modulus of yeast cell using AFM with sharp tip had reported the Young's modulus in the same order. Thus, the sharp tip result in this research is considered to be reliable. The two different tips evaluating the Young's modulus of a yeast cell in different ways. And I believe that both of them are suitable for evaluating the Young's modulus of yeast cell.

Contents

Chapter 1 **Introduction**

1.1 Background

A unicellular organism is an organism that consists of a single cell [1-4]. It contains lots of creatures such as cyanobacteria, *Escherichia coli*, and yeast. There are lots of studies about unicellular organisms in different fields. For example, cyanobacteria are a kind of photosynthetic bacteria which live in a wide variety of moist soils and water [5]. It has been used as a model microorganism in a wide range of studies in areas such as photosynthesis [6-9], biofuel [10-12], and environmental stress adaptation [13-16]. *Escherichia coli* is a kind of facultative anaerobic, rod-shaped, coliform bacterium of the genus Escherichia. It is widely studied in the field of ecology [17-19], public health [20, 21], and protein production [22, 23]. Yeast is a kind of eukaryotic which is widely used in in studies involving protein production [24-26], gene analysis [27-29], cell cultivation [30-32].

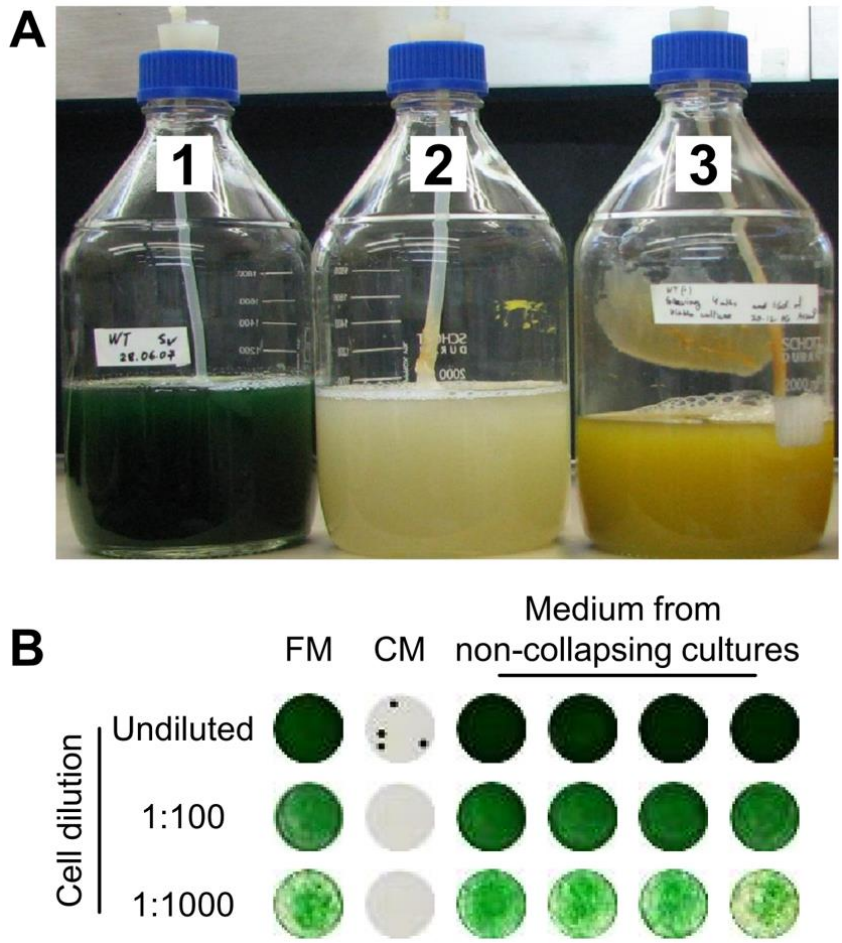

Figure 1.1 Different fates of aged cultures of the cyanobacterium S. elongatus.
(A) Cultures maintained at stationary phase were characterized by dark blue-green pigmentation up to about 3 months (culture No. 1). Older cultures either rapidly collapsed (culture No. 2), or gradually acquired a yellowish color (culture No. 3) and further survived. Cultures No. 1 and 2 are about 3 months old, whereas culture No. 3 is 6 months old. (B) Conditioned medium (CM) of a collapsing culture induced rapid cell death of exponentially growing cells of S. elongatus in contrast to medium from non-collapsing cultures, which did not affect viability. Cells were inoculated into fresh medium (FM) as a control. 5 µl of undiluted cultures or cultures diluted 1:100 or 1:1000 was 'spotted' on solid growth medium, following exposure to the different media. [42]

To study the cell, it is important to evaluate the cell condition. There are lots of methods to analyze cells. One kind of method to study the cells is to operate or measure cells in the form of liquid suspension or film on agar [42], as shown in Figure 1.1. Cells are studied as a group and the parameter of a group of cells such as optical density [34,35] and culturing conditions are analyzed [42]. Another method is to analyze a single target cell using specific devices. The single cell analysis has drawn lots of attentions [33] because its ability to analyze a cell specifically. The single cell analysis includes lots of methods, such as the fluorescent label [36-38] and single nucleus RNA sequencing [39-41].

Among the single cell analysis studies, the mechanical property of a single cell, such as Young's modulus, has drawn lots of attentions in recent years [43-47]. The mechanical property of a single cell would be affected by numerous factors, including cell variation [48,49], chemical treatment [50,51], viral infection [52,53] and environment conditions [54]. Thus, measuring the mechanical property of a single cell can help us understand the more about cells. Considering the fact that there are lots of cells with different size and different properties to be studied, different methods have been proposed to meet different needs. This research focus on measuring the Young's modulus of unicellular organism with small size, such as cyanobacteria and yeast cells. The diameter of cyanobacteria and yeast cell is around several micrometers. The small size of these unicellular organism makes it difficult to operate or measure the target cell. The methods proposed by other researchers have different advantages which make them not suitable or convenient for measuring cyanobacteria or yeast cells. Thus, it is important to propose a method to

measure the Young's modulus of cells with small size. Firstly, I will briefly introduce some methods proposed by other researchers in the next section.

1.2 Mechanical property measurement methods

To evaluate the mechanical property of a cell, it is usually needed to deform the target cell and measure some related parameters. Most of the proposed methods are based on such kind of principle. The methods used to evaluate the mechanical property of a single cell including micromanipulation method, micropipette aspiration method, optical tweezers method, micro-constriction channel method, robot integrated microfluidic chip method, and the atomic force microscopy (AFM) method. Here I will briefly introduce these methods.

1.2.1 Micromanipulation method

The micromanipulation method utilizes micro-structures which are fabricated using the micro and nano fabrication technology to evaluate cell by deforming it and measuring the force applied.

The micro-structure can be fabricated on a substrate. For example, Liu et al. fabricated a poly(dimethylsiloxane) (PDMS) cell holding device for measuring forces applied to an oocyte cell. The elastic and viscoelastic properties of a single oocyte cell was measured by indenting the target cell using a micropipette as shown in Figure 1.3 [54], and analyze the data using a large-deformation mechanical model which was developed to extract the mechanical properties from the measured force‐deformation data [55].

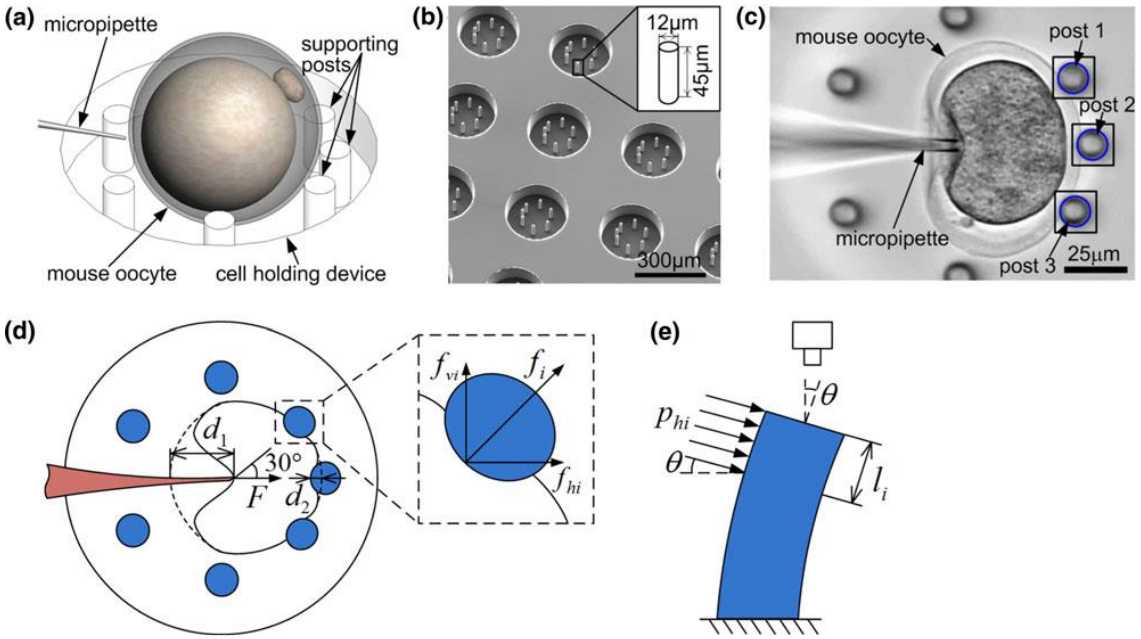

Figure 1.3 Vision-based force measurement of mouse oocytes. (a) Schematic of the working principle. (b) SEM image of a PDMS cell holding device. (c) Indentation forces deform the mouse oocyte and deflect three supporting posts. (d) Force balance on the cell under indentation. (e) Post deflection model [55].

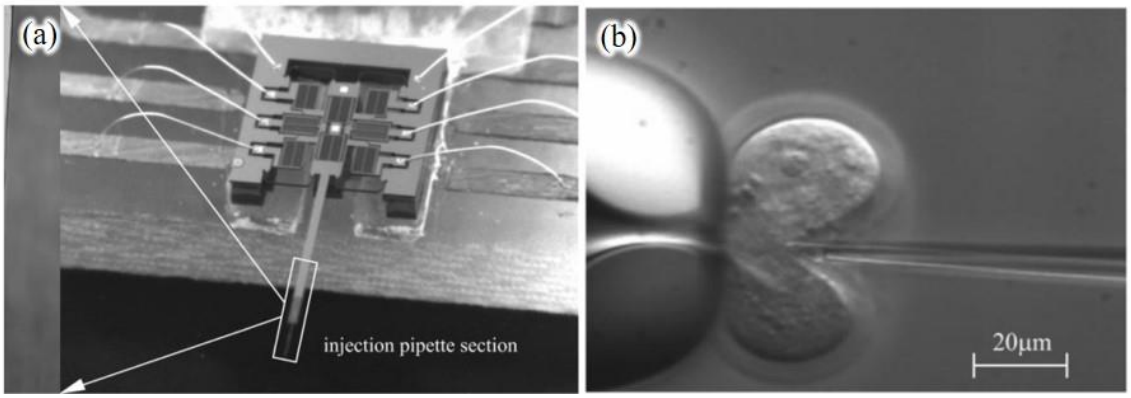

Figure 1.2 (a) Micromanipulator with a wire-bonded force sensor. (b) Force-deformation curve measurement of a mouse oocyte zona pellucida [57].

The micro-structures can also be fabricated to make an isolated micromanipulator. For example, Sun et al. developed a micromanipulator consisted of a 2-degree of freedom

capacitive force sensor and a probe [56]. It was used to measure the stiffness of a mouse oocyte, as shown in Figure 1.2, by indenting the cell with the force sensor attached probe.

Some other researchers succeeded in measuring the mechanical property of a tomato cell by compressing the cells between the flat end of an optic fiber (the micromanipulation probe) and a glass surface, as shown in Figure 1.4 [46]. The probe was mounted on a force transducer, which in turn was mounted on a micromanipulator. This allowed the probe to be driven at a chosen speed towards the slide, compressing the cell [47,65].

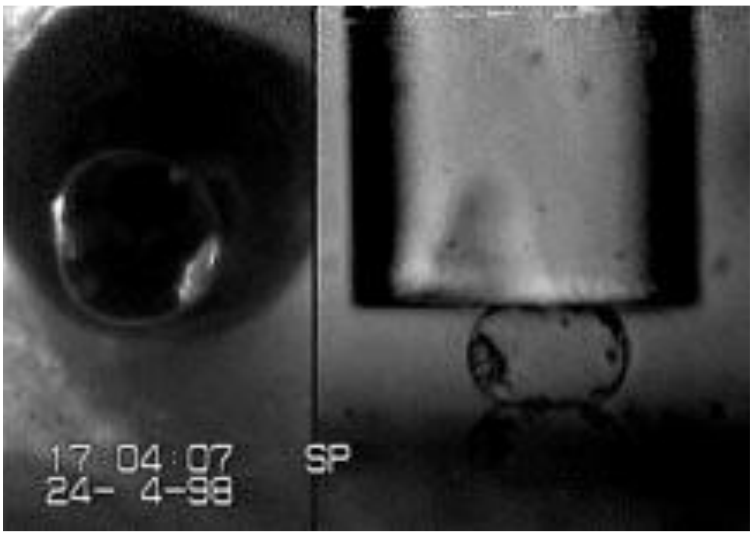

Figure 1.4 Video image of bottom and side views of a cell under deformation [46].

1.2.2 Micropipette aspiration method

Micropipette aspiration method utilize a tube whose inner diameter is slightly small than the target cell to aspirate it as shown in Figure 1.5 [58]. And then evaluate the cell mechanical property according to the pressure applied on the tube and the cell deformation [59-62]. This method is usually used to measure soft some cells with a Young's modulus smaller than 1 kPa, such as chondrocyte and endothelial cells [59]. There are also researches which study the force model for describing the aspiration of a target cell to calculate the mechanical property of the target cell more accurately [63,64].

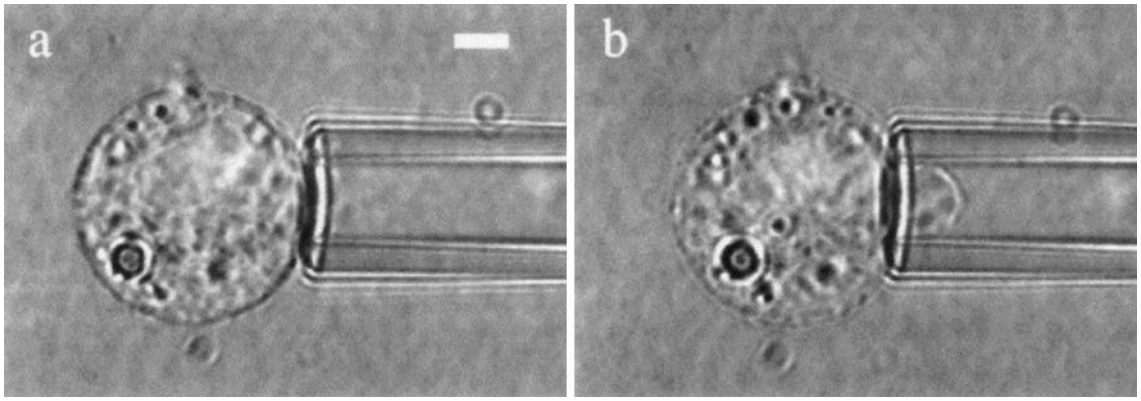

Figure 1.5 Micropipette aspiration test to evaluate cell stiffness. (a) Application of tare pressure and (b)incremental pressure application [58].

1.2.3 Optical tweezers method

The optical tweezers are technique which utilize a focused laser beam to manipulate particles with a size in the order of nanometer or micrometer. It was proposed around 50 years ago [66,67] and has been widely used for lots of researches [68-70]. Measuring the mechanical property of a single cell can also been achieved by using optical tweezers. Because the optical tweezers can only apply force in the order of piconewton (pN) [71]. They are usually used to measure soft cells such as human red blood cell [72] or cancer cell [73,74]. The optical tweezers trap microbeads to apply force on a target cell by stretching, as shown in Figure 1.6 [72]], or by indenting, as shown in Figure 1.7 [74].

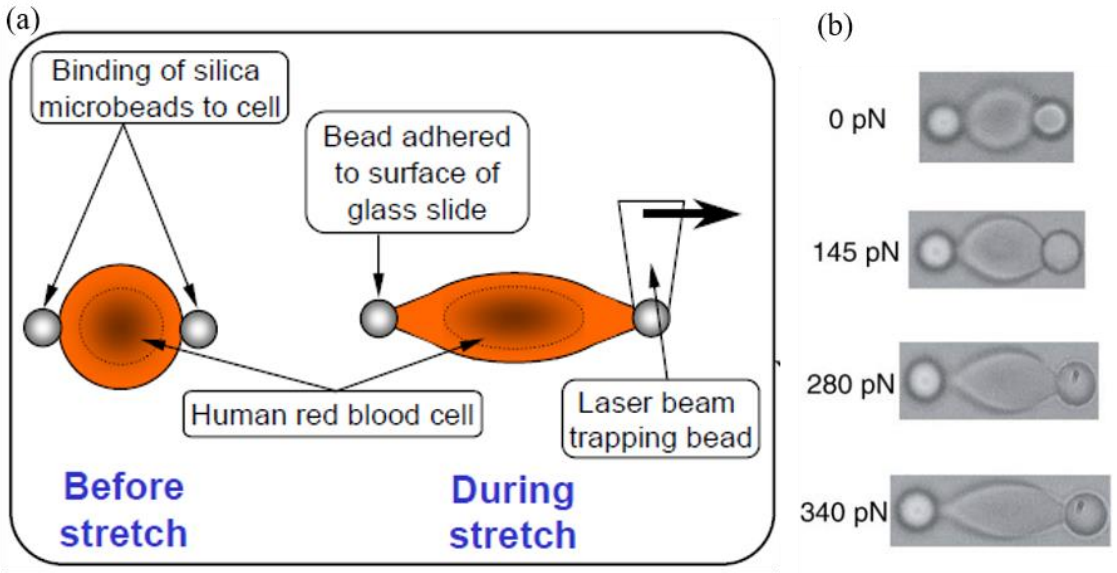

Figure 1.6 (a) Concept of the stretching experiment. The left bead is anchored to the surface of the glass slide. The right bead can be trapped using the laser beam and stretching force applied to it via the movement of the laser beam. (b) Experimental observations of the stretched red blood cell loaded from 0 to 340 pN. Diameter of the bead is 4.12 μm [72].

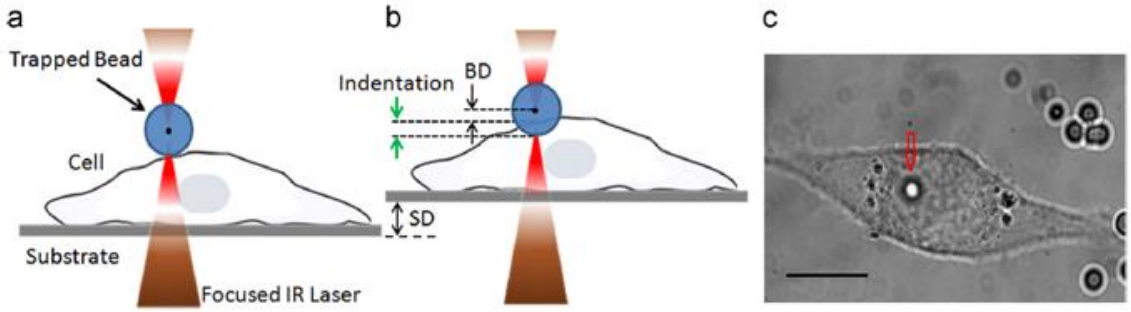

Figure 1.7 Schematic of the experimental procedure. (a) The cell is positioned below the trapped bead, (b) the stage is moved up by SD and the cell interacts with the bead displacing it by BD, while the bead indents the cell and (c) optical microscope image of the bead above the cell, bead indicated by arrow, scalebar10 μm [74].

1.2.4 Microfluidic chip method

Microfluidic chip is a chip with patterned microchannels and some other structures such as microvalve, micropump and microsensors as shown in Figure 1.8. It has been greatly developed for decades [75-77] in the field of particle sorting [79], DNA analysis [80], cell analysis [81-83], biomedical [84] and so on [85-87]. There are several ways to evaluate the mechanical property of a single cell using microfluidic chips.

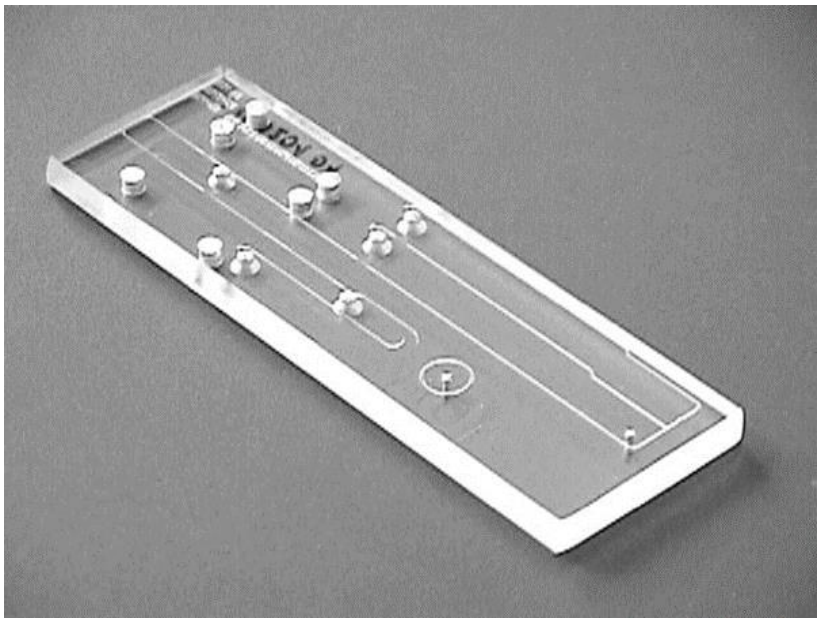

Figure 1.8 Picture of a microfluidic chip [78].

One of the methods to evaluate the mechanical property of a single cell using a microfluidic chip is called micro-constriction channel method. The micro-constriction channel method is a little similar with the micropipette method. The micro-constriction channel method evaluates the mechanical property of the target cell by forcing the cell going through a channel whose diameter is smaller than the cell [88,89], as shown in Figure 1.9 [75]. Different from the micropipette aspiration method, the micro-constriction channels are usually fabricated on a microfluidic chip and can realize high-throughput single-cell mechanical property characterization [90-92]. This method is usually used to evaluate soft cells such as red blood cells [89], white blood cells [90,93,94], and cancer cells [92,95-97].

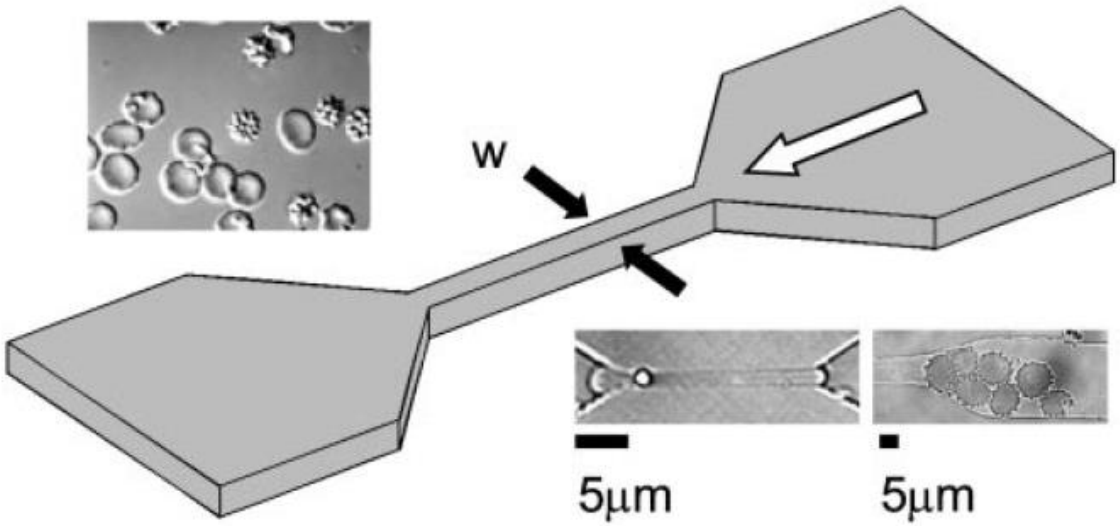

Figure 1.9 Schematic illustrating the geometry of the microchannel. The constricted segment of the channel (width denoted by w) was sized at 8, 6, 4, and 2 μm. The white arrow represents the direction of fluid flow. (Upper Inset) A differential interference contrast image of normal (smooth) and infected RBCs. (Lower Left Inset) A normal RBC passing through a 2- μm constriction. (Lower Right Inset) Infected RBCs blocking a 6- μm constriction. [89].

Another way to evaluate the mechanical property of a single cell is to apply fluidic force on a cell and record its deformation using high speed camera [98-100] as shown in Figure 1.10 [97]. This method delivers the cells to a special flowing field uniformly by using the inertial focusing. The cells are deformed at high strain rates, imaged with a

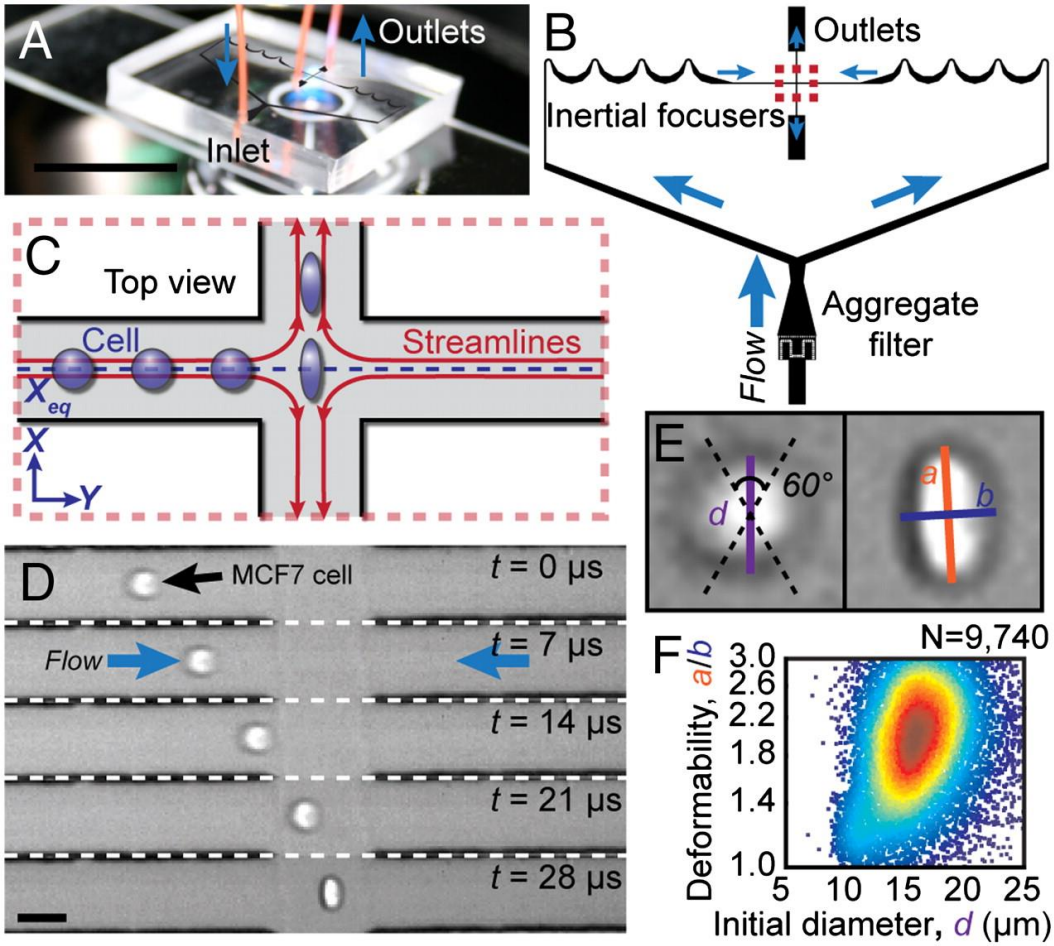

Figure 1.10 Principles of deformability cytometry. (A) *A picture of the chip.* (B) *A schematic of structure which makes cells to the channel centerline before delivering them to the stretching extensional flow.* (C) *A schematic of the deformation of a cell delivered to the center of an extensional flow by being previously aligned at an inertial focusing position,* (D) *High-speed microscopic images of a deformed cell (Scale bar: 40 μm.)* (E) *Definitions of the shape parameters extracted from images.* (F) *Summarized result of the human embryonic stem cells [98].*

high-speed camera, and computationally analyzed to extract quantitative parameters. This method has a high through output as much as 2000 cells per second. But only suitable for soft cells which can be deformed easily by the shear stress in a laminar flow, such as human stem cells [98].

Deforming the target cell with a probe or a pair of probes integrated on a specifically designed microfluidic chip. And then, sensing the cellular force using an on-chip force sensor is another method to measure the mechanical property (such as stiffness) of a single cell [101-103]. The cell will be compressed between two flat surfaces which connected to a force sensor to measure the force during compression, as shown in Figure 1.11 [102]. The force sensor on the microfluidic chip is usually a folded beam sensor. By designing the force sensor properly, the microfluidic chip is capable to measure different cells in different conditions.

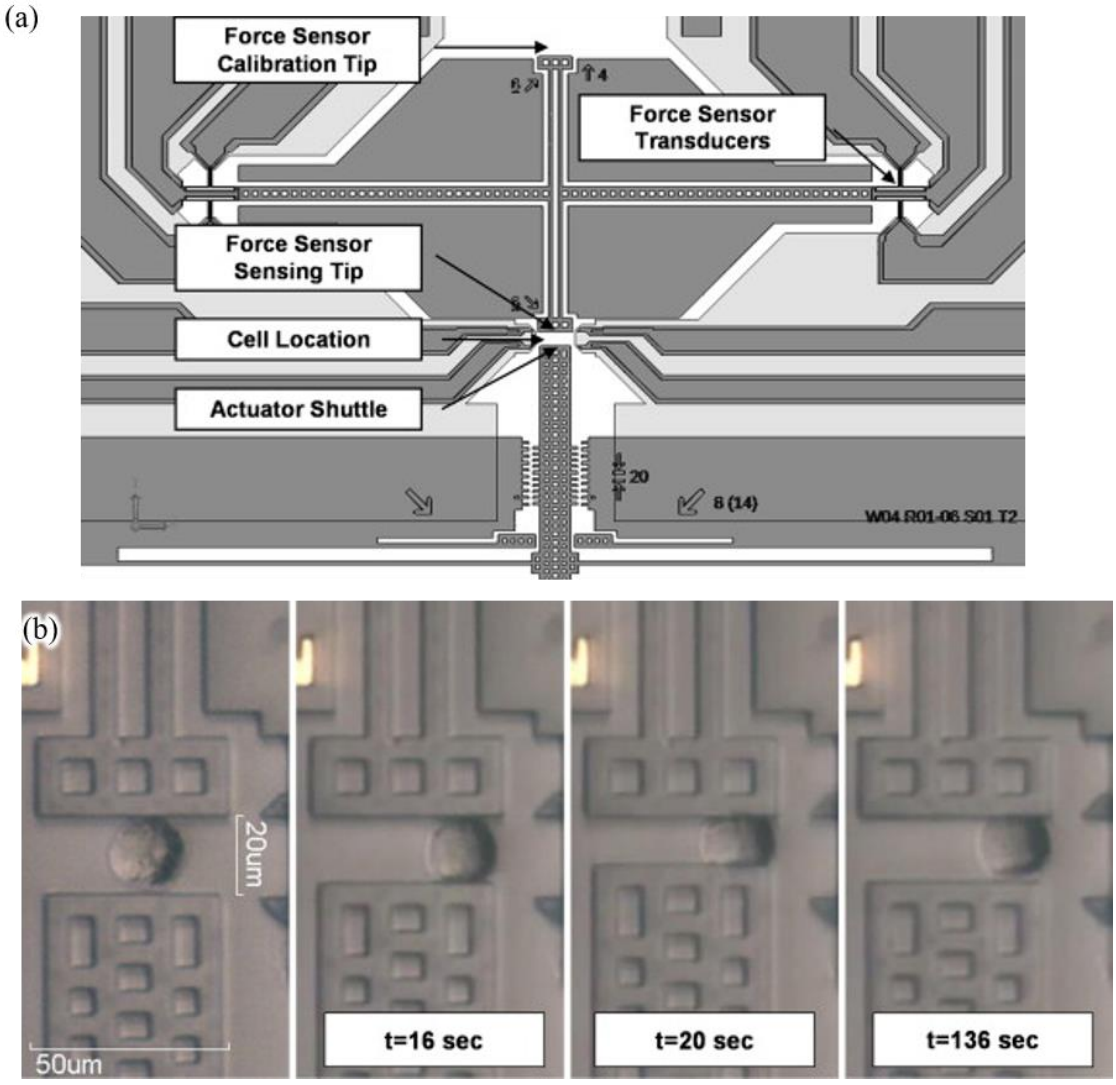

Figure 1.11 (a) Diagram of a chip with force sensor structures and actuator structures (b) Experiment figures of the compression of a single NIH 3T3 cell [103].

1.2.5 AFM method

Atomic force microscopy (AFM) is a type of scanning probe microscope (SPM) with high resolution. It is widely used device for studying biological structures and processes on cellular [104,105] and molecular scales [106,107]. There are many different designs of AFMs, but the main parts of almost any AFM are similar: a flexible cantilever (usually mounted with a sharp tip) that acts as a spring, a laser diode whose light is focused on the cantilever, a photodiode that detects the laser beam reflected by the cantilever, and a piezo device for positioning the sample relative to the tip in three dimensions [108], as shown in Figure 1.12 [107].

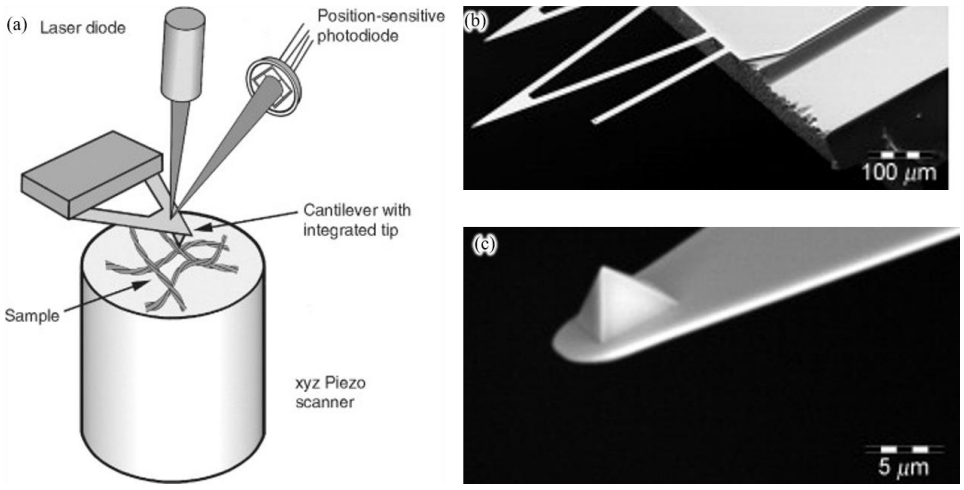

Figure 1.12 (a)Principal components of an AFM: cantilever with integrated tip, laser diode and photodiode for deflection sensing, and a piezo device for positioning the sample relative to the tip. (b) AFM cantilever. (c) Sharp tip of the AFM cantilever [108].

It can not only scan the surface of a sample, but also measure the mechanical property of the sample by indenting the sample with the cantilever, as shown in Figure 1.13 [112]. There are lots of researches who studied the cell mechanical property using AFM [109-112]. By indenting the target cell using the cantilever with a sharp tip or a sphere tip, the cell mechanical property could be evaluated according the indentation depth and the cantilever deflection.

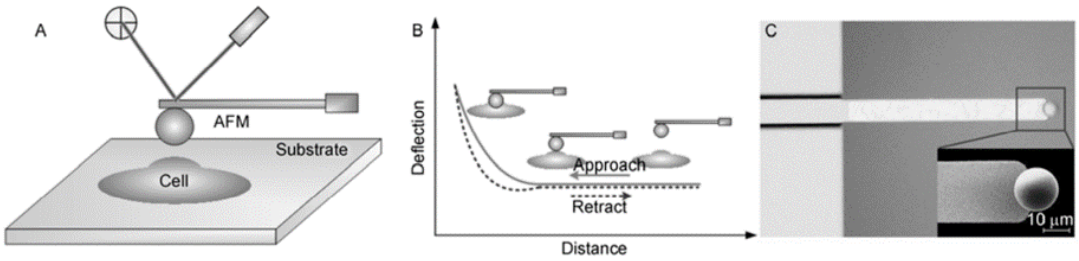

Figure 1.13 Principle of measuring cellular mechanical properties with a spherical AFM probe. A, Cell is attached onto the substrate, while a sphere is glued onto a tipless cantilever. B, Approach, contact, and retraction to obtain force profiles on the cell surface. C, Optical and SEM images (inset) of a cantilever with a glued sphere [113].

1.3 Measurement of unicellular organism using robot integrated microfluidic chip

As mentioned above, there are lots of methods to measure the mechanical property of a single cell. The stiffness of several kinds of cell, human red blood cell and stem cell for example, have been investigated. Even though there are several methods to evaluate the mechanical properties of single cells which has been proposed by previous researchers, it is not suitable to utilize those method for evaluating some unicellular organism, such as the *Synechocystis* sp. strain PCC6803 (hereafter *Synechocystis*) because of its small size. The diameter of a *Synechocystis* cell is approximately 2 μm, as shown in Figure 1.14 [116]. The micromanipulation methods need to operate a micromanipulator to operate or deform the cell, but *Synechocystis* is so small to be operated using the micromanipulators. Micropipette aspiration method, optical tweezers deforming method and micro-

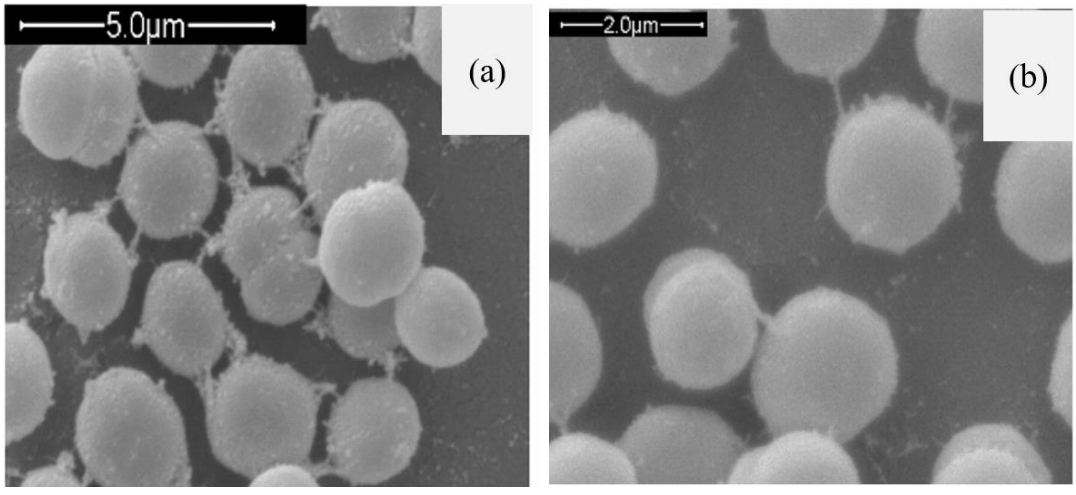

Figure 1.14 Scanning electron microscopy (SEM) of Synechocystis sp. strain PCC 6803 cells from agar plates. (a) magnification 12000 (scale bars, 5 μm). (b) magnification 24000 (scale bar, 2 μm [116].

constriction channel method can only deform soft cells such as cancer cells. The cell wall around *Synechocystis* cell makes it stiffer than cancer cells. The Young's modulus of a Synechocystis cell might be in the order of million-pascal, but the cancer cell is in the order of kilopascal [48]. Microfluidic chip can deform the *Synechocystis* cell, but it is difficult to move the *Synechocystis* cell to the measurement point using the flow control because it is too small. AFM method might be able to deform the cell, but it needs to immobilize the cell on a substrate tightly, which means the *Synechocystis* cell is not measured in a nature state. Considering the fact that *Synechocystis* is a model unicellular phototrophic cyanobacterium [113,114]. And it has been widely used as a model microorganism widely used and studied in different research areas such as, photosynthesis [115], biofuel [10-12], and environmental stress adaptation[15,16]. It is necessary to propose a method to evaluate the Young's modulus of the *Synechocystis* cell to help researchers understand more about the cellular mechanism.

The small size of the cyanobacteria leads to two difficulties to measure its mechanical property. One difficulty is to evaluate deformation of the cell and the applying force during the deforming process accurately. The other difficulty is to operate the cell accurately, such as moving the cell to a specific point. The micromanipulation method could manipulate or compress the cell. However, this technique does not have enough accuracy or resolution to measure the *Synechocystis* cells. The micropipette aspiration method and optical tweezers method are only suitable for soft cells as I introduced in previous sections. Sugiura et al. [119,120] reported their work which utilizes the fluid control for cell manipulation. But it is difficult to utilize the flow control on cells as small as *Synechocystis*. The position of the small cells are easily affect by the fluid flow.

Therefore, it takes long time to move the cell to a proper position. Microgripper [121] is another method for single cell manipulation. But it is not easy to isolate suspended cells. It is well known that the microfluidic chips are widely used in the study of biology. It is able to be designed specifically to realize different needs, including high sensing resolution of course. In addition, optical tweezers can apply small force (in the order of pN) on small transparent objects. It is possible to manipulate small particles suspended in liquid, such as suspending cells. The trapping force of optical tweezers is not big enough to deform *Synechocystis* cells, but large enough to trap and move them. Thus, I combined the robot integrated microfluidic chip with optical tweezers to measure the mechanical properties, such as stiffness, of single *Synechocystis* cells.

1.4 Measurement of unicellular organism using atomic force microscopy (AFM)

AFM is a widely used method to measure the mechanical property of a single cell as I introduced previously. Even though there are few researches about the mechanical property of *Synechocystis* cells using AFM. Lots of studies on yeast cells, which is also a widely studied unicellular organism, have been reported. The measurement of cell mechanical property using AFM is different with the robot integrated microfluidic chip method. The conventional AFM measures the the mechanical property of a single cell by indenting the cells using a tip mounted cantilever. While the microfluidic chip measure the mechanical property of a single cell by compressing it between two flat surfaces. This leads to a question that whether the measurement results of these two methods are similar to each other. It is reasonable if the measurement results are similar when the target is a PDSM beads because it is homogeneous. But cells are complicated and have lots of structures such as cell wall, nucleus, and cytoplasm. It is necessary to know that whether the AFM method and the robot integrated microfluidic chip have a similar result when measuring the same cell strain in a similar condition. Thus, I proposed to measure the stiffness of a single yeast cell using AFM and microfluidic chip.

There is another problem about applying AFM in measuring single yeast cells. AFM is a popular device for investigating the mechanical properties of a single yeast cell [122-124]. The yeast cells are usually trapped in a hole of a substrate for immobilization and scanned, as shown in Figure 1.15.

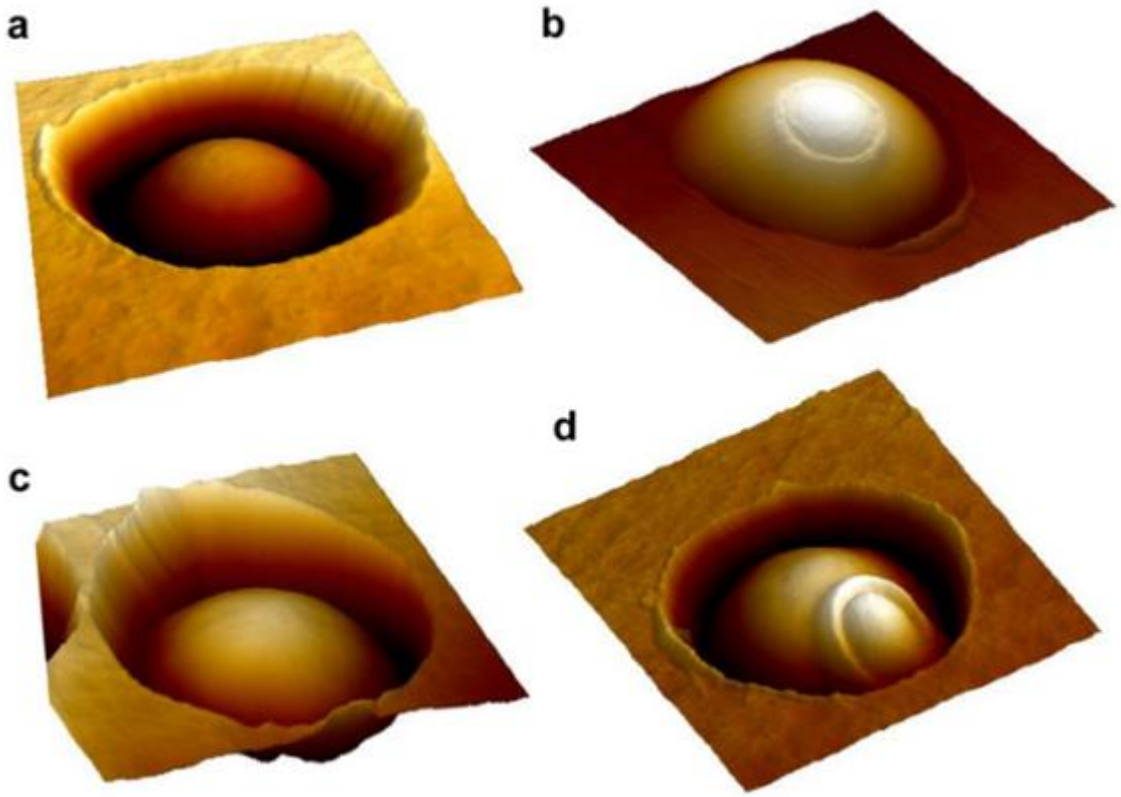

Figure 1.15 Imaging living yeast cells. AFM height images ((a), 6 μm × 6 μm, z-range: 400 nm; (b), 6 μm × 6 μm, z-range: 1500 nm; (c), 7 μm × 7 μm, z-range: 400 nm; (d), 7 μm × 7 μm, z-range: 1500 nm) of Saccharomyces carlsbergensis ((a), (b)) and S. cerevisiae ((c), (d)) recorded in buffered solution (sodium acetate; pH 4.75; 1 mM $CaCl_2$ + 1 mM $MnCl_2$). While some cells showed homogeneous surfaces ((a), (c)), others clearly showed the presence of a bud scar ((b), (d)). Cells were trapped into a porous polymer membrane for non-invasive, in situ imaging [124].

Even though the mechanical properties of cells are often determined using similar AFM methods, different researchers often report different values for the Young's modulus. For example, Young's modulus values reported by different groups range from 0.15 ± 0.02 MPa [54] to 2.62 ± 1.03 MPa [125], which corresponds to an order of magnitude difference. Moreover, the results obtained from AFM can also be quite different from those acquired using a microfluidic chip system with micromanipulators

such as 9.35 MPa (Hertzian model) or 276.4 MPa (Capsule Contact Model)[126]. Such differences may be due to cell culturing conditions, measurement parameters, and/or the immobilization method. Additionally, the sharp AFM tip itself presents some disadvantages that may cause variations in measurement results. Specifically, differences may arise if the value of the tip shape parameter applied in the deformation model is different from the true value, or if the tip radius and the indentation depth are on the same order of magnitude. The resulting modelling error causes miscalculation of the Young's modulus based on analysis of the indentation data.

To overcome this problem, I proposed to measure the yeast cell using an AFM cantilever with a flat tip. The whole target cell would be compressed between the tip bottom and the substrate, thereby avoiding any error caused by the tip shape. This compression method is similar to the microfluidic chip system, which uses micromanipulators with flat surfaces [128,129].

In this study, firstly, I measured the Young's modulus of a poly(dimethylsiloxane) (PDMS) bead using a sharp tip to reveal the error caused by the tip shape. Then, a PDMS bead was measured using a flat tip to check the feasibility and accuracy of this method. Finally, measurements were performed on single cells of a wild type strain of budding yeast, *Saccharomyces cerevisiae* BY4741, which is a widely used laboratory strain [130,131]. The cell is compressed between the flat tip bottom and the substrate, and the Young's modulus is calculated as the mechanical property of the whole cell. For comparison, this property of the cell is also measured using a microfluidic chip with two probes, based on a previously pubished method [129].

1.5 Thesis Overview

1.5.1 Research aim and target

There are lots of methods to study the mechanical property of a single cell. It is difficult to measure the mechanical property of a cell such as cyanobacteria whose diameter is as small as 2 μm and whose Young's modulus is in the order of million pascal. Thus, I would like to propose a method which could be used to measure the mechanical property of a stiff single cell with small size.

1.5.2 Outline of the thesis

This thesis consists of five chapters.

Chapter 1.

I introduce the background of the research and describe the research target in this chapter.

Chapter 2.

I proposed the measurement system used to measure the mechanical property of a single cyanobacteria cell. I introduce the concept of the measurement system, microfluidic chip design and fabrication, and the calibration of the spring constant of the beam sensor integrated on the chip.

Chapter 3.

I introduce the cell that I used for experiment. I showed the measurement process and experiment data of two types of cells in three different conditions. The summarized result

of the Young’s modulus of the single cell shows clearly difference. While the diameters of the cell have no obvious difference.

Chapter 4.

I introduce the measurement of a single cell using AFM and compare the result with these obtained in the measurement system proposed in Chapter 2. A typical unicellular organism, yeast, is measured using AFM. The yeast cell is measured by AFM in two different methods. In one method, the yeast cell is indented by a sharp tip to measure the local stiffness of the measurement point. In the other method, the yeast cell is compressed as a whole and the Young’s modulus of the whole cell is measured. Microfluidic chip method proposed in Chapter 2 is carried out and compared with the two methods using AFM.

Chapter 5

I summary this thesis and discuss the future work.

Chapter 2 **Measurement system used to measure mechanical property of single cell**

2.1 Introduction

As mentioned in the previous section, to measure the mechanical property of a single cell with small size such as cyanobacteria, I constructed a measurement system which

combines optical tweezers and microfluidic chip. The optical tweezers could apply a force in the order of pN, which is used to trap the target cell and transport it to the gap between the gap between two probes. And the robot integrated microfluidic chip is used to compress the target cell and sense the reactive force.

2.2 Concept

2.2.1 Concept of the measurement system

As mentioned previously, it is necessary to deform the cell to measure its stiffness. And the sensing during the deforming process should be high enough to evaluate the deformation and force. But the small size of *Synechocystis* whose diameter is about 2 μm leads to a challenge. In this thesis, I propose an on-chip measurement system to investigate the mechanical properties of *Synechocystis* on the single cell level as shown in Figure 2.1. I combined the robot integrated microfluidic chip with optical tweezers to measure the mechanical properties of single *Synechocystis* cells. The main system contains two parts, the optical tweezers and the robot integrated microfluidic chip. The optical tweezers are utilized to trap and transport the cells. The chip is utilized to carry,

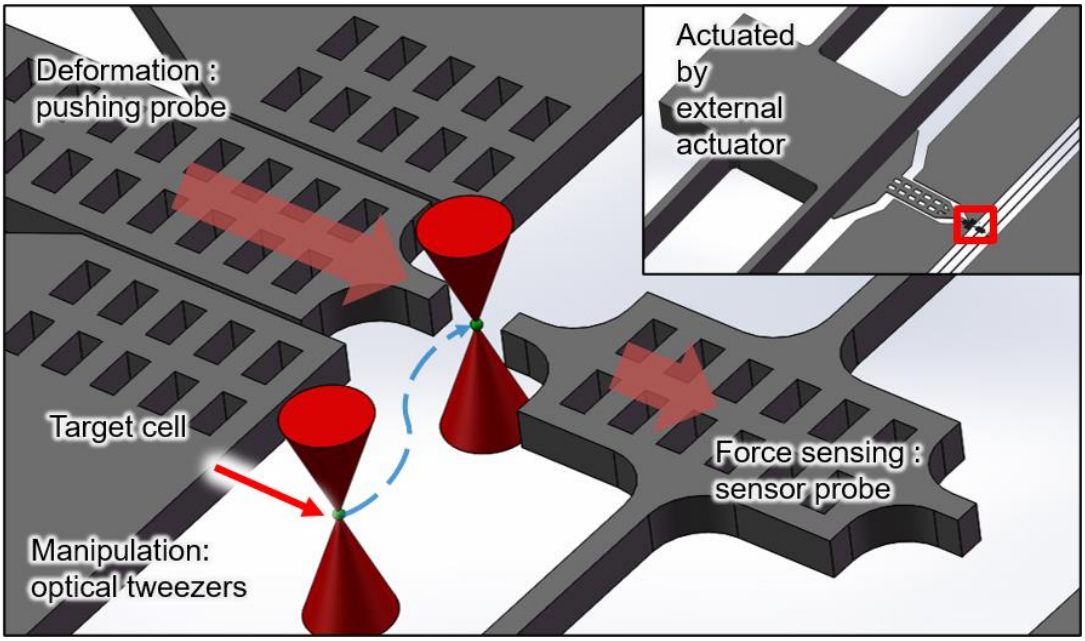

Figure 2.1 Schematic diagram of the system (probes on the chip and optical tweezers transporting the target cell).

deform and sensing the cell. There is a pair of probes with a flat top integrated on the chip. The two probes are called the pushing probe and the sensing probe (or sensor probe). The pushing probe can move in one dimension and is motivated by an external piezoelectric actuator. The sensing probe is connected to the chip through a folded beam spring force sensor. The concept of the cross section of the chip is shown in Figure 2.2. The microfluidic chip is made of a silicon on insulator wafer.

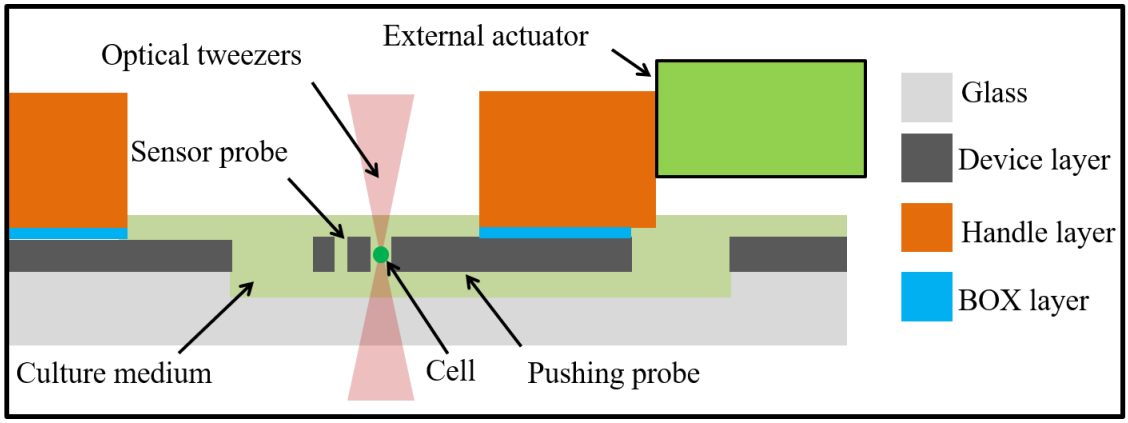

Figure 2.2 Schematic diagram of the cross section of the microfluidic chip

The parameters of the beam are designed to achieve an appropriate spring constant, as indicated in Section 2.3. A special displacement measurement method, called the sampling moiré method, is applied for high resolution sensing (see Section 2.2.4 for details). The cell is trapped by the optical tweezers at first. Secondly, it is transported to the gap between the probes. An external piezoelectric actuator actuates the pushing probe to compress the cell between the pair of probes. The displacements of the two probes are recorded during the process. The cell diameter, deformation, and reactive force can be calculated from the recorded displacement. At last, the force-deformation curve is fitted with a Hertzian model [132] to calculate the stiffness of the tested cell.

2.2.2 Compression model

Synechocystis cells from different test groups are tested to know their Young's modulus by compressing and sensing using the chip. The pushing probe pushes and compresses the cell to the sensor probe. The sensor probe is connected to a spring force sensor that can transduce the force to displacement. To measure the initial distance between the pair of probes, the pushing probe is actuated to touch the sensor probe just before compression, and their displacements are recorded. The schematic diagram of the compression process of a cell is shown in Figure 2.3.

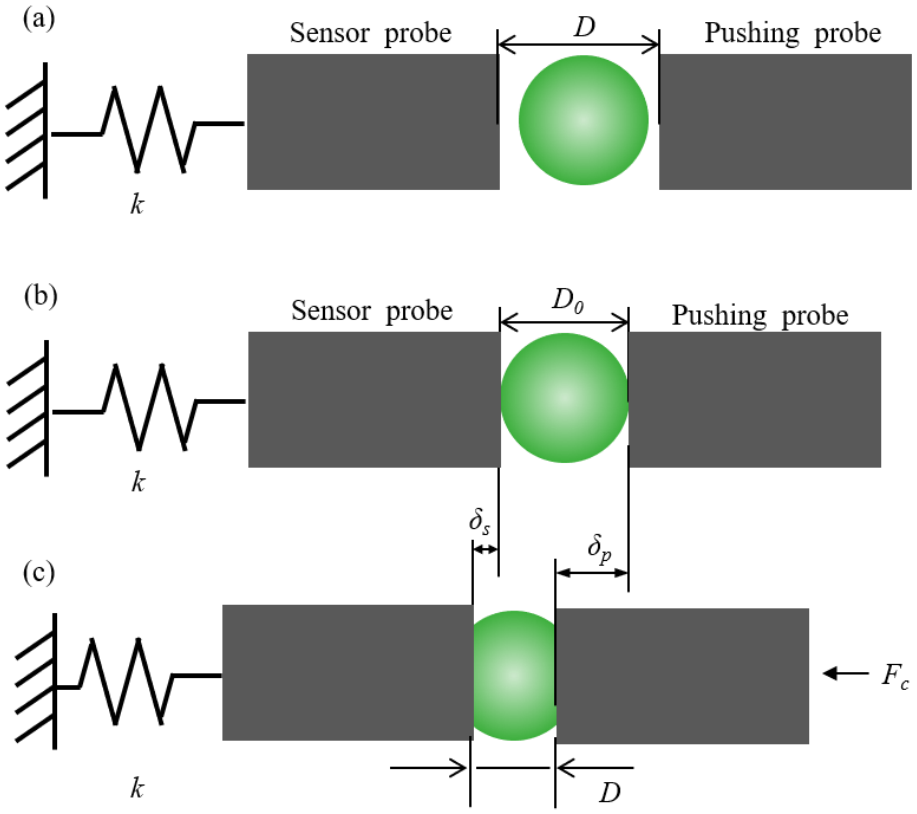

Figure 2.3 Schematic diagram of cell compression, (a) before compression, (b) start of compression and (c) during compression.

The target cell is moved to the gap between the probes as shown in Figure 2.3(a). The cell is pushed and touch the sensor probe when the pushing probe moves forward. Diameter of the tested cell, D_0, is acquired during the compression process. The diameter is measured by recording the distance between the two probes when the sensor probe starts moving, as shown in Figure 2.3(b). The displacement of the sensor probe δ_s and pushing probe δ_p are measured by recording the displacement of the sensor probe and pushing probe. I employed a Hertzian model which is widely used in studies involving Young's modulus measurement of the cellular Young modulus E_c. The deformation of silicon at the contact area can be ignored because the Young's modulus of silicon is approximately 170 GPa [133]. It is much greater comparing to the stiffness of cells (in the order of million pascal). The equation for the Hertzian model used for the measurement of single *Synechocystis* cell can be simplified as follows:

$$F_c = \frac{4(D_0/2)^{1/2}}{3} \cdot \frac{E_c}{1-\nu^2} \cdot \left(\frac{\delta_c}{2}\right)^{3/2} \tag{2.1}$$

The Poisson's ratio v is taken to be 0.5. This is to simplify the analyzing model and is widely used base on the assumption that the measured target is made of materials which are incompressible. The deformation of the cell δ_c and the cellular reactive force F_c can be calculated from the spring constant of the on-chip force sensor k, the displacement of sensor probe δ_s, and pushing probe δ_p as follows:

$$\delta_c = \delta_p - \delta_s \tag{2.2}$$

$$F_c = k\delta_s \tag{2.3}$$

2.2.3 Optical tweezers and microfluidic chip

As mentioned above, the challenges in measuring the stiffness of *Synechocystis* are manipulating, deforming, and sensing. To manipulate single *Synechocystis* cells, an optical tweezers system that is developed by other members in Arai Lab, Nagoya University [134] is used.

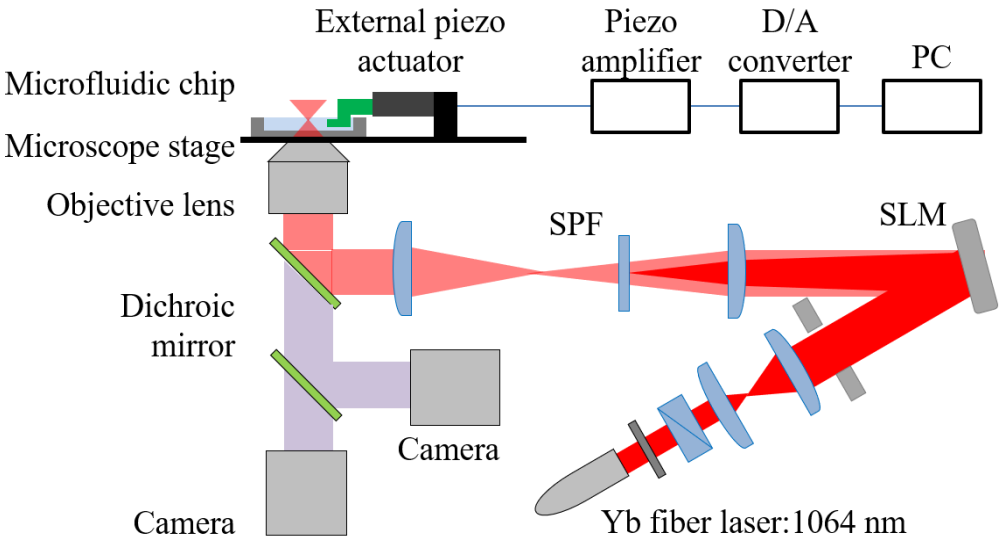

Figure 2.4 Schematic diagram of the optical tweezers used for cell manipulating.

The optical tweezer system is composed of a converted optical microscope, two cameras and an external optical system. A spatial light modulator (SLM) is used to change the phase distribution of the laser, which in turn changes the position of the focal point of the laser, as shown in Figure 2.4. I could transport a single cell by controlling the position of the focal point. An Yb fiber laser with a wavelength of 1064 nm is utilized as the laser source of the system. Because it has low damage to cells [135]. And its low absorption by the silicon substrate prevents the temperature rising at the exposed point. The chip and

an external piezo actuator are installed onto the microscope stage using a jig. One camera is used for recording the video during experiment for displacement measurement. Another camera is connected to the computer which is used to operate the optical tweezers.

To specifically deform a single cell, the deformation part of the chip must be fabricated on a scale similar to the diameter of the cell, i.e., less than 10 μm. However, the chip must also have a rigid component in the order of one hundred micrometers in size, so that it is strong enough for not being destroyed during the immobilization, cleaning, or interacting with other devices. Thus, a silicon on insulator (SOI) wafer was used. This kind of wafer consists of three layers, the device layer, the buried oxide (BOX) layer and the handle layer. In this thesis, the thicknesses of those three layers are 7.5, 1, and 225 μm, respectively. The device layer and handle layer consist of single crystal silicon, on which structures can be fabricated as a plane. I fabricated the pair of probes on the device layer and the rigid part, to triggered by an external actuator, on the handle layer. As shown in Figure 2.1 and Figure 2.2, a pair of flat top probes was fabricated on the device layer. One is called a pushing probe. It is triggered by an external piezoelectric actuator and can move in one dimension. The other probe is the sensor probe, which is connected through a folded beam spring force sensor and can transduce the force to displacement. The folded beam sensor provides good linearity in actuation direction. It also rigid in constrained directions [136].

2.2.4 Sampling moiré method to improve the measurement accuracy

Moiré fringes are large-scale interference patterns that can be produced when an opaque ruled pattern with transparent gaps is overlaid on another similar pattern. For the moiré interference pattern to appear, the two patterns must not be completely identical, but rather displaced, rotated, or have slightly different pitch [137].

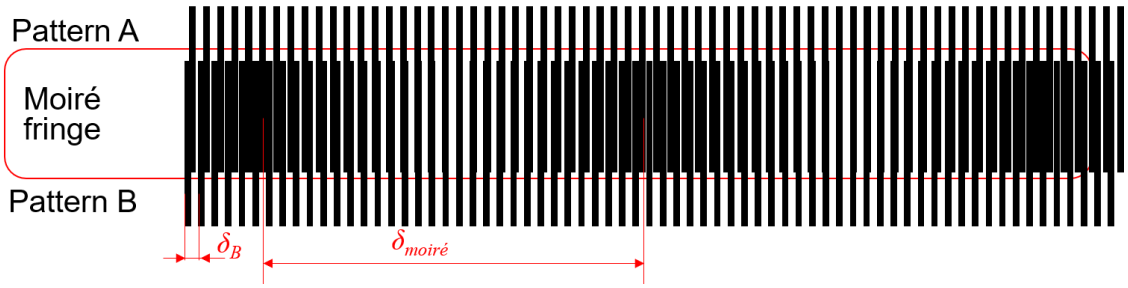

Figure 2.5 Moiré fringe (generated by two similar gratings) can amplify mutual displacement.

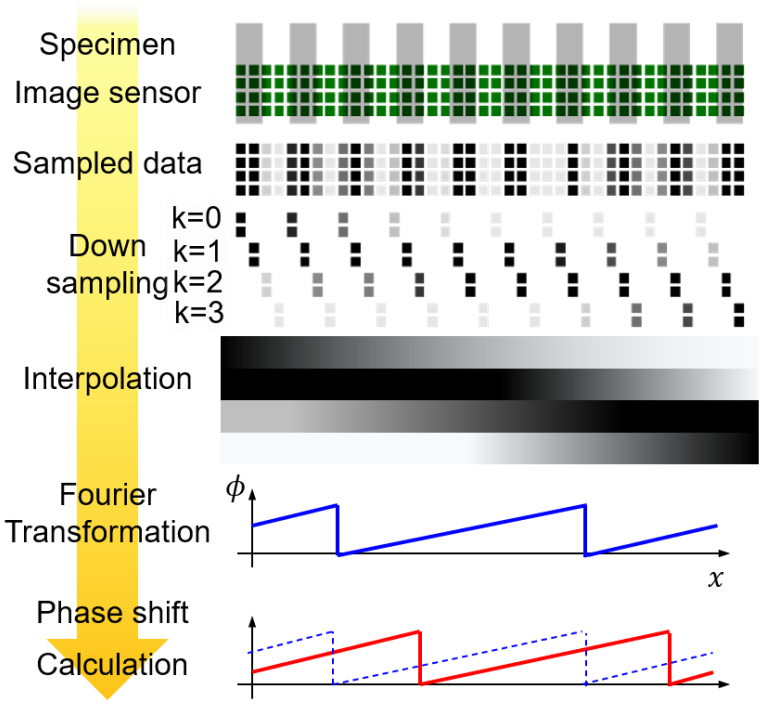

Figure 2.6 Principle of the sampling moiré method [119,120].

As detailed above, the force sensing resolution is mainly decided by the spring constant and displacement measurement accuracy. Displacement measurement by edge detection using a microscopy image has a limit resolution of approximately 0.2 μm, which is insufficient to establish the difference between the target cells. To realize high measurement resolution, I used a technique called the sampling moiré method. Similar methods have been reported in other work [138,139]. The sampling moiré method which I used in this work is proposed by another member in Arai laboratory. This method can greatly improve the resolution of the displacement measurement, which can improve the accuracy of the experimental data [119,120].

The principle of this method is shown in Figure 2.6. First of all, grating patterns with a constant period are fabricated on the chip. And a grayscale image is obtained from the microscope using a charge-coupled device (CCD) camera. Subsequently, a down sampling process is applied for every few pixels (every four pixels in the example shown in Figure 2.6) of the image and an interpolation process is then applied to reveal the moiré fringe. This fringe is called the sampling moiré fringe. The displacement of the probe could be calculated by analyzing the phase shift before and after the moving of the probe. To calculate the phase of the sampling moiré fringe, a Fourier transformation method is applied to the intensity of sampled image. Thus, the position of the probe is related to the light intensity distribution of the sampled fringe. I can establish the displacement by calculating the phase shift. The details are described in the previous research in Arai laboratory [119,120].

2.3 Chip design and fabrication

2.3.1 Design of the force sensor

For evaluating the stiffness of single *Synechocystis* cells, it is necessary to sense the force applied on the cell during cell compression. Thus, a proper design of the force sensor on is necessary. To design the force sensor, I firstly estimated the force applied on a *Synechocystis* cell during compression. Considering the Hertzian model, as shown in equation (2.1), it is necessary to know some parameter of a cell, such as diameter, Young's modulus, Poisson's ratio, and deformation, to calculate the cellular reactive force. The diameter is around 2 μm as mentioned in Section 1.3. The Poisson's ratio is set to be 0.5, which is common in researches about cell stiffness. The deformation assumed as 0.2 μm which is 10% of the cell diameter to meet the small deformation assumption of the Hertzian model. But Young's modulus of the *Synechocystis* is not known. Considering the presence of the cell wall of Synechocystis, the Young's modulus of Synechocystis should be bigger than animal cells. Yeast cell, which is also a kind of unicellular organism with cell wall, is measured using AFM by other researchers to study its stiffness. According to previous researches, Young's modulus of yeast cell is around several million pascals [122]. Thus, I assume the Young's of Synechocystis to be 1 MPa. Thus, the cellular reactive force at 10% deformation ratio $F_{10\%}$ is calculated to be 56 nN according to equation (2.1). Assuming that the resolution of the force sensor is one percent of $F_{10\%}$, the required resolution of the force sensor on the microfluidic chip should be 0.56 nN. In this thesis, a folded beam force sensor, as shown in Figure 2.7, is designed to realize such a high resolution.

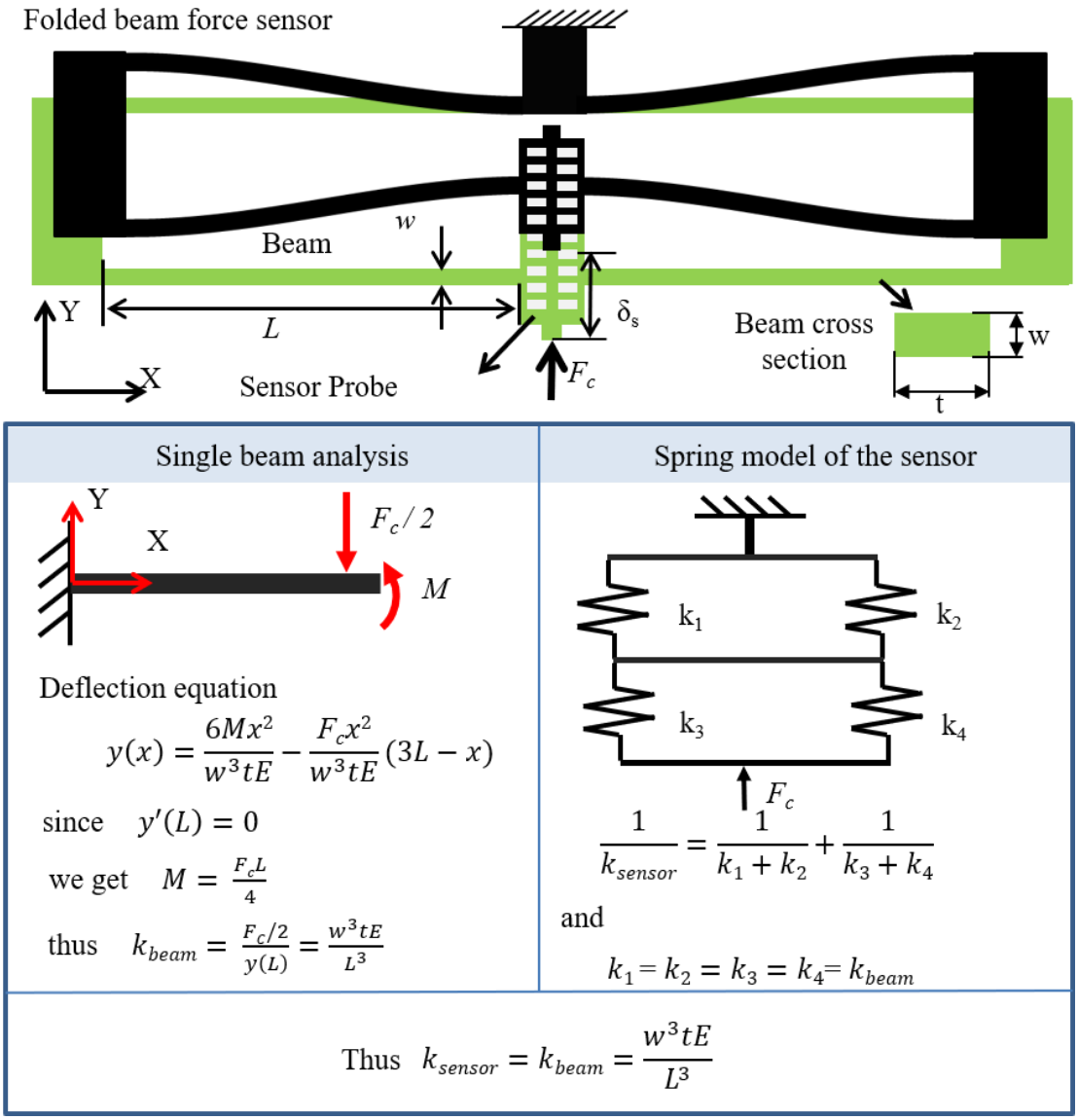

Figure 2.7 Force analysis of the folded beam sensor

The resolution of a spring-based force sensor depends on two parameters, the spring constant *k*, and the displacement measurement resolution δ_{res}. To design the force sensor, both of these two parameters need to be considered carefully.

As shown in Figure 2.7, the folded beam force sensor consists of four beams, two trusses and a sensor probe. When force is applied to the sensor probe, beams are deformed, and eventually the sensor probe moves. The trusses allow expansion or contraction of the beams along the x-axis [140].

Assuming that the trusses and sensor probe are rigid, the applied force F_c and the sensor tip displacement δ_s have a relationship which can be written by,

$$F_c = \delta_s w^3 t E / L^3 \qquad (2.4)$$

where E is Young's modulus, L is beam length, w is beam width, and t is the beam thickness. The value of t is decided by the chip used to fabricate the sensor. In this research, force sensor is fabricated on the device layer of an SOI chip, thus t has the same value with the thickness of the device layer as 7.5 μm. Since silicon is anisotropic material, the value of E depends on the crystal orientation. Crystal orientation is a parameter describing crystal structures. In this thesis, orientation of the crystal at force beams' direction is <110>, thus E of the sensor beam should be 170 GPa. Therefore, the spring constant can be decided by two parameters w and L. Thus, the resolution of the force sensor is,

$$F_{res} = \delta_{res} w^3 t E / L^3 \qquad (2.5)$$

Considering that E and t are consistent value, the force resolution depend on three parameters, w, L, and δ_{res}.

It is well known there is a limit of the resolution of an optical microscope. The lens used in this thesis has a numerical aperture of 1.4, thus the resolution of the optical microscope is around 200 nm.

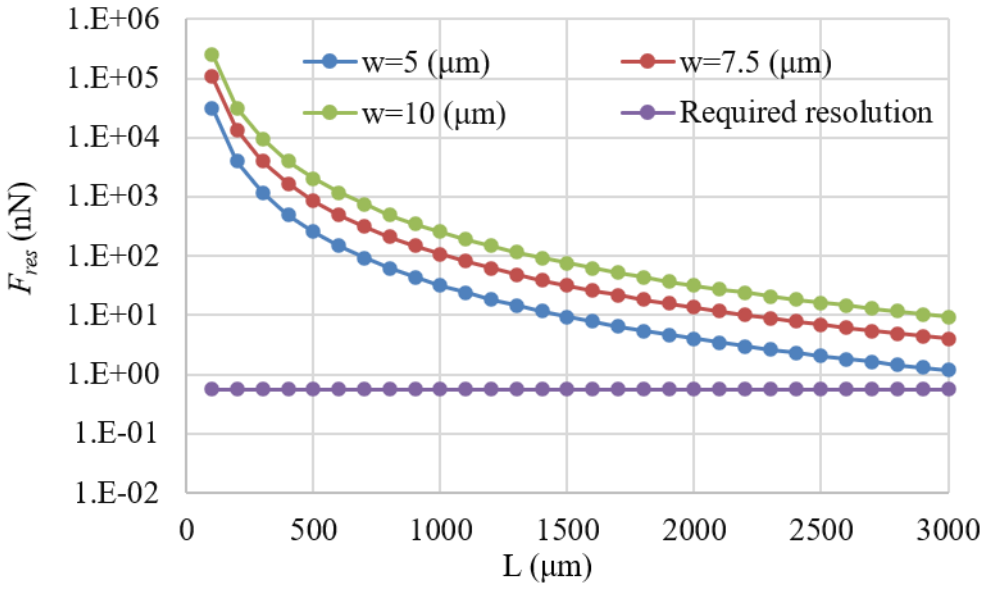

Figure 2.8 The relationship between length of the beam, L and the force resolution F_{res} when δ_{res} is 200 nm.

As shown in Figure 2.8, the force resolution of different w and L cannot meet the required force resolution (no curve intersect with the parallel purple line) when the displacement measurement resolution δ_{res} is 200 nm, the force sensor can hardly reach the requirement of the force resolution. This is because of the fabrication of the beam sensor would be more and more difficult when the beam gets longer and thinner. If a beam is longer than 3000 or thinner than 5 μm, it is difficult to fabricate. Thus, I introduced the sampling moiré method proposed by another member in Arai laboratory [119,120]. In this thesis, the sampling moiré method is adjusted to suit better for the microfluidic chip (see detail in Section 2.3.2). This method improved the displacement

resolution to 4.7 nm. Thus, the situation is improved, and the required resolution could be realized as shown in Figure 2.9. Considering the convenient for fabrications process and force sensing resolution, *L* and *w* of the beam are designed to be 1500 and 5 μm, respectively.

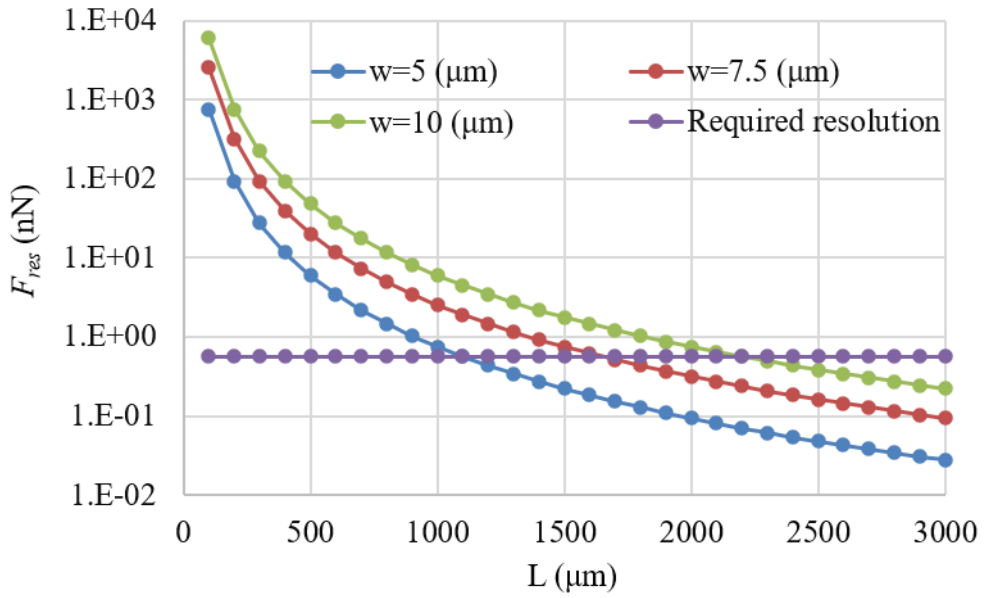

Figure 2.9 The relationship between length of the beam, L and the force resolution F_{res} when δ_{res} is 4.7 nm.

2.3.2 Improvement of the sampling moiré fringe

The sampling moiré fringe method is proposed and used by other members in Arai laboratory. This thesis also used the sampling moiré method to improve the displacement sensing accuracy. The grating structures designed on the sensor probe and pushing probe are usually has a pitch larger than 10 μm [117-120]. The grating structures of the chip for *Synechocystis* cell measurement was initially designed to have a pitch of 10 μm, but some big errors as much as 0.2 μm had occurred. This might because of the target cell in this study is small. A lens of 100 times magnification is utilized to observe the small *Synechocystis* cells. Thus, the view of the camera is quite narrow, only a rectangle area of around 100 *75 μm. To include the pushing probe and sensing probe in this narrow

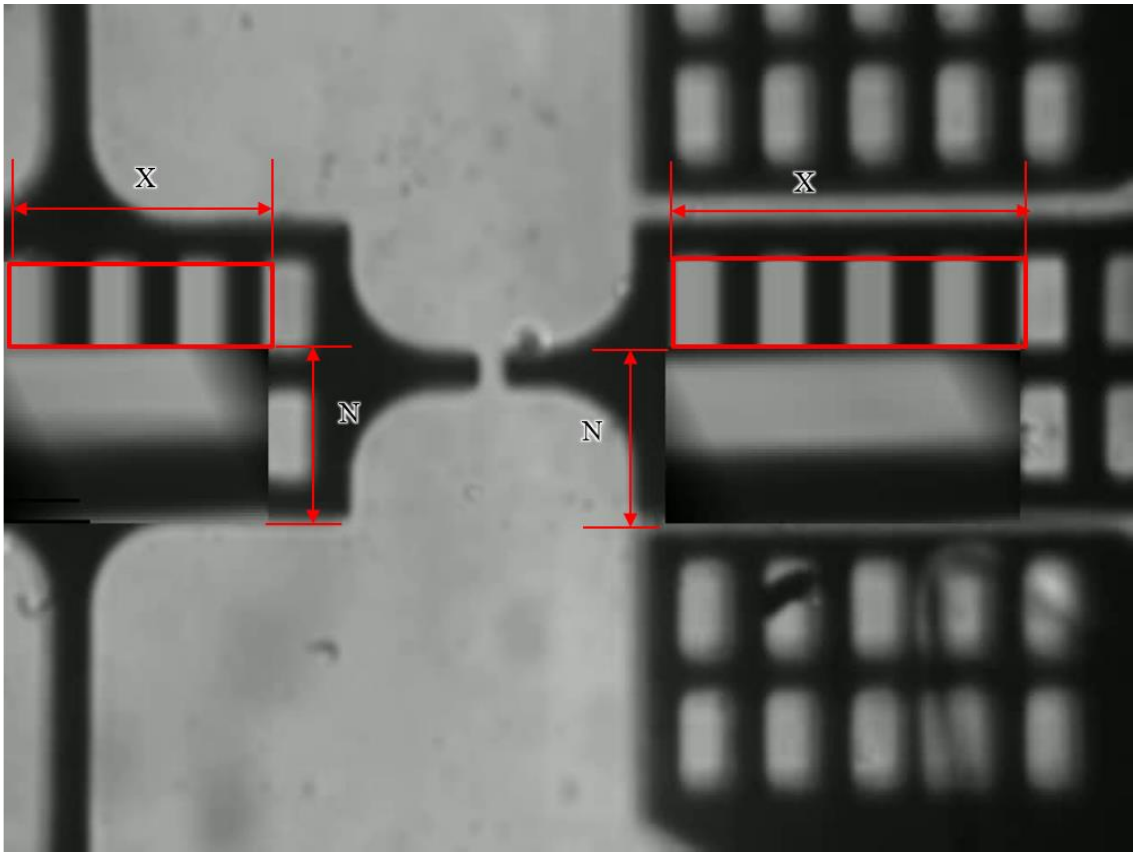

Figure 2.10 An example figure showing the analysis area in sampling moiré fringe method.

view, they are designed small and only one or two grating structures could be included in the sampling moiré fringe process.

To improve the performance of the sampling moiré method in the measurement of *Synechocystis*, a simulation is carried out based on C++ and OpenCV to study the influence of the sampling length *X*, the down sampling number *N*, and the grating shape, as shown in Figure 2.10. The accuracy of the sampling moiré method could be affected by lots of factors, such as light intensity, noise, camera pixel and so on. I only analyzed these three factors because they can be controlled by chip design and coding the sampling moiré fringe analysis software. Firstly, a pattern without noise is fabricated by coding as shown in Figure 2.11. The pattern on the figure would move a constant displacement every frame which is set in the program. And the accuracy of the moiré fringe is estimated based on the error of the measured displacement using the sampling moiré method. The

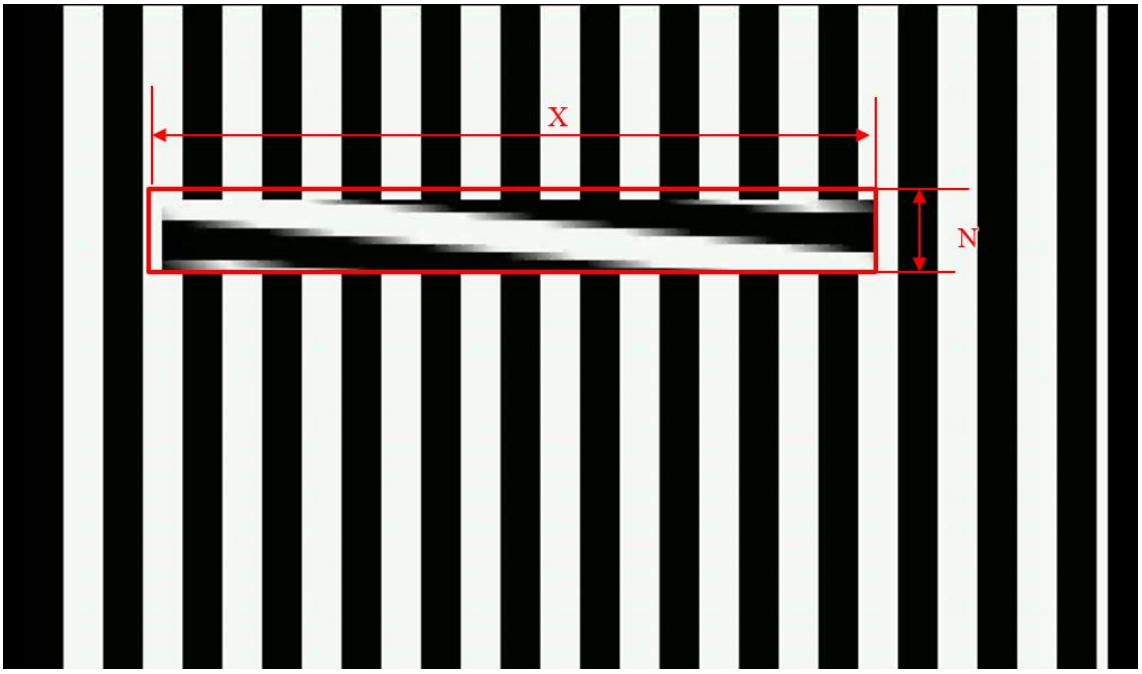

Figure 2.11 Simulation to study the sampling moiré fringe method.

influences of X, N and grating shape are shown in Figure 2.12, Figure 2.13, and Figure 2.14.

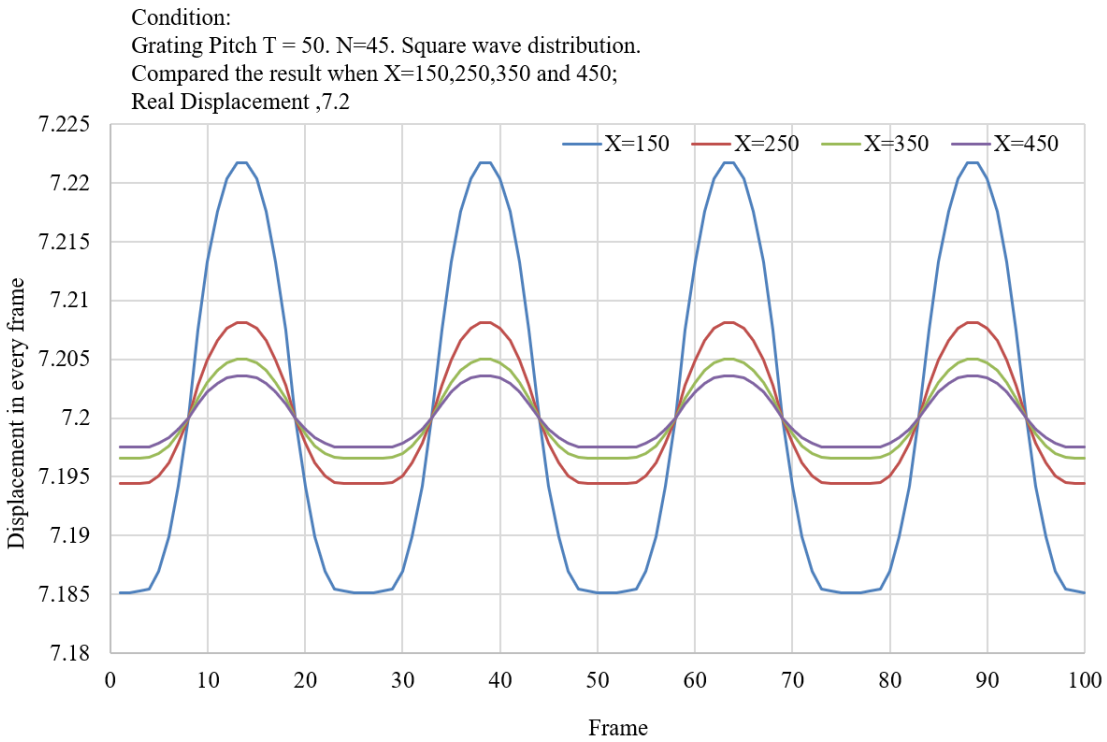

Figure 2.12 Relationship between X and sampling moiré measurement result.

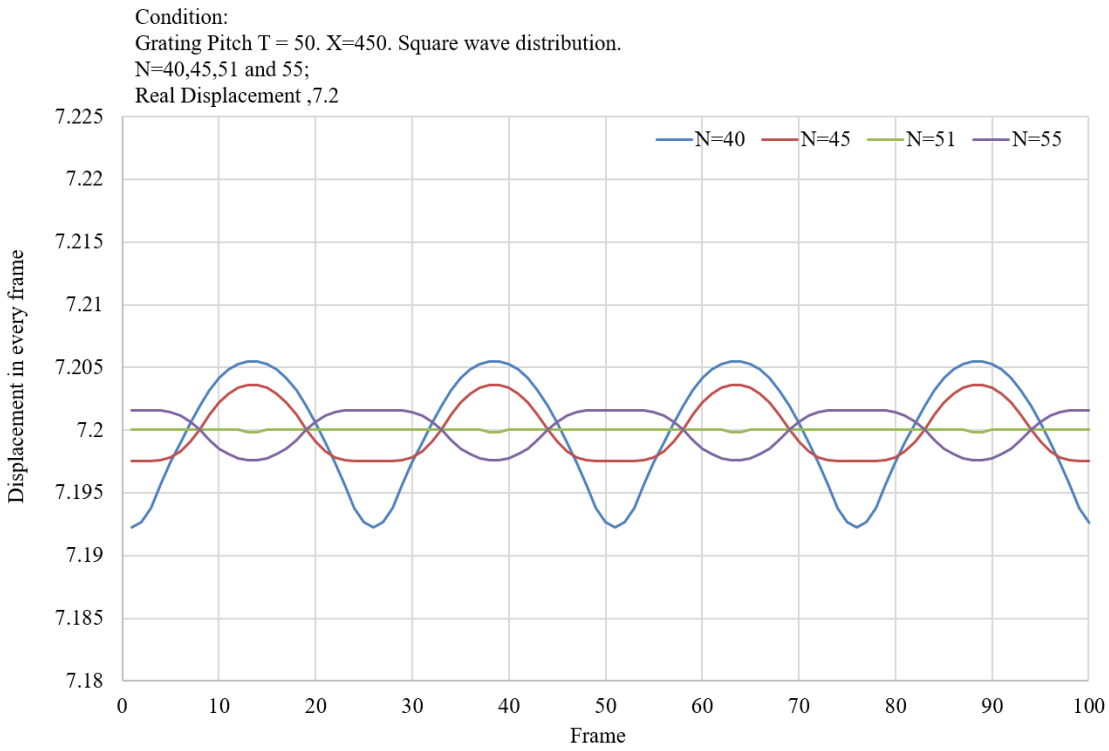

Figure 2.13 Relationship between N and sampling moiré measurement result

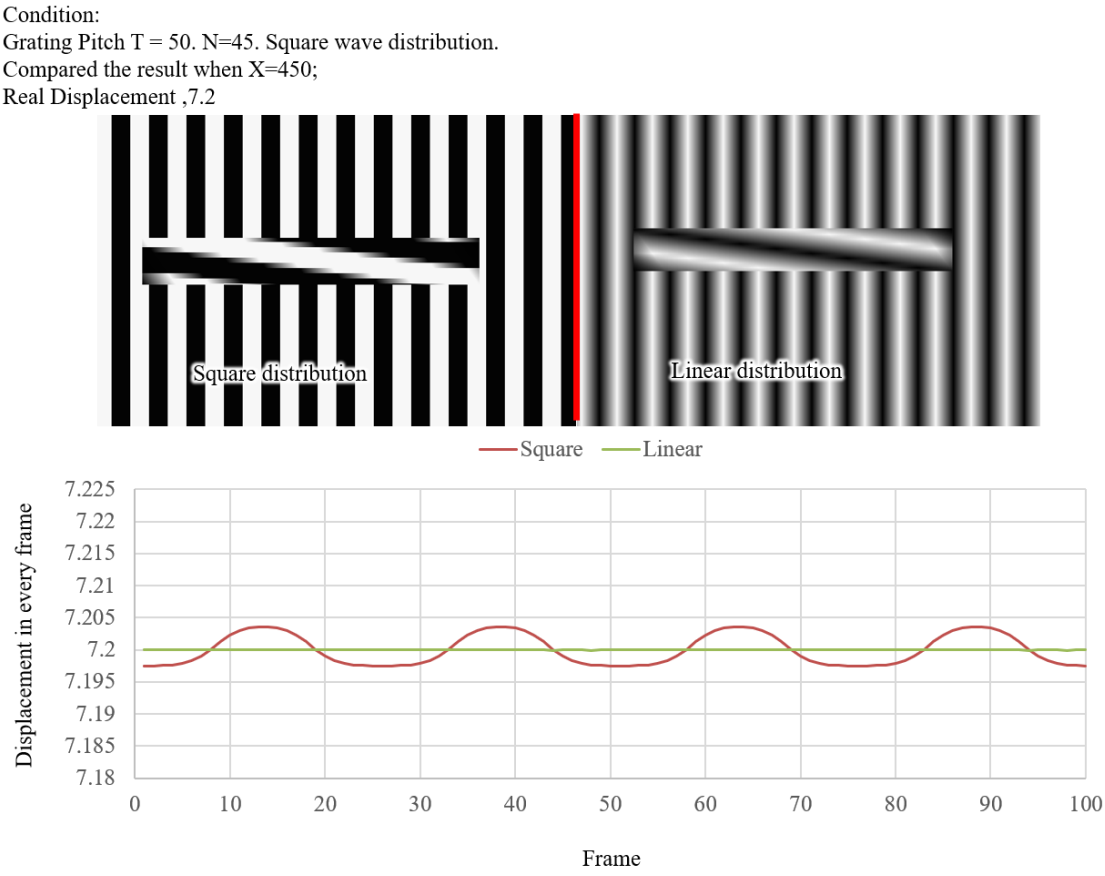

Figure 2.14 Relationship between grating shape (distribution) and sampling moiré measurement result

According to above figures, by increasing *X*, setting an *N* similar with the grating pitch, and using Linear distribution, the sampling moiré method would have a better accuracy. To increase *X* means including more grating pitches in the sampling moiré area, thus, longer *X* should be used, and smaller grating pitch should be designed on the probes. A proper *N* could be found by adjusting the *N* until moiré fringe reaches the biggest magnification times. The linear distribution could be realized by fabricating diamond shape gratings. But the small diamond gratings are very difficult to fabricate, as shown in Figure 2.15. Moreover, there is a fabrication limit that it is difficult to make small grating

structures lower than 2 μm because of diffractions, thus, a grating structure of 4 μm was designed and fabricated.

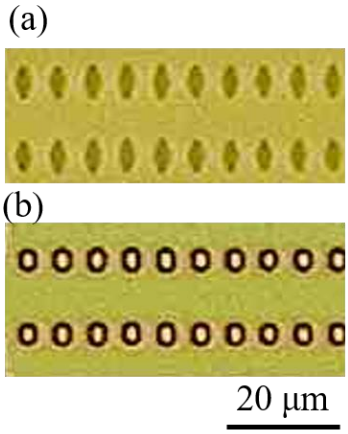

Figure 2.15 Failure of the diamond shape gratings. (a) Diamond shapes have no uniformity which makes the linear distribution nonlinear. (b)Diffraction occurred, turning diamond gratings into sphere-like gratings

The accuracy of the fabricated chip was verified by measuring the displacement of the sensor for 5 sec without motivating. The sensor should have a displacement of zero,

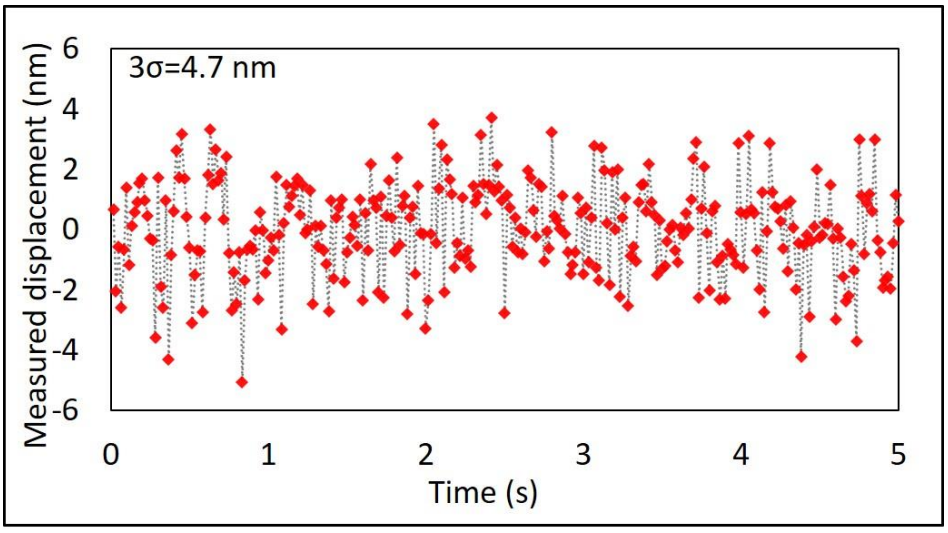

Figure 2.16 Stability of displacement measurement.

but due to the noise, small displacement was detected by the sampling moiré method. The result is shown in Figure 2.16. Three times of the standard deviation is regarded as the displacement resolution [118,119].

2.3.3 Fabrication of the chip

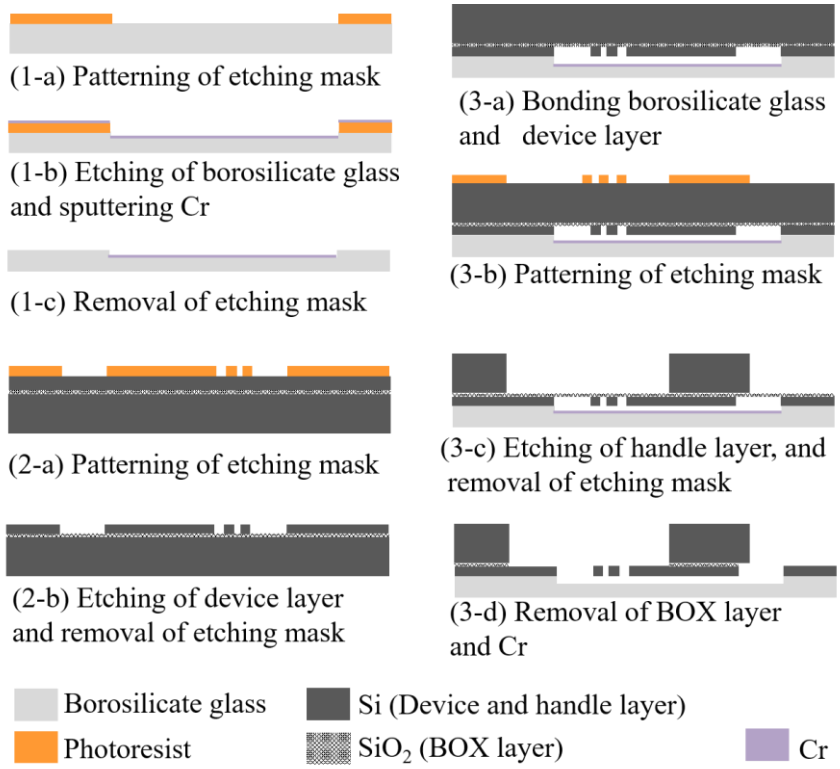

Figure 2.17 Fabrication process of the chip used in this thesis.

As mentioned in previous section, the chip is integrated of two different chips, an SOI chip and a borosilicate glass chip. The silicon chip has structure for sensing and pushing. The glass chip is only used for supporting the silicon structure and be transport for observing using a convert microscope. The fabrication process is shown in Figure 2.17. There are nine steps in total to fabricate the chip. From step (1-a) to (1-c), the glass chip is fabricated. From (2-a) to (2-b), the device layer of the SOI chip is fabricated. From (3-a) to (3-d), the two chips are bonded and fabricated as a whole chip.

(1-a) SU-8 3010, a negative photoresist, is spin-coated onto the surface of a borosilicate glass chip, and then patterned using a mask aligner.

(1-b) The glass chip was etched using deep reactive-ion etching (DRIE) to approximately 6 μm. This process prevents friction between the probes and the glass. A thin layer of Cr was then sputtered onto the etched side of the glass. The Cr layer protects the movable parts (the force sensor and the pushing probe) from bonding to the glass.

(1-c) The photoresist on the glass is removed using piranha solution. The Cr attached to the photoresist is removed at the same time. Thus, only the etched part are covered with Cr.

(2-a) OFPR, a positive photoresist, is patterned onto the device layer as an etching mask. This photoresist is thinner than SU-8 and is therefore useful for fabricating small structures on the device layer.

(2-b) The device layer is etched using a special etching process called deep reactive-ion etching (DRIE). This etching process has a good performance in making vertical side wall. The etching mask was then removed using piranha solution.

(3-a) The glass and device layer are bonded together using anodic bonding.

(3-b) SU-8 was spin-coated and patterned onto the surface of the handle layer as an etching mask. The pattern on the handle layer do not need high accuracy and has a large etching depth. Thus, it is better to use SU-8 than OFPR because of its thicker photoresist layer.

(3-c) Handle layer is etched using DRIE and the etching mask is removed by oxygen plasma ashing.

(3-d) The BOX layer is removed using buffered hydrogen fluoride (HF) solution. HF solution is a kind of highly poison and corrosive liquid.

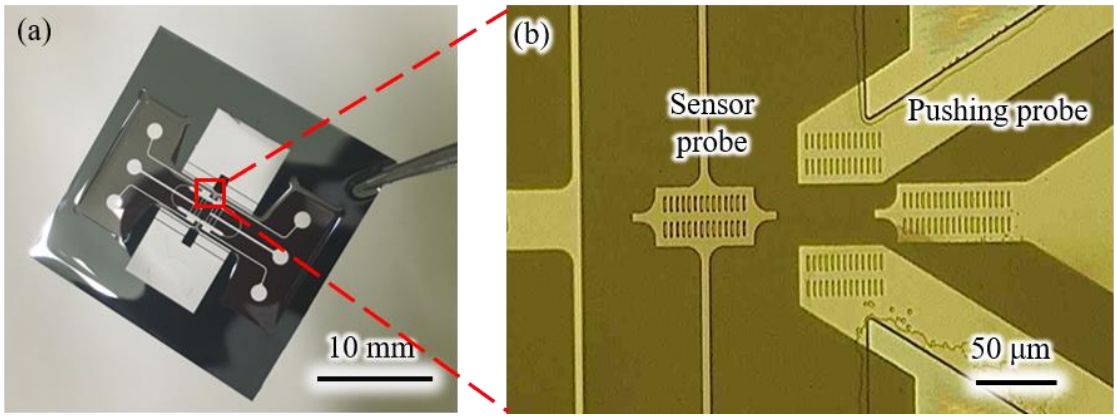

Figure 2.18 (a) Complete view of the fabricated microfluidic chip. (b) Photograph of the probes of the chip under optical microscope.

The fabricated microfluidic chip is shown in Figure 2.18 (a) and Figure 2.18 (b). The complete view of the fabricated chip is shown in Figure 2.18 (a).Figure 2.18 (b) shows a magnified picture of the chip under an optical microscope. The length of the fabricated beam is 1500 μm. And the width of the fabricated beam is 4.5 μm measured by an optical microscope. The sensor beam has a different width compared with its design value. This is due to the errors of the machine, photoresist patterning, silicon etching and so on. The thickness of the beam *t* was 7.5 μm, which is as same as the thickness of the device layer. Therefore, the theoretical spring constant of the beam sensor which has been fabricated on the microfluidic chip is 0.0344 N/m according to equation (2.4).

2.4 Calibration of the force sensor

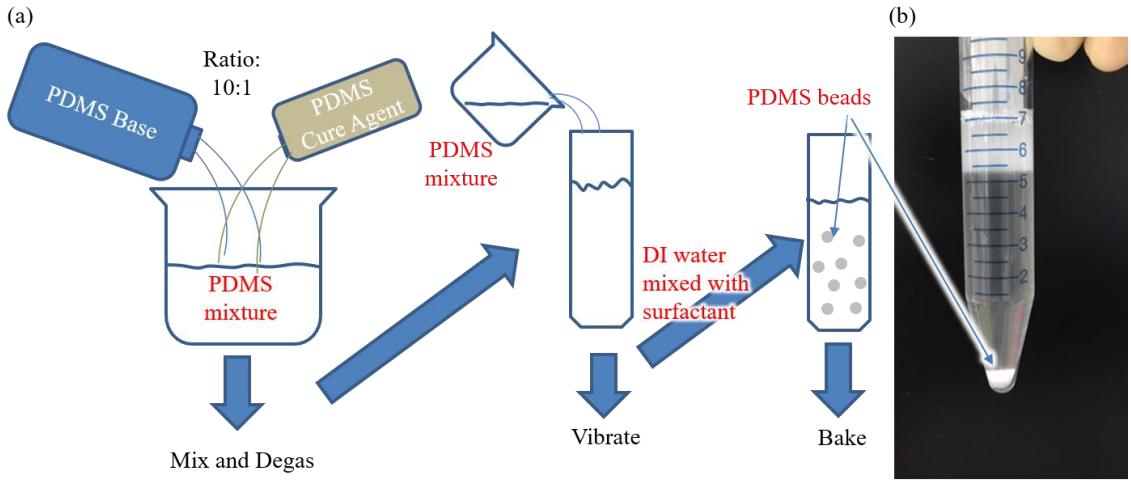

Figure 2.19 Fabrication process of PDMS beads (a) and the fabricated PDMS beads in a tube (b).

It is necessary to calibrate the force sensor before using the microfluidic chip. Usually, there are several methods to calibrate a beam force sensor. For example: measuring the geometry accurately to compute the spring constant, applying a known load using a calibrated force sensor, and measuring the resonate frequency. For the force sensor described in this section, it is very difficult to measure the geometry accurately because of its small size and the resolution limit of the optical microscope. Another method which utilizes another calibrated force sensor is neither suitable. The force sensor is so sensitive that few force sensors can be used to apply a proper force to the chip sensor. Resonate frequency is neither suitable for this sensor calibration because the size of the sensor beam is not easy to be measured accurately, which means the mass of the spring cannot be

calculated accurately. Thus, the spring constant cannot be calculated from the resonate frequency.

In this thesis, the spring constant is calibrated using polydimethylsiloxane (PDMS) beads. A commercial viscous prepolymer (Sylgard 186, Dow Corning) was used. The prepolymer consisted of a viscous base and a liquid curing agent. The fabrication process of the PDMS beads is shown in Figure 2.19(a). The base and cross-linking agent were mixed at a ratio of 10:1 by weight. The mixture was then poured into deionized water (DI water). One drop of surfactant (Ajax dish soap) is added into the DI water to prevent the beads from gathering. The vessel containing the DI water and PDMS mixture was then vibrated using Vortex-Genie-2 at 3200rpm to form spherical beads. The container was subsequently baked at 80°C for 2 hours. The fabricated PDMS beads are shown in Figure 2.19(b).

A piece of PDMS film was also fabricated under the same conditions from the same mixture. The Young's modulus of the PDMS film is measured using a commercial tensile test device (EZ-LX, Shimadzu Cooperation). The average Young's modulus of the PDMS film is approximately 1.15 MPa. Considering that the PDMS has a risk that the crosslink reaction is not totally finished during baking, which might lead to increasing the Young's modulus of PDMS have the possibility to become stiffer after baking, 4 PDMS film samples are measured once a day for 14 days. And no obvious increase is observed as shown in Figure 2.20. The PDMS beads are measured in day 14 for calibration. The Young's modulus of PDMS beads and PDMS films should be same because of their same fabrication process.

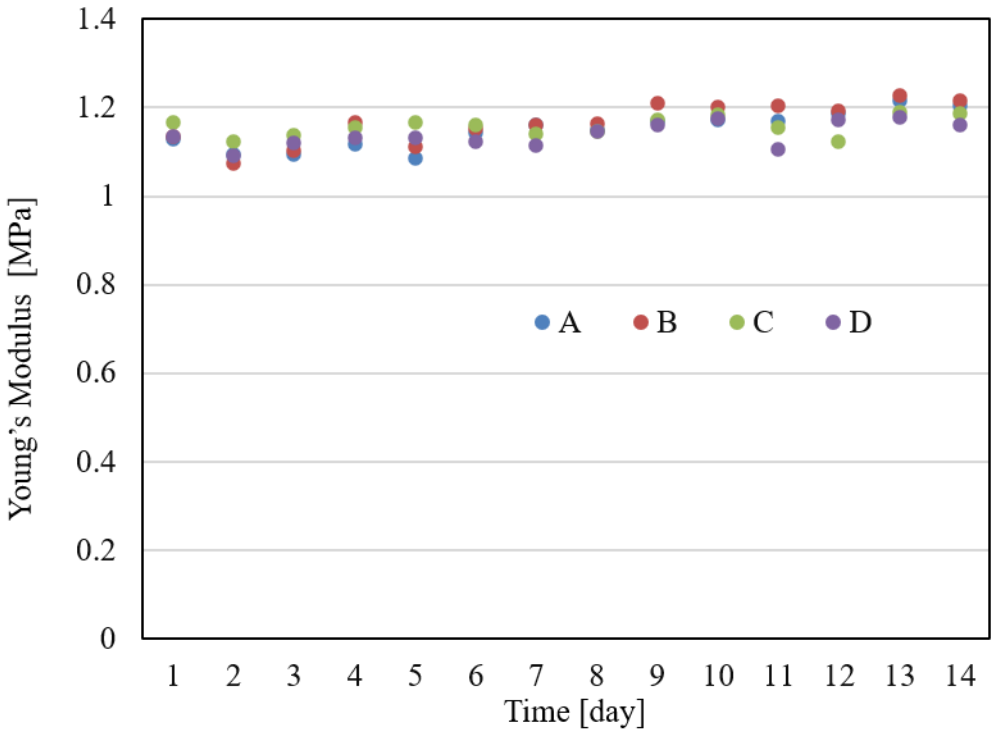

Figure 2.20 Young's modulus of four PDMS film samples measured in 14 days.

Ten PDMS beads were measured using the robot integrated microfluidic chip to calibrate the force sensor's spring constant. For each bead, the spring constant is calibrated using equations (2.1) to (2.3) assuming the E to be 1.15 MPa. The average calibrated spring constant was 0.0326 ± 0.0017 N/m (mean ± standard deviation, n = 10). This value is close to the theoretical value from equation (2.4). Figure 2.21 shows an example of the calibration data. The blue dots represent the force data measured by the chip, and the red curve is the theoretical value of force after calibration. From these results, the spring constant is 0.0326 N/m. This value is used in later calculations.

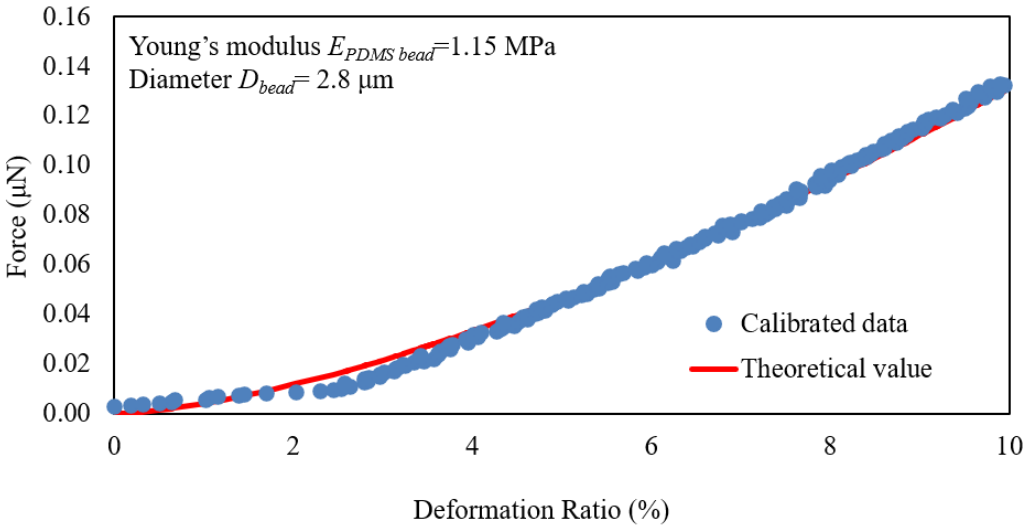

Figure 2.21 An example of the calibration data of the folded beam force sensor. Blue dots are the data measured using the microfluidic chip after calibration and red curve is the theoretical value when the Young's modulus is 1.15 MPa.

2.5 Summary

In this chapter, I propose a system for measurement of the stiffness of single *Synechocystis* cells. Firstly, I showed the design of the measurement system and the chip. My system uses optical tweezers to trap and transport a cell, and two probes fabricated on a microfluidic chip to deform it. The chip has an external actuated pushing probe and a force sensor probe. A single cell could be located between the tip of both probes using the optical tweezers and was then deformed using the probes. The sampling moiré method was used to achieve high measurement resolution. A Hertzian model is used to fit force curve for calculating the Young's modulus. Secondly, I described the fabrication process of my chip. After that, pictures of the fabricated chip are shown. Finally, I show the calibration of the force sensor. The sensor is calibrated using PDMS beads whose Young's modulus is known.

Chapter 3 Measurement of the mechanical property of single cyanobacteria cell

3.1 Introduction

As mentioned in the previous sections, *Synechocystis* is a model unicellular phototrophic cyanobacterium that has been used as a model microorganism in a wide range of studies in areas such as photosynthesis [115], biofuel [10-12], and environmental stress adaptation[15,16]. Cells have developed lots of mechanism to survive from different environmental conditions. It is well known that the cell membrane is a kind of semipermeable membrane. Thus, the osmolarity is an important factor for cell life

because it affects the water flow across the semipermeable membrane, as shown in Figure 3.1.

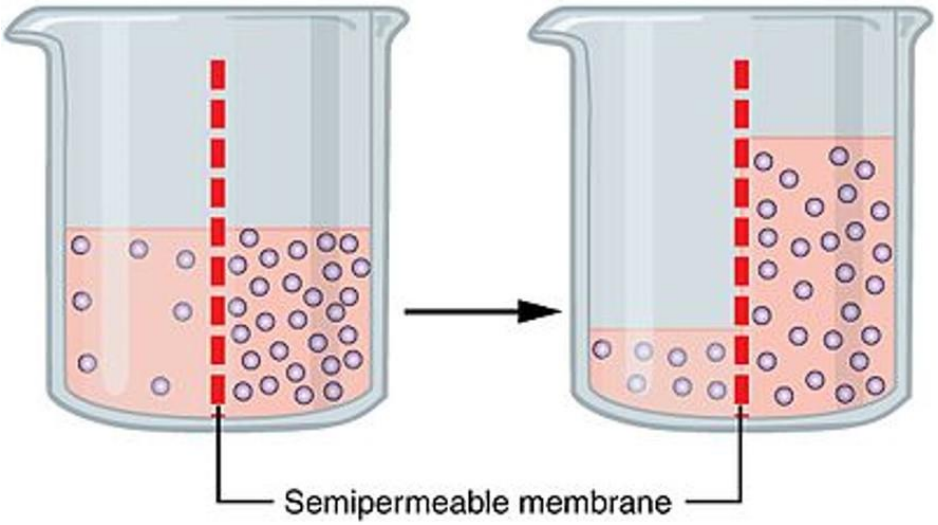

Figure 3.1 The process of osmosis over a semi-permeable membrane. The dots represent particles driving the osmotic gradient. [141]

Synechocystis has an osmoadaptation mechanism that allows it to survive osmotic concentration shifting in the external environment. This mechanism is of fundamental importance for growth and survival [142]. Mechanosensitive (MS) channels, one of the ion channels on the cell membrane, play important roles in the osmoadaptation mechanism. MS channels are reported to sense the cell membrane tension and release intracellular material into the extracellular environment to protect the cell in osmotic down shift [143,144]. To maintain intracellular pressure, *Synechocystis* regulates ion channels. When extracellular osmotic concentration increases, intracellular water molecules pass out into the extracellular environment, resulting in an intracellular pressure decrease. In this situation, MS channels does not work. Conversely, when extracellular osmotic concentration decreases, water

molecules enter into the cell across the cell membrane (and cell wall). Simultaneously intracellular pressure and the cell membrane tension increase. MS channels sense the change of the tension and release intracellular materials from the cells by opening their gate to keep the cell integrity from hypo-osmotic change. I previously reported on the function of several ion channels in the osmoadaptation mechanism using size differences observed in microscopy images [16]. However, when the size changes are too small to be detected, I must consider an alternative method of evaluating the activity of the MS channels.

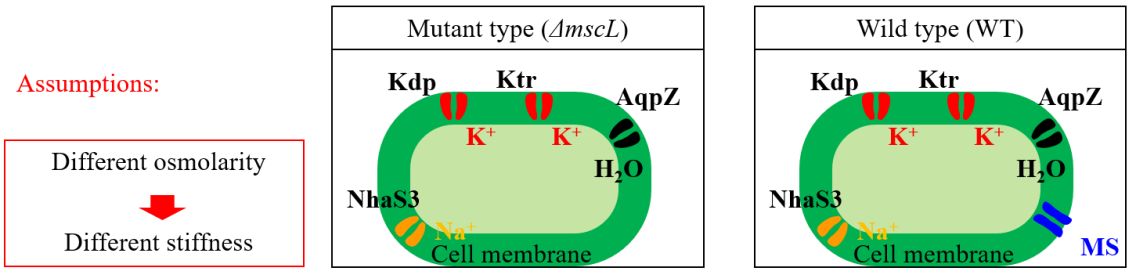

High osmolarity	Stiffness of *ΔmscL*	≈	Stiffness of WT
Normal osmolarity	Stiffness of *ΔmscL*	>	Stiffness of WT
Low osmolarity	Stiffness of *ΔmscL*	>	Stiffness of WT

Figure 3.2 Assumptions of the effect of the MS on the stiffness of single Synechocystis cell.

Because intracellular pressure is regulated by the MS channels under external low osmotic conditions, I propose that the activities of MS channel could be evaluated by measuring stiffness of the cell. For this purpose, I tested *Synechocystis* wild type (WT) (without genetic modification) and MscL-defective mutant (*ΔmscL*). As mentioned above, MS channels have different activities in different osmolarities. Thus, I measured the

stiffness of WT and *ΔmscL* cells in different osmolarities to evaluate the activities of MS channels. As shown in Figure 3.2, I assume that the WT and *ΔmscL* cells should have similar stiffness in high osmolarity because the MS channels do not work. While in normal osmolarity, the stiffness of the WT cells should increase, while *ΔmscL* cells should have a higher stiffness than WT cells. This is because MS channel on the cell membrane of WT cells allow the efflux of intracellular materials. Furthermore, in low osmolarity, the stiffness of cells should be higher than that in normal osmolarity because of higher tension of cell membrane.

As described in Chapter 2, I proposed a measurement system which consists of optical tweezers and a robot integrated microfluidic chip to investigate the stiffness of *Synechocystis* on a level of single cell. I evaluate the Young's modulus of WT and *ΔmscL* cells in three different osmotic concentrations.

3.2 Sample preparation

3.2.1 Cell culturing and preparation

The cells used in this thesis are the model cyanobacterium *Synechocystis* sp. strain PCC6803. Two types of the *Synechocystis* cells are measured, the wild type (WT) (without genetic modification) and MscL-defective mutant (*ΔmscL*). WT cells and *ΔmscL* cells were grown at 29°C in liquid BG11 medium [144]. Continuous illumination was provided by a 3.5 W LED white light source (AS ONE CORPORATION, BLS/3-6229-02) which was set 150 mm away from the cell suspension. The mutant type *ΔmscL* was genetically modified by insertion of a Spe resistance cassette into *SyMscL* (*slr*0875) as described in previous research [144]. To evaluate the influence of MS channels, WT and *ΔmscL* cells were measured in three different solutions, as shown in Figure 3.3.

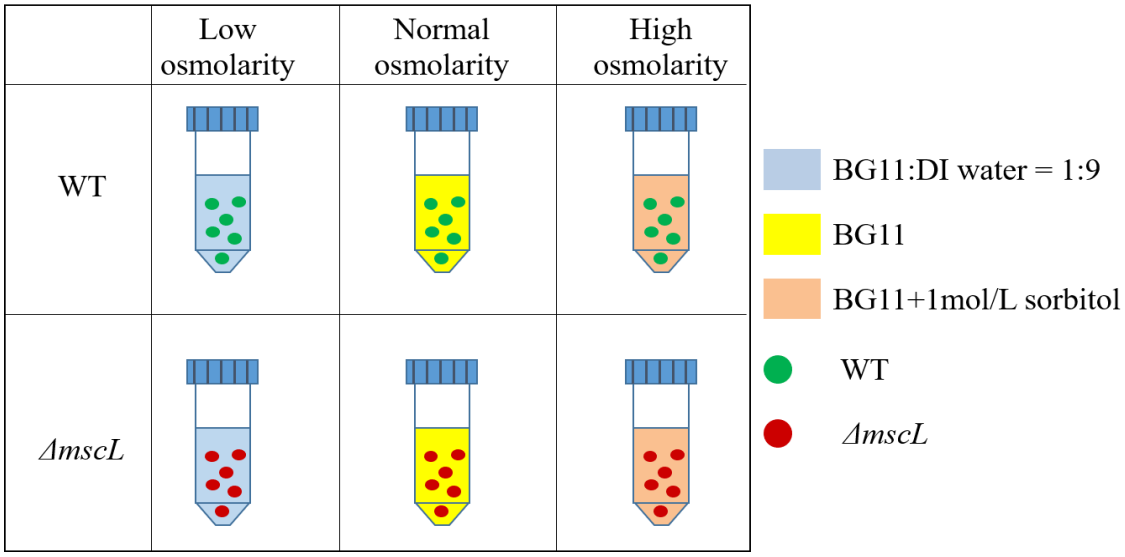

Figure 3.3 The diagram of sample preparation for further experiment.

BG11 is a liquid culture medium used for culturing *Synechocystis* and was therefore used as the normal osmotic concentration solution. BG11 containing 1 mol/L sorbitol was used as the high osmotic concentration solution. The concentration of sorbitol is based on previous research. And BG11 mixed with deionized water at a ratio of 1:9 (by volume) was used as the low osmotic concentration solution. Before measurement, both WT and *ΔmscL* cells were centrifuged at 4°C and resuspended in one of the three solutions. The cell is assumed to be made of incompressible materials as mentioned previously. But water flowing across the cell membrane after applying osmolarity stress will makes the cell swell or shrink. Therefore, cells were cultured in the particular solution for more than 2 hours prior to measurement, and I assume they are considered as stable state when I measure them [144].

3.2.2 Chip cleaning before each experiment

To measure reactive force of the target cell when it is deformed, the most important parameter is the width of the sensor beam because it greatly affects the spring constant as shown in equation (2.4). In the fabrication processes of microfluidic chip, the width of beam may have the small difference of several hundred nanometres. Thus, I decided to use the same chip which has the calibrated force sensor in my experiments to compare the results. To prevent contamination between cell types and culture medium with different osmolarity, I clean the chip to make sure there is no residual cells or culture medium after measuring one group of cells. The chip cleaning process is described as follows. Firstly, the chip is put into acetone for two hours. Then, wash the chip using ethanol and deionized water (DI water) separately to remove all the acetone attached on the chip. After that, the chip is put into piranha solution (sulfuric acid: Hydrogen peroxide = 2:1 in volume) and wait for half hours. Then, I put the chip into a cup of new piranha solution and wait for another half hours. Finally, the chip is washed gently and carefully using deionized water for three times. Thus, the chip is totally clean and no cells remaining on it. For each experiment, the chip would be wetted using the corresponding solution to make sure the concentration of the cell culture medium does not change.

3.3 Experiment

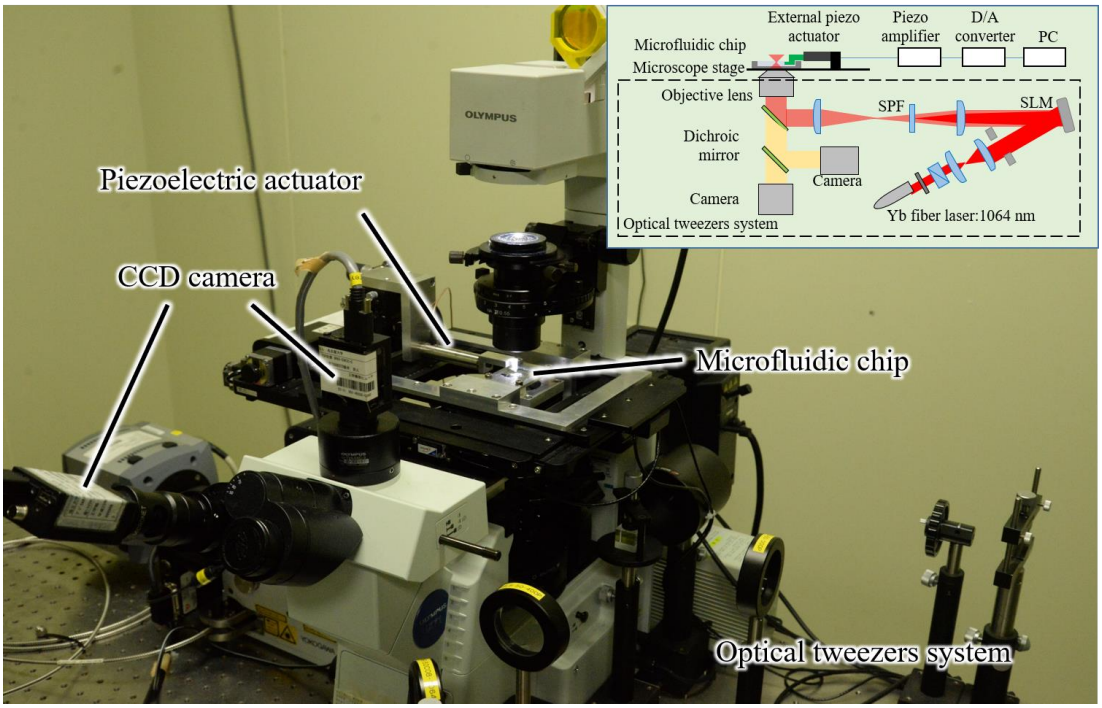

Figure 3.4 Photograph of the experimental setup.

The setup of the measurement system is shown in Figure 3.4. This system is mainly made up of two parts, the optical tweezer system and the robot integrated microfluidic chip. The chip was fixed to the microscope. A PC controls a piezoelectric actuator according to a D/A converter. There were two CCD cameras assembled on the microscope. One was used to observe the target cell during manipulation. The other was used for the sampling moiré method.

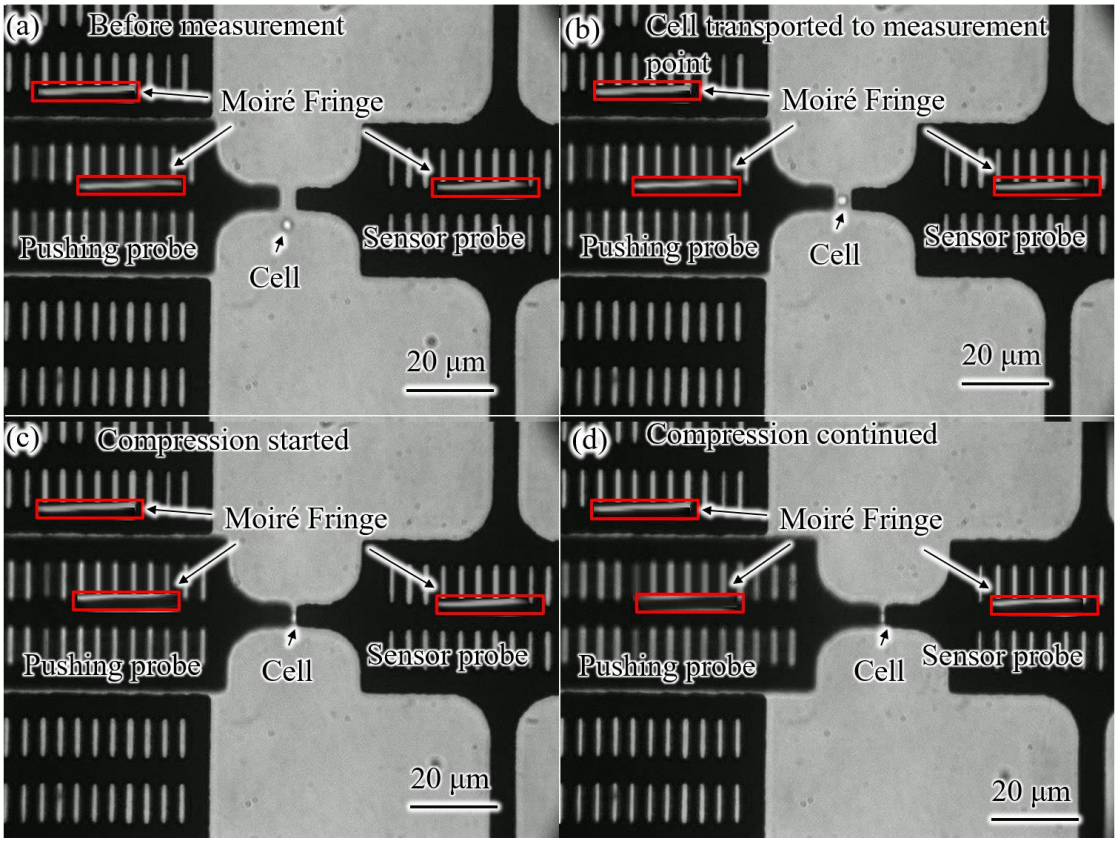

Figure 3.5 Experimental process for one single cell. (a) Before compression. (b) Cell transported to measurement point by optical tweezers. (c) Start of compression process. (d) Continued compression

An example of a measurement is shown in Figure 3.5(a) to Figure 3.5(d). The chip is fixed onto the stage of the microscope and a drop of cell suspension is added to the surface of the microfluidic chip. The process of measurement is described below. First, a single cell is trapped by the optical tweezers and transported close to the measurement point, as shown in Figure 3.5(a). The pushing probe is then actuated to contact the sensor without a cell present, to record the initial distance between these two probes. Following this, the cell is transported to the gap between the probes, as shown in Figure 3.5(b). Finally, the pushing probe is actuated again compressing the cell between the two probes, as shown

in Figure 3.4(c) and Figure 3.5(d). During this compressing process, the displacement of the two probes was recorded by the CCD camera.

As mentioned previously, I used Hertzian model to calculate the Young's modulus of a single cell. There are lots of contact force models to describe the contact between two objects. The Hertzian model is a small deformation contact model. It is necessary to know the deformation limit of the small deformation ratio. There is a research show that when the deformation of a sphere compression test is less than 10%, Hertzian model and Tatara model [145] which is a contact force model suitable for both of small deformation and large deformation, would be similar with each other [146]. Thus, I calculated the Young's modulus for cases where deformation was less than 10%.

In Hertzian model, the material is considered to be elastic. Previous researchers discovered that animal cells have poroelasticity [147] and viscoelasticity [148]. Moreover, another research shows that living mammalian cytoplasm exhibits different mechanical properties, including viscoelasticity, poroelasticity and elasticity in different conditions [149]. In this thesis, the target is to evaluate the influence of MS channel on the stiffness of the whole cell, and the poroelasticity is ignored in the calculation of Young's modulus. In the case of Synechocystis cells, dynamic property is not well investigated. What's more, the difference between the fitting curve using viscoelastic model and poroelastic model is very small [147]. In this experiment, the compression of a single cell takes several seconds, the damping effect of the viscoelasticity could be ignored. This can be proved because the experiment data fits Hertzian model well. In this thesis, the focus is to build a system which can evaluate the stiffness of a single cell whose diameter can be as small as 2 μm and compare the measurement result between wild type and *ΔmscL* to evaluate

the function of MS channel and how does it influence the stiffness of cell in different osmolarity conditions. Thus, I choose a simple and commonly utilized model, Hertzian model, with the elastic assumption to calculate the Young's modulus.

3.4 Result and discussion

To investigate the function of MS channels in the osmoadaptation mechanism of *Synechocystis*, I conducted a series of six experiments. WT and *ΔmscL* cells were separately measured in three different osmotic concentrations.

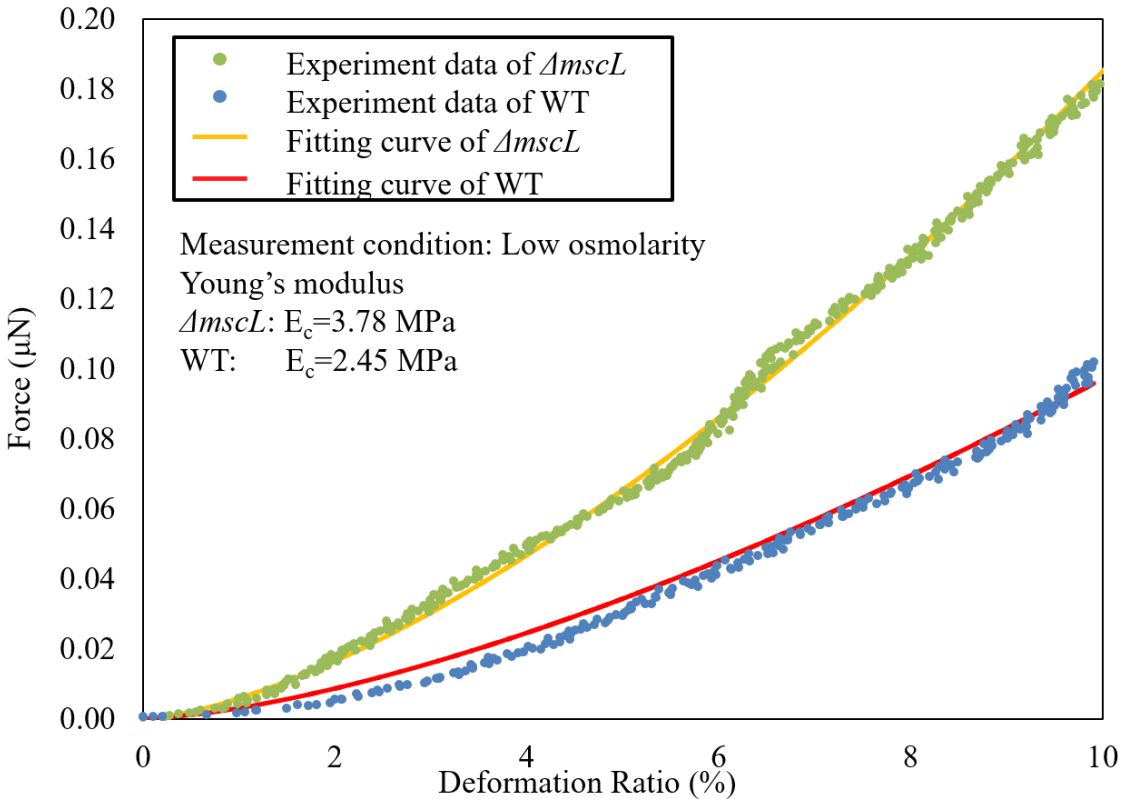

Figure 3.6 Examples of the result of a single WT cell and a single ΔmscL cell in low osmolarity. Blue and green dots represent for experimental data of WT and ΔmscL, respectively. Red and orange curve show the fitting value of Hertzian model of WT and ΔmscL, respectively.

Two examples of the typical measurement data and their fitting curves are shown in Figure 3.6. One is the WT cell, and another is the *ΔmscL* cell. Both cells are measured in

the low osmolarity condition. Blue and green dots represent for experimental data of WT and *ΔmscL* cells, respectively. Red and orange curves are the fitting curve of WT and *ΔmscL* cells using Hertzian model, respectively.

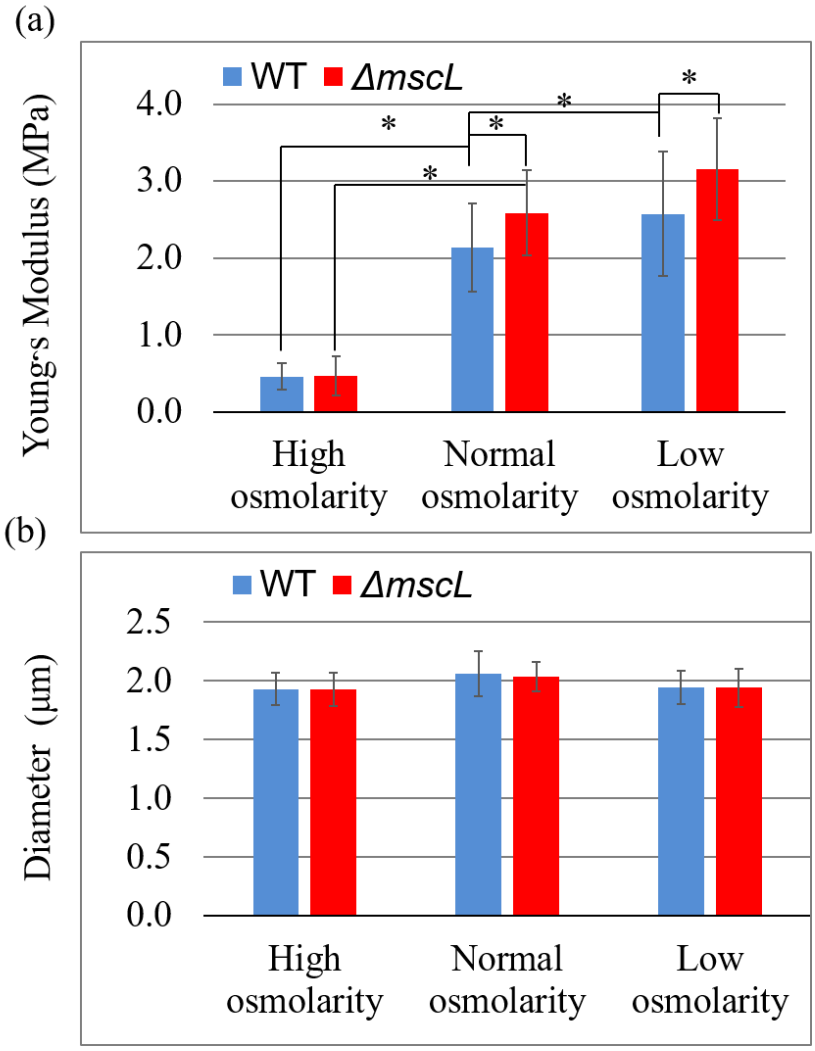

Figure 3.7 Young's modulus (a) and diameter (b) of WT cells and ΔmscL cells in three osmotic concentrations. Blue data is WT and red data is ΔmscL. The sample number for each series is ten. The error bars show standard deviation. A significant difference between WT and ΔmscL was analyzed by Student's t test ($p < 0.05$).*

In total, ten cells were measured in each experiment and the summarized Young's modulus data are shown in Figure 3.7(a). The blue bars represent WT cells and red bars represent *ΔmscL* cells. The error bars show standard deviation (SD). In high osmotic concentrations, the Young's modulus of WT and *ΔmscL* were 0.46 ± 0.17 MPa (mean ± SD, n = 10) and 0.47 ± 0.25 MPa (mean ± SD, n = 10), respectively. There is no significant difference between the two cell types. At normal osmotic concentration, a Young's modulus of *ΔmscL* cells (2.57 ± 0.57 MPa) (mean ± SD, n = 10) was significantly higher than to that of WT (2.14 ± 0.57 MPa) (mean ± SD, n = 10). And in low osmotic concentrations, a Young's modulus of *ΔmscL* cells (3.16 ± 0.66 MPa) (mean ± SD, n = 10) was significantly higher than to that of WT (2.59 ± 0.82 MPa) (mean ± SD, n = 10) respectively. These results show that cells without MS channels were stiffer than cells with MS channels in solutions with normal and low osmotic concentrations. What's more, the Student t-test is also carried out to test whether there is a significant difference for the same bacteria strain between normal and low osmolarities. As a result, there is a significant difference for *ΔmscL* between normal and low osmolarities. While, t-test for WT between normal and low osmolarities shows that the difference is not significant. The diameter of each cell is also summarized in Figure 3.7(b). As stated, the diameter of each cell was also measured. The distance between the pushing and sensing probe was recorded when the sensor started moving during the compression process. I regarded the distance as the diameter of the cell. Although the displacement measurement is very accurate using this chip, no clear difference between cell types or osmotic concentration was observed.

The diameters measured in this research revealed no clear variation between different osmotic concentrations or different cell types. It was difficult to see the change in the size of the cell including cell wall in different osmolarities. As mentioned above, the diameter of the cell is measured by recording the distance between the two probes when the sensor probe starts moving. I think that there is no significant difference in cell size between each condition because of the tiny change of the cell wall in this measurement method. However, distinct differences in Young's modulus were observed.

The diameter of the cell is not change obviously in this experiment. But in some previous studies, which evaluating the volume of the cell in different methods (such as electron paramagnetic resonance (EPR) spectrometry [13], light microscopy analysis [16] and optical density measurement [144]), show that the volume of the cell decreased when it is coming across hyperosmolarity condition. The volume of the cell which is treated with hyperosmotic condition is around 60%~70% of the volume before hyperosmotic treatment [13, 16]. The difference between this thesis and previous studies might be caused by the usage of different methods. It is well known that plasmolysis would happen when a cell with cell wall comes across the hyperosmolarity environment [150] as shown in Figure 3.8. The cell membrane would separate from the cell wall, the size of the cell wall does not change much, but the size of cytoplasm decrease. In this thesis, the diameter of a cell is measured during the compression process, the distance between the two probes when the sensor probe starts moving in the cell compression test is considered as the diameter of the cell. It means that the diameter measured is the diameter of the cell wall. Thus, the diameter did not change in different osmolarity conditions in this thesis. But in previous studies, where the cells are observed or measured using indirectly, the volume

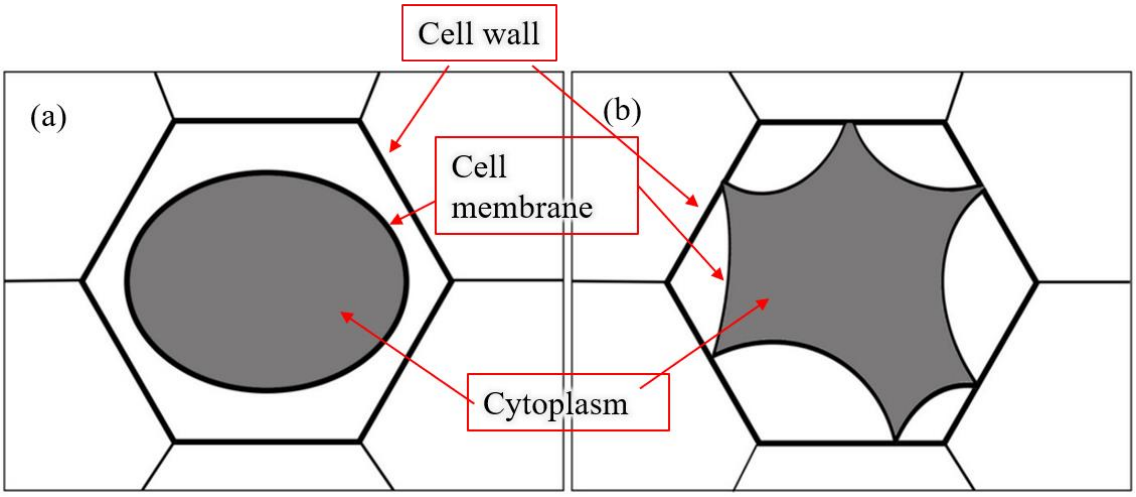

Figure 3.8 Schematic of the two major plasmolysis forms; (a) convex plasmolysis; (b) concave plasmolysis [150].

of cytoplasm is evaluated. Thus, the volume would decrease when the cell come across hyperosmolarity environment.

MS channels work by opening a protein gate and releasing material from the intracellular materials to the extracellular environment in response to changes in cell membrane tension [151,152]. The mechanism of an MS channel is shown schematically in Figure 3.9. When the tension of the cell membrane is low, the MS channel is closed (Figure 3.9(a)). When the membrane tension increases due to osmotic down shift, the MS channel reacts to the increase and opens (Figure 3.9(b)). Some materials inside the cell, such as water and ions, can then flow out of the cell from this gate to protect the cell from bursting. In this chapter, when cells were kept in an environment with high osmotic concentration the cell membrane was consequently not tight. While in normal and low osmotic concentrations, the cell membrane was kept tight, and the membrane tension was high. The MS channels were stimulated and responded to the tension increase by releasing some materials inside the cell into the extracellular environment. In contrast, *ΔmscL* cells

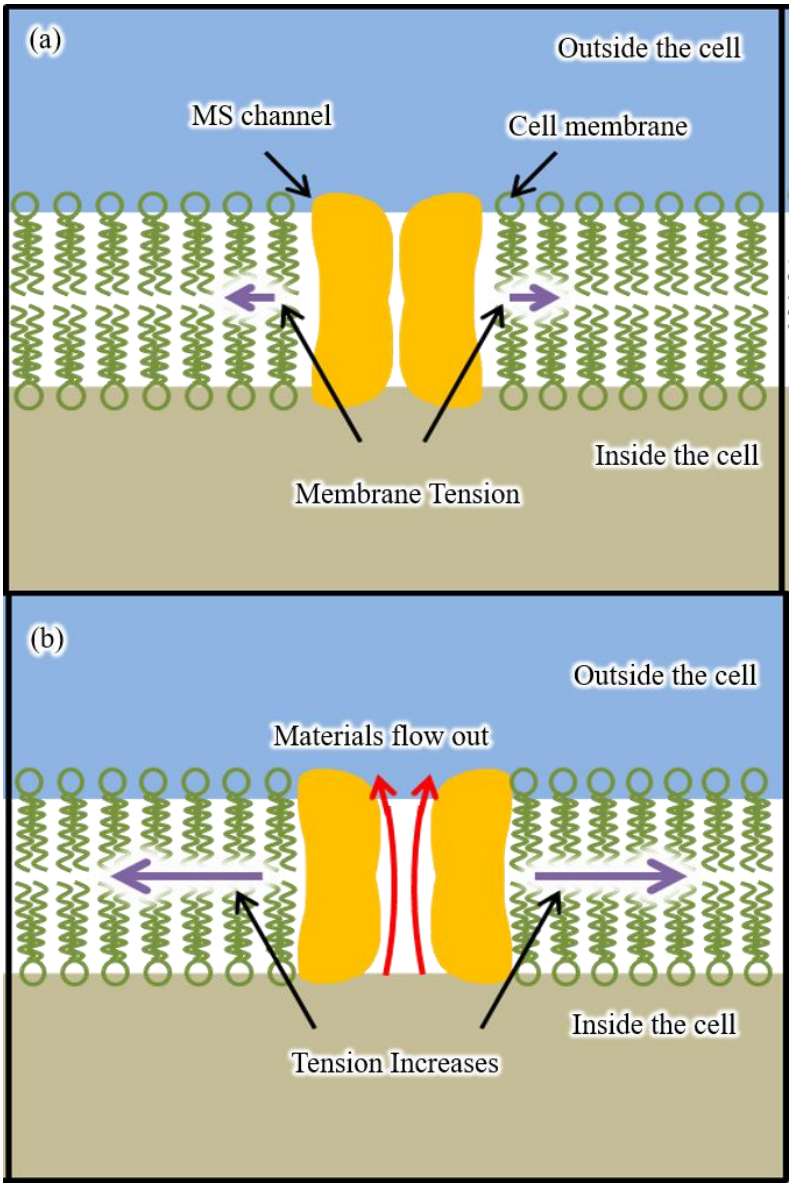

Figure 3.9 A schematic representation of the mechanism of an MS channel sensing membrane tension and opening to allow materials to flow out of the cell. (a) Membrane tension is small and MS channel is closed. (b) Membrane tension increases, and MS channel opens a gate for materials inside the cell to flow out

could not respond to the tension increase because of a defect in the MS channel, therefore, materials inside the cell could not be transported across the membrane. Consequently, the *ΔmscL* cells have a higher Young's modulus than WT cells. In general, the results are consistent with the biological function of MS channels. These results support the theory

that MS channels can sense the tension within the cell membrane and release materials inside the cell to the environment as a result. When the cell size change cannot be detected, the developed measurement system helps to dissect the function and physiological role of MS channels in single microorganism in response with the natural osmotic changes.

3.5 Summary

In this chapter I utilized the measurement system proposed in Chapter 2 to measure single *Synechocystis* cells. The diameter and Young's modulus of WT and *ΔmscL* cells in high osmotic concentration (BG11 containing 1 mol/L sorbitol), normal osmotic concentration (BG11), and low osmotic concentration (BG11: DI water = 1:9 in volume) were studied. There was no clear variation in cell diameter between different cells types or osmotic concentration conditions, however there was a distinct difference in Young's modulus. Clear differences in Young's modulus between WT and *ΔmscL* cells were detected. The proposed evaluation method for comparing WT and mutant cells could contribute to clarifying the effect of ion channels based on the measurement of the stiffness of single cells in three different osmotic concentrations. The study about Young's modulus can help reveal more about the function of MS channels in the osmoadaptation mechanism.

Chapter 4 AFM measurement system for the mechanical property

4.1 Introduction of yest cell

Yeast is a type of eukaryotic cell, and it is widely used in studies involving protein production [24], gene analysis [27], cell cultivation [30], and biofuels [153]. The rigid cell wall of yeast leads to a Young's modulus as large as millions of pascals (Pa). It has been reported that the mechanical properties of yeast can be influenced by numerous factors, including genetic modification [122], cell viability [102], chemical pretreatment [159], and environment conditions [54]. Therefore, evaluating the mechanical properties of a single yeast cell can help us understand more about it. In this chapter, I evaluate the Young's modulus of individual yeast cells as an indicator of its mechanical properties, specifically stiffness.

4.2 Concept

AFM is a type of scanning microscopy technique. It can scan the sample surface and/or measure mechanical properties by indenting the sample with the cantilever, as shown in Figure 4.1. The deflection of the cantilever, d, is measured by a photodiode detector when the holder moves downwards causing the tip of the cantilever to make an indentation in the sample. The indentation depth, δ, is calculated based on the displacement of the holder, D, and the cantilever deflection using equation (4.1).

$$\delta = D - d \qquad (4.1)$$

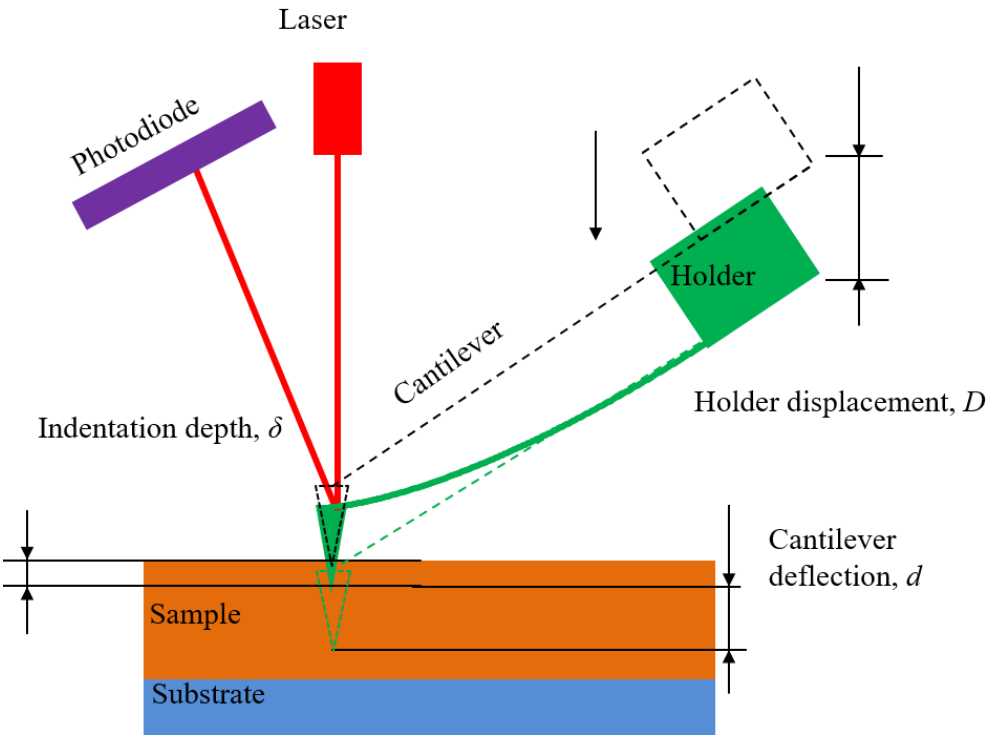

Figure 4.1Schematic diagram showing how AFM measures a sample's mechanical properties.

The force, F, is calculated from the cantilever spring constant, *k*, and its deflection using equation (4.2).

$$F = kd \qquad (4.2)$$

By fitting the force curve (*F* vs. δ) using the Hertzian model [132] shown in equation (4.3), or the Sneddon model [154] shown in equation (4.4), Young's modulus, *E*, can be determined. These calculations assume the sample to be incompressible which means that their Poisson's ratio, *v*, should be 0.5.

$$F = \frac{4}{3}\frac{E}{1-\nu^2}R^{1/2}\delta^{3/2} \qquad (4.3)$$

$$F = \frac{2}{\pi}\frac{E}{1-\nu^2}\delta^2 \tan\theta \qquad (4.4)$$

Equation (4.3) is applicable when the tip shape is nearly spherical with a radius of *R*. Alternatively, equation (4.4) is applicable when the tip radius is ignored, and the tip is treated as a cone with a half opening angle of θ.

This is a method that is widely utilized for evluating the mechanical properties of cells or tissues [155,156]. However, the use of a sharp tip has some disadvantages in the case of yeast cell indentation.

According to equations (4.3) and (4.4), the tip radius and the tip half opening angle are very important parameters for calculating Young's modulus. However, the values of these tip shape parameters used in the equations might differ from their true values. Usually, the typical or nominal value provided by the production company is input into the equations (4.3) and (4.4) [157], but the value provided by the company may not be the

real value. For example, a sharp tip cantilever (MLCT, Bruker Nano Inc.) has a nominal tip radius of 20 nm, but the maximum radius can be as large as 60 nm, which can potentially lead to an error of up to 50%. Additionally, many sharp tips have pyramidal shapes, but they are considered cone-shaped in calculations [122]. Moreover, a sharp tip has a higher risk of fracturing or introducing contamination during measurements [158], which would also cause measurement and calculation errors. Generally, it is not easy to manually check these parameters before each experiment.

Another complication stems from the fact that the indentation depth and the tip radius are on the same order of magnitude. Many sharp AFM tips have a radius between 10 nm and 60 nm, and the indentation depth during the experiment ranges from 40 nm [125] to 100 nm [54]. This means that the sharp tip can neither be treated as a sphere (because the indentation depth would sometimes be larger than the tip radius), nor as a cone (because the tip radius is too large to be neglected). Consequently, neither presented model (Hertzian or Sneddon) is proper for accurately calculating the Young's modulus in this situation. The Hertzian model may only be viable in cases where the indentation depth is smaller than the tip radius. However, this requires the tip radius to be checked before each experiment, which is not practical.

Herein, I describe a method of measuring Young's modulus, *E*, of a single yeast cell using a cantilever with a flat tip whose surface area would be larger than the cell, as shown in Figure 4.2(a). The procedure involves compressing the target cell between the flat cantilever tip and the substrate. Thus, the Hertzian model is effective for the analysis.

$$\delta_f = \delta_1 + \delta_2 \qquad (4.5)$$

$$\delta_1 = \delta_2 \qquad (4.6)$$

$$F_f = \frac{4}{3}\frac{E}{1-\nu^2}(D_{cell}/2)^{1/2}\delta_1^{3/2} \qquad (4.7)$$

In equations (4.5) to (4.7), δ_1 and δ_2 represent the deformation at the flat tip and the substrate, respectively, δ_f is the deformation measured by the AFM instrument, D_{cell} is cell diameter, and F_f is the force applied by the flat tip, as measured by the AFM. Based on equations (4.5) to (4.7), the relationship between F and δ is expressed as shown in equation (4.8).

$$F_f = \frac{1}{3}\frac{E}{1-\nu^2}D_{cell}^{1/2}\,{\delta_f}^{3/2} \qquad (4.8)$$

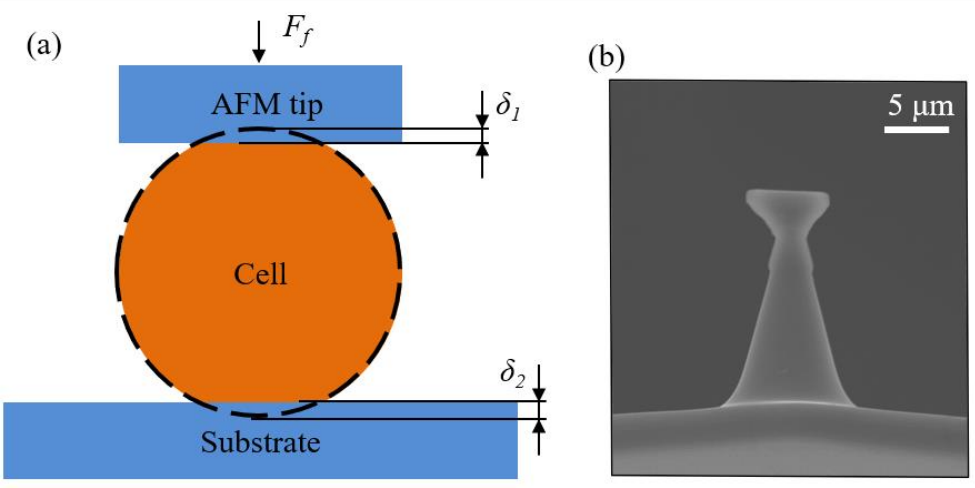

Figure 4.2 (a) Schematic diagram depicting how the mechanical stiffness of a single cell is measured using a flat AFM tip. (b) An SEM photograph of the flat AFM tip

The F vs. δ curves generated in this study were obtained using an AFM (Cellhesion 200, JPK) which was assembled on an inverted microscope (IX73, Olympus Corporation). A sharp tip (BL-AC40TSA, Olympus Corporation) with a spring constant of 0.097 N/m and a customized flat tip (Nanotools GmbH), as shown in Figure 4.2(b) with a spring constant of 48 N/m, are used to obtain the force curve.

PDMS beads are measured to determine the measurement error occured when using the AFM cantilever with the sharp tips. The measurements on PDMS beads and single yeast cells were performed after immobilizing the respective samples on the glass bottom dish (substrate) and compressing them using the AFM cantilever with the flat tip. The force curves were fitted using equation (4.8). Then, measurements were performed on single cells of a wild type strain of budding yeast, *Saccharomyces cerevisiae* BY4741, which is a widely used laboratory strain as mentioned in Section 1.4. This method employs an AFM cantilever with a flat tip whose area is larger than a single yeast cell. The cells are compressed between the bottom of the flat tip and the substrate, and Young's modulus of the whole cell is calculated to evaluate its mechanical property. For comparison, this property of the cell is also measured using the microfluidic chip with two probes, based on the method proposed in Chapter 2. Also a sharp tip is utilized to measure the mechanical property at the surface of a single yeast cell to compare the result between sharp tip measurement and flat tip measurement.

4.3 Sample preparation

The *Saccharomyces cerevisiae* BY4741 was used for the experiments in this chapter. The cells were cultured on a YPD (1% (w/v) yeast extract, 2% (w/v) polypeptone, 2% (w/v) dextrose) containing 2% (w/v) agar plate stored at 29 °C. Before the experiment, the cells were transferred into liquid YPD medium and cultured for one day. Then, 0.1 mL of the preculture was added to 4 mL liquid YPD medium by scratching the cell on the agar medium slightly using a pipette tip and dipping it into a tube containing the liquid medium. the cells in the liquid YPD medium are cultured for 6 hours to allow growth to reach the log phase. The log phase is a period the number of new cells appearing per unit time is proportional to the present population. This yeast cell in log phase is usually used for analyzing cell properties in other researches [153,156,159]. The cells were then collected by centrifugation at 2000 rpm for 1 min and resuspended in liquid buffer solution (20 mM sodium acetate, adjusting the pH to 5.5 using sodium hydroxide and acetic acid). All buffer solutions used in this research had the same pH and composition. In the next step, the cells were washed using the acetate buffer to remove the YPD culture. After repeating the washing process twice, the cells were suspended in the buffer solution. They were ready for the measurements at this point.

Microorganisms such as bacteria and yeast have a small area of contact with a flat substrate, so these cells can easily detach from the substrate when compressed by the AFM probe. Therefore, it is necessary to immobilize the target cell on the substrate during the AFM measurement. Several immobilization methods have been reported, such as air

drying [155], using a chemical-coated substrate [160], or mechanical trapping [161]. In this chapter, I used a concanavalin A (ConA)-coated glass substrate to immobilize the yeast cells [123,166].

ConA is a lectin that binds specifically to a mannose residue of mannan polymers on the yeast cell surface, and it has been widely used to immobilize yeast cells [166]. The ConA from Canavalia ensiformis (Jack bean), Type VI, lyophilized powder, was purchased from Sigma-Aldrich. The ConA solution contained 20 mM sodium acetate, 1 mM $CaCl_2$, 1 mM $MnCl_2$, and 1mg/mL ConA, and was adjusted to pH 5.5, which is similar to other studies [123].

To immobilize a yeast cell, the ConA solution was added to a glass bottom dish and allowed to stand still for 1 hour at room temperature to fully coat the glass substrate with ConA. Then, the ConA solution was drained using a pipette, and the dish was washed gently three times using the buffer solution containing 20 mM sodium acetate. Then, yeast cells suspended in the buffer solution were added to the ConA-coated glass bottom dish and left for 30 mins at room temperature. Finally, the cell suspension was drained, and the buffer solution was gently added to the dish.

The PDMS beads and PDMS film used in this study were fabricated using a viscous commercial prepolymer (Silpot 184, Dow Corning), employing a similar process as described previously [129]. The base and cross-linking agent were mixed completely in a weight ratio of 10:1, degassed, and then poured into deionized (DI) water. The vessel containing the DI water and PDMS mixture was then vibrated using a Vortex-Genie-2 at

3200 rpm to form spherical PDMS beads. The container was subsequently baked at 80 °C for 2 hours. The PDMS film was fabricated under the same conditions.

The Young's modulus of the PDMS film is acquired from a commercial tensile test device (EZ-LX, Shimadzu Corporation) for comparison with the PDMS beads and yeast cells. The average measured Young's modulus of the PDMS film was approximately 1.45 ± 0.06 MPa (mean ± SD, n = 10) (the value is different from that in Section 2.4 because these two experiments are not operated at the same time, and thus the samples are different). Because the PDMS beads and PDMS film are fabricated under the same conditions, they are assumed to have the same value of Young's modulus. To eliminate the effect of measurement error, the PDMS beads are immobilized on a glass bottom dish following the same procedure used for the yeast cells. The mechanical properties of these beads were then measured using the AFM cantilever with sharp tip and flat tip separately.

4.4 Experiment and result

4.4.1 PDMS experiment

First, I conducted measurements on the PDMS beads by indenting the samples using a sharp cantilever tip as mentioned previously. I used the analytical model expressed in equation (4.3), because this equation better fit the experimental force curve, relative to the model expressed by equation (4.4). The tip radius used for the calculation was 10 nm (the value provided by the company), and Poisson's ratio is 0.5 [122]. Ten different beads were tested, and the average Young's modulus was determined to be 2.08 ± 0.95 MPa (mean ± SD, n = 10). This is much larger than the Young's modulus measured by the commercial tensile tester, which was 1.45 ± 0.06 MPa (mean ± SD, n = 10).

Next, PDMS bead stiffnesses were measured by compressing them between the flat AFM tip and the glass substrate. Ten PDMS beads were measured in this way, and the average Young's modulus of a PDMS bead calculated from equation (4.8) was 1.49 ± 0.27 MPa (mean ± SD, n = 10), which is similar to the tensile test results.

4.4.2 Cell experiment using AFM

After measuring the PDMS beads using AFM, single cells from the yeast strain are subjected to measurements by compressing a target cell between the glass substrate and the flat tip. Also, to compare the result between sharp tip measurement and flat tip measurement, a sharp tip is utilized to measure the stiffness of yeast cell. The sample cells are immobilized on a glass bottom dish using ConA as described in Section 4.3. The immobilization is verified by checking the location of the tested cell before and after the compression. The maximum force applied during sharp tip indentation is 2 nN. And the maximum force applied during flat tip compression is 1000 nN so that the deformation of the sample is smaller than 10% to meet the small deformation assumption [146] of the Hertzian model.

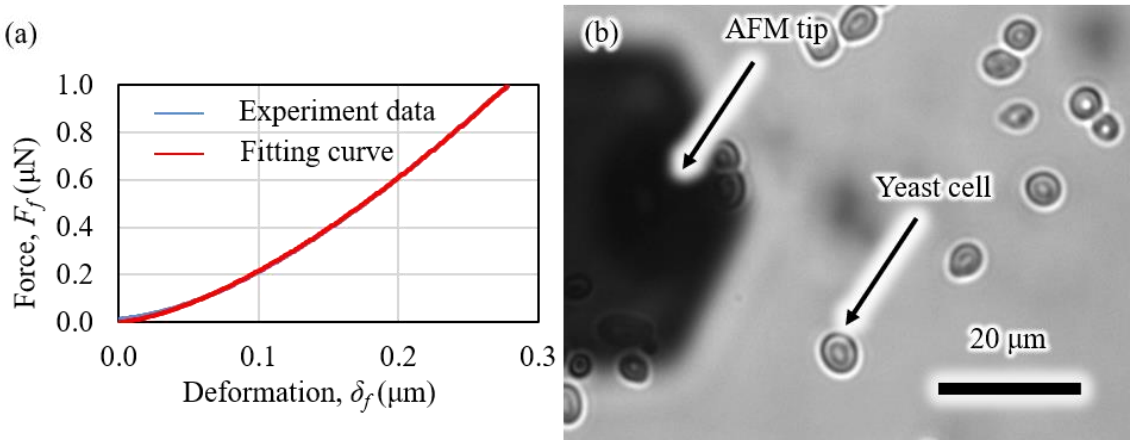

Figure 4.3 (a) Force curve for a single yeast cell obtained using AFM with a flat-tipped cantilever. The blue curve is the experiment data, and the red curve is the data fitted with the Hertzian model (equation 4.8). (b) A photograph of the flat AFM tip and immobilized yeast cells, taken with a converted optical microscope.

A photo of a target cell and a plotted force curve are shown in Figure 4.3. The stiffness of a yeast cell is calculated by fitting the experimental force data using equation (4.8).

The radius of each cell is measured according to the images acquired from the inverted microscope before compression. Ten yeast cells are measured, and the Young's modulus of the yeast cells is 5.09 ± 1.51 MPa.

4.4.3 Cell experiment using microfluidic chip

In the measurements using the microfluidic chip system, cells are floating in the buffer solution and transported to the measurement point using optical tweezers. Therefore, this method is quite convenient because the immobilization process is not necessary.

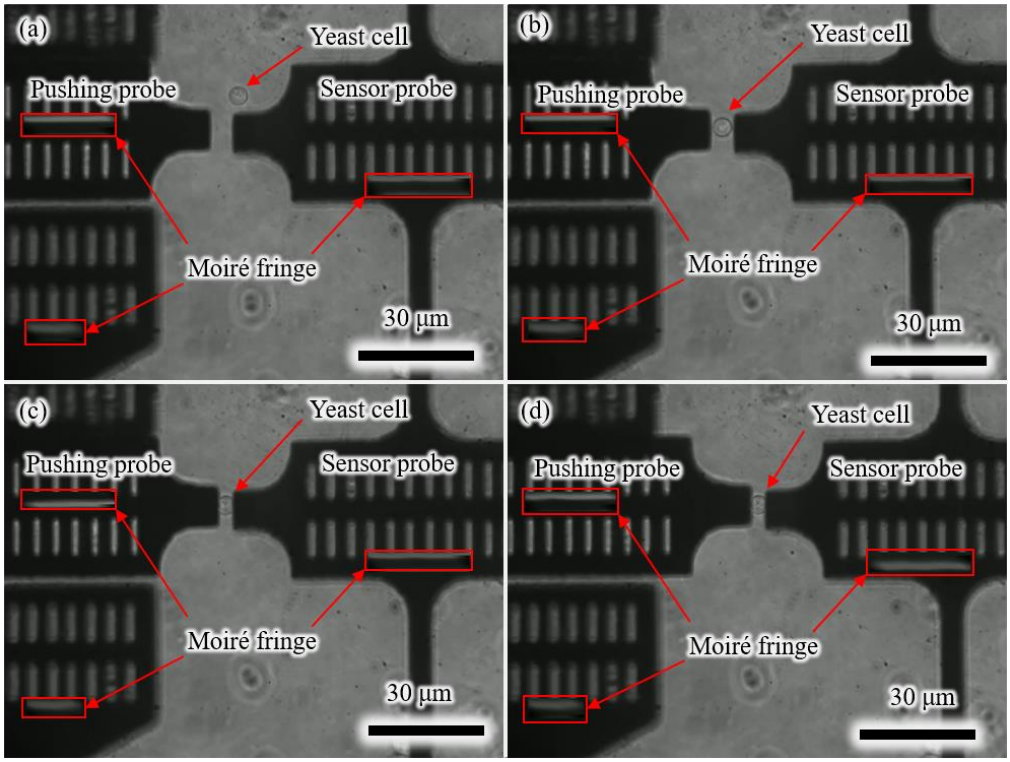

Figure 4.4 On-chip experimental process for measuring the stiffness of a yeast cell: (a) Before compression; (b) Yeast cell transported to the gap between the two probes; (c) Pushing probe moves towards the cell when compression is about to start; (d) The cell is compressed by the pushing probe and sensor probe.

The measurement procedure is shown in Figure 4.4. First, a single cell is moved to the gap between the two probes. Then, the pushing probe is activated by an external piezoelectric actuator. It is motivated to move towards the sensor probe. The cell is compressed by the two probes, and the displacements of both probes are recorded and analyzed using a sampling moiré method [129].

In this chapter, the spring constant of the sensor probe (0.066 N/m) is determined by calibration as described in Chapter 2. The PDMS beads used for calibration here is same with the beads used in AFM measurement. Then, ten yeast cells are measured using the same microfluidic chip. The stiffness of the yeast cells measured using this method is 4.54 ± 0.81 MPa. This is slightly different from the result obtained from AFM measurements. However, there is no significant difference based on Student's t-test.

4.5 Discussion

The PDMS beads experiments clearly demonstrated the problem with performing measurements with the sharp-tipped AFM cantilever. The Young's modulus obtained by this technique (2.08 MPa) was 43% higher than the value acquired by the tension test. This error may be due to the difference between the true tip radius and the typical tip radius provided by the company.

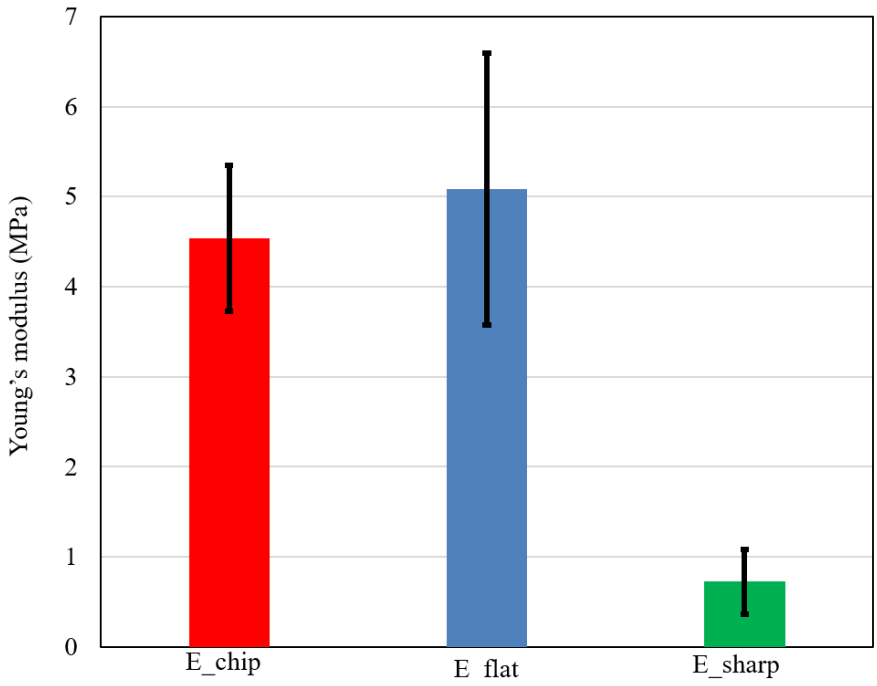

Figure 4.5 Comparison of the values of Young's modulus of a single whole yeast cell, as measured by a microfluidic chip system (red), by AFM with a flat tip (blue) or by AFM with a sharp tip (green). The error bars represent the standard deviation, and there is no significant difference between red and blue bar according to Student's t-test. While obvious difference is shown between sharp tip method result and two other methods result.

But there are possibilities that the difference might be caused by the difference between PDMS sheet sample and PDMS beads, or the error in AFM cantilever calibration.

Thus, anther experiment is carried out to verify the error caused by the sharp tip. A PDMS sheet was fixed on a glass substrate and measured by AFM. The PDMS sheet is measured by a sharp tip, and a tip with a sphere (diameter 3.7 μm measured by optical microscopy). The PDMS sheet measured by sharp tip has a Young's modulus of 2.57 ± 0.41 MPa (mean ± SD, n = 10). But the PDMS sheet measured by sphere tip has a Young's modulus of 1.47 ± 0.06 MPa (mean ± SD, n = 10). Since the diameter of the sphere tip could be measured by optical microscopy, the error caused by the shape parameter error is prevented. Thus, the result of the sphere tip AFM measurement is considered to be accurate, and it is similar with the tensile test. But the sharp tip measurement result of the PDMS sheet has a big difference with both the tensile test and the sphere tip measurement result. Even though there might be some other possibilities leading to the error of sharp tip measurement result beside the shape error, it is obvious that the sharp tip indentation measurement using AFM might have some errors.

The use of a flat-tipped AFM cantilever, which compressed the PDMS beads between two parallel surfaces, effectively eliminated the error, and a Young's modulus of 1.49 MPa (similar to the tension test result) is obtained. These results confirm that using a sharp tip for such measurements can introduce errors when evaluating the Young's modulus, whereas using a flat tip helps avoid this problem.

To verify the reliability of the flat tip measurement method, I measured single cells of the yeast strain with the flat-tipped AFM and with a microfluidic chip system. Both of these processes compressed the individual yeast cells between two parallel surfaces. The small difference in the results provided by these two methods may originate from the variation of cell properties, the error in measuring the cell diameters, or the calibration of

the AFM cantilever spring constant. Despite these uncertainties, similar values for Young's modulus are acquired using two different measurement systems described. These results indicate that the proposed flat-tipped method is effective for determining the stiffness of a whole yeast cell.

Table 4.1 Summary of the stiffness of yeast cell measured by other researchers.

Stiffness of yeast cell (mean ± SD)	Measurement method	Analysis model
0.6 ± 0.4 MPa [162]	AFM	Sneddon model
0.7 ± 0.2 MPa [124]		Sneddon model
1.12 ± 0.02 MPa [162]		Hertzian model
0.483 ± 0.061 MPa [164]		Sneddon model
0.389 ± 0.007 MPa [165]		Sneddon model
1.62 ± 0.22 MPa [122]		Sneddon model
2.62 ± 1.03 MPa [125]		Sneddon model
0.15 ± 0.02 MPa [54]		Sneddon model
9.3 ± 3.1 N/m [128]	MEMS squeezers	Spring model
9.35 ± 4.81 MPa [126]	Flat tip optical fiber	Hertzian model

In this thesis, I discussed the problem of sharp tip indention experiments designed to evaluate Young's modulus of whole yeast cells. This issue was evident in the error produced when calculating Young's modulus of a PDMS bead using the AFM cantilever

with a sharp tip. Then, PDMS beads were compressed between the substrate surface and the bottom surafce of the flat tip attached on the AFM cantilever. The obtained force curve was fitted with a Hertzian model and utilized to calculate Young's modulus. The result from these measurements was similar to the data obtained by the commercial tension test. Therefore, the error was effectively avoided by using the AFM cantilever with a flat tip.

Table 4.1 showed some measurement result of different researchers who studied the stiffness of single yeast cell. It shows that the range of the Young's modulus measrued by AFM with sharp tip indentation is in around 1 MPa. A research which compress the yeast cell using flat optical fiber reported a cellular Young's modulus of 9.35 MPa by analyzing the force curve using Hertzian model. And the Young's modulus of the cell wall would be 276.4 MPa when the same force curve is analyzed using capsule contact model [168]. The yeast cells are also tested using conventional AFM sharp tip method. The measurement result 0.72 ± 0.36 MPa (mean ± standard deviation, n = 10), which is quite different from the flat tip measurement result in this research, as shown in Figure 4.5. But it is similar with some other researches which studied yeast cell using sharp tips [122,157]. On the other hand, the flat tip measurement result is similar with the results obtained by some researches when the yeast cell was compressed between two flat surfaces which is about 9.35 MPa[126]. This result indicates that the stiffness of the whole cell is different from the stiffness of the local point on the surface of the cell. For a PDMS bead, it is reasonable to expect a similar result from the sharp tip and flat tip measurement. Because the bead is made of the same material and can be considered as homogeneous, which means that the whole stiffness and the local stiffness at the surface should be the

same. A yeast cell consists of cell wall, cytoplasm filled by organelles and so on, therefore, it is reasonable that the whole stiffness is different from the local stiffness at the surface. Actually, a cell is more like a capsule than a sphere. Considering a sphere shell full of water, the stiffness of the whole sphere is decided by its shell thickness, Young's modulus of the shell, and its turgor pressure which is applied by the water in the shell. But the thickness of the cell wall cannot be measured in vivo, and the turgor pressure is also difficult to evaluate, thus it is difficult to calculate the stiffness of the cell wall and the turgor pressure accurately. Even though there are researches which analyzed the cell wall thickness, cell wall material stiffness, and the turgor pressure[167], it is not appropriate nor accurate for single cell analysis. That is for the reason that an average of cell wall thickness was utilized. And the cell wall thickness cannot be measured in real time. In conclusion, both of the sharp and the flat tips can be utilized to evaluate the mechanical property of a single yeast cell. Measurement using sharp tip evaluates the stiffness of the cell wall. And the flat tip evaluates the stiffness of the whole cell.

4.6 Summary

In this chapter, I discussed the problem of sharp tip indention experiments designed to evaluate Young's modulus of whole yeast cells. This issue was evident in the error produced when calculating Young's modulus of a PDMS bead using the AFM cantilever with a sharp tip. Then, PDMS beads were compressed between the AFM cantilever with a flat tip and the substrate surface. The obtained force curve was fitted with a Hertzian model and used to calculate Young's modulus. The result from these measurements was similar to the data obtained by the commercial tensile tester. Therefore, the error was effectively avoided by using the AFM cantilever with a flat tip in the case of PDMS bead measurement.

The method employing the flat tip was further used to measure the Young's modulus of the yeast cells, and the results were compared with those obtained using a microfluidic chip system. The Young's modulus value for a whole yeast cell measured by these two methods was 5.09 MPa and 4.54 MPa, respectively, and no significant difference was observed according to Student's t-test. Thus, I determined that employing AFM with a flat cantilever tip is an effective method for evaluating the mechanical stiffness of a single yeast cell based on whole cell deformation. A measurement using sharp tip is also applied on the yeast cell, and different Young's modulus of 0.72 MPa is acquired. This indicates that the surface stiffness measured by sharp tip and the whole stiffness measured by flat tip is different from each other, which meet the fact that the yeast cell is composed of cell wall, cytoplasm and so on. Thus, the flat tip method should be used when analysing the stiffness of the whole cell, and the sharp tip method should be used when analysing the stiffness of a local point.

Chapter 5 **Conclusion**

5.1 Summary

In summary, I proposed a measurement system which is capable of measure small unicellular organism with a size as small as 2 μm. The measurement result of wild type and mutant type of *Synechocystis* in different osmotic condition prove the fact that mechanical measurement could help us understand more about unicellular organism. I also carried out experiment on yeast BY4741. The measurement result using AFM with sharp tip, AFM with flat tip and the robot integrated microfluidic chip shows that Young's modulus of the whole cell and the cell surface is greatly different with each other. Measuring the mechanical property of the whole cell give us another view to understand the cell structure.

Chapter 2

I proposed the measurement system used to measure the mechanical property of a single cyanobacteria cell. I introduce the concept of the measurement system, microfluidic chip design and fabrication, and the calibration of the spring constant of the beam sensor integrated on the chip.

Chapter 3

I introduce the cell that I used for experiment. I showed the measurement process and experiment data of two types of cells in three different conditions. The summarized result of the Young's modulus of the single cell shows clearly that wild type cell and mutant cell (*ΔmscL*) have different Young's modulus in different osmolarity conditions (BG11 condition and BG11 mixed with DI water condition). In contrast, the diameters of the cell have no obvious difference.

Chapter 4

I introduce the measurement of a single cell using AFM and the measurement system proposed in Chapter 2. A typical unicellular organism, yeast, is measured using AFM by two different methods. The yeast cell is measured by AFM in two different methods. In one method, the yeast cell is indented by a sharp tip to measures the local stiffness of the measurement point. In the other method, the yeast cell is compress as a whole and the Young's modulus of the whole cell is measured. Microfluidic chip method proposed in Chapter 2 is carried out and compared with the measurement result using AFM with sharp tip and flat tip. The yeast cells are measured in buffer solution (pH 5.5) containing 20

mM sodium acetate. This condition is similar with some other researches which studied yeast cell using AFM.

5.2 Future work

As I mentioned previously, I have succeeded in measuring the Young's modulus of small unicellular organisms using robot integrated microfluidic chip and AFM. In the future, the research could be developed to several directions.

Combine the robot integrated microfluidic chip with other microfluidic systems such as temperature control and microvalve. By combining different functions and systems, I would be able to measure the mechanical property of the target cell in different environment conditions.

Measuring different types of genetically modified cells to understand more about the cell life, gene expression and environmental adaptation.

Integrating the microfluidic chip with computer and coding. It would be able to achieve automatic measurement for cell properties.

Only cells of sphere shapes are measured in this study. In the future, it is possible to measure cells with other shapes such as ellipse or thin rod. This might need to propose special force models.

Bibliography

1. Moses, Tessa, et al. "Synthetic biology approaches for the production of plant metabolites in unicellular organisms." Journal of Experimental Botany 68.15 (2017): 4057-4074.
2. Bäuerlein, Edmund. "Biomineralization of unicellular organisms: An unusual membrane biochemistry for the production of inorganic nano‐and microstructures." Angewandte Chemie International Edition 42.6 (2003): 614-641.
3. Soininen, Janne. "Macroecology of unicellular organisms–patterns and processes." Environmental microbiology reports 4.1 (2012): 10-22.
4. Egawa, Tsuyoshi, and Syun-Ru Yeh. "Structural and functional properties of hemoglobins from unicellular organisms as revealed by resonance Raman spectroscopy." Journal of inorganic biochemistry 99.1 (2005): 72-96.
5. Dodds, Walter K., Dolly A. Gudder, and Dieter Mollenhauer. "The ecology of Nostoc." Journal of Phycology 31.1 (1995): 2-18.
6. Appel, Jens, et al. "The bidirectional hydrogenase of *Synechocystis* sp. PCC 6803 works as an electron valve during photosynthesis." Archives of microbiology 173.5-6 (2000): 333-338.
7. Scott, Matt, et al. "Mechanism of the down regulation of photosynthesis by blue light in the cyanobacterium *Synechocystis* sp. PCC 6803." Biochemistry 45.29 (2006): 8952-8958.
8. Vermaas, Wim FJ. "Photosynthesis and respiration in cyanobacteria." e LS (2001).

9. MacIntyre, Hugh L., et al. "Photoacclimation of photosynthesis irradiance response curves and photosynthetic pigments in microalgae and cyanobacteria 1." Journal of phycology 38.1 (2002): 17-38.
10. Quintana, Naira, et al. "Renewable energy from Cyanobacteria: energy production optimization by metabolic pathway engineering." Applied microbiology and biotechnology 91.3 (2011): 471-490.
11. Tian, Xiaoxu, et al. "Quantitative proteomics reveals dynamic responses of *Synechocystis* sp. PCC 6803 to next-generation biofuel butanol." Journal of proteomics 78 (2013): 326-345.
12. Savakis, Philipp, and Klaas J. Hellingwerf. "Engineering cyanobacteria for direct biofuel production from CO2." Current opinion in biotechnology 33 (2015): 8-14.
13. Akai, Masaro, et al. "Aquaporin AqpZ is involved in cell volume regulation and sensitivity to osmotic stress in *Synechocystis* sp. strain PCC 6803." Journal of bacteriology 194.24 (2012): 6828-6836.
14. Kanesaki, Yu, et al. "Salt stress and hyperosmotic stress regulate the expression of different sets of genes in *Synechocystis* sp. PCC 6803." Biochemical and biophysical research communications 290.1 (2002): 339-348.
15. Mikami, Koji, et al. "The histidine kinase Hik33 perceives osmotic stress and cold stress in *Synechocystis* sp. PCC 6803." Molecular microbiology 46.4 (2002): 905-915.
16. Nanatani, Kei, et al. "Comparative analysis of kdp and ktr mutants reveals distinct roles of the potassium transporters in the model cyanobacterium *Synechocystis* sp. strain PCC 6803." Journal of bacteriology 197.4 (2015): 676-687.

17. Jang, Jeonghwan, et al. "Environmental Escherichia coli: ecology and public health implications—a review." Journal of applied microbiology 123.3 (2017): 570-581.
18. Hartland, Elizabeth L., and John Leong. "Enteropathogenic and enterohemorrhagic E. coli: ecology, pathogenesis, and evolution." Frontiers in cellular and infection microbiology 3 (2013): 15.
19. Luo, Chengwei, et al. "Genome sequencing of environmental Escherichia coli expands understanding of the ecology and speciation of the model bacterial species." Proceedings of the National Academy of Sciences 108.17 (2011): 7200-7205.
20. Van Elsas, Jan Dirk, et al. "Survival of Escherichia coli in the environment: fundamental and public health aspects." The ISME journal 5.2 (2011): 173-183.
21. Edberg, S. C. L., et al. "Escherichia coli: the best biological drinking water indicator for public health protection." Journal of applied microbiology 88.S1 (2000): 106S-116S.
22. Papaneophytou, Christos P., and George Kontopidis. "Statistical approaches to maximize recombinant protein expression in Escherichia coli: a general review." Protein expression and purification 94 (2014): 22-32.
23. Chen, Rachel. "Bacterial expression systems for recombinant protein production: E. coli and beyond." Biotechnology advances 30.5 (2012): 1102-1107.
24. Deaner, Matthew, Julio Mejia, and Hal S. Alper. "Enabling graded and large-scale multiplex of desired genes using a dual-mode dCas9 activator in Saccharomyces cerevisiae." ACS synthetic biology 6.10 (2017): 1931-1943.

25. Idiris, Alimjan, et al. "Engineering of protein secretion in yeast: strategies and impact on protein production." Applied microbiology and biotechnology 86.2 (2010): 403-417.
26. Cereghino, Geoffrey P. Lin, and James M. Cregg. "Applications of yeast in biotechnology: protein production and genetic analysis." Current opinion in biotechnology 10.5 (1999): 422-427.
27. Varela, Cristian, et al. "Quantitative analysis of wine yeast gene expression profiles under winemaking conditions." Yeast 22.5 (2005): 369-383.
28. Lashkari, Deval A., et al. "Yeast microarrays for genome wide parallel genetic and gene expression analysis." Proceedings of the National Academy of Sciences 94.24 (1997): 13057-13062.
29. Ryan, Owen, et al. "Global gene deletion analysis exploring yeast filamentous growth." Science 337.6100 (2012): 1353-1356.
30. Edlich, Astrid, et al. "Microfluidic reactor for continuous cultivation of Saccharomyces cerevisiae." Biotechnology progress 26.5 (2010): 1259-1270.
31. Hahn-Hägerdal, Bärbel, et al. "Role of cultivation media in the development of yeast strains for large scale industrial use." Microbial cell factories 4.1 (2005): 1-16.
32. Aguilar‐Uscanga, B., and J. M. Francois. "A study of the yeast cell wall composition and structure in response to growth conditions and mode of cultivation." Letters in applied microbiology 37.3 (2003): 268-274.
33. Stuart, Tim, and Rahul Satija. "Integrative single-cell analysis." Nature Reviews Genetics 20.5 (2019): 257-272.

34. Myers, John A., Brandon S. Curtis, and Wayne R. Curtis. "Improving accuracy of cell and chromophore concentration measurements using optical density." BMC biophysics 6.1 (2013): 4.
35. Sutton, Scott. "Measurement of cell concentration in suspension by optical density." Microbiol 585 (2006): 210-8336.
36. Shao-Fang, Zhu, et al. "PKH26 as a fluorescent label for live human umbilical mesenchymal stem cells." In Vitro Cellular & Developmental Biology-Animal 47.8 (2011): 516.
37. Zhu, Chunlei, et al. "A potent fluorescent probe for the detection of cell apoptosis." Chemical Communications 47.19 (2011): 5524-5526.
38. Le Guével, Xavier, et al. "Highly fluorescent silver nanoclusters stabilized by glutathione: A promising fluorescent label for bioimaging." Nano Research 5.6 (2012): 379-387.
39. Habib, Naomi, et al. "Massively parallel single-nucleus RNA-seq with DroNc-seq." Nature methods 14.10 (2017): 955-958.
40. Ding, Jiarui, et al. "Systematic comparison of single-cell and single-nucleus RNA-sequencing methods." Nature biotechnology (2020): 1-10.
41. Li, Bo, et al. "Cumulus provides cloud-based data analysis for large-scale single-cell and single-nucleus RNA-seq." Nature Methods 17.8 (2020): 793-798.
42. Cohen, Assaf, et al. "Collapsing aged culture of the cyanobacterium Synechococcus elongatus produces compound (s) toxic to photosynthetic organisms." PloS one 9.6 (2014): e100747.

43. Berdyyeva, Tamara K., Craig D. Woodworth, and Igor Sokolov. "Human epithelial cells increase their rigidity with ageing in vitro: direct measurements." Physics in Medicine & Biology 50.1 (2004): 81.
44. Carmichael, B., et al. "The fractional viscoelastic response of human breast tissue cells." Physical biology 12.4 (2015): 046001.
45. Rosenbluth, Michael J., Wilbur A. Lam, and Daniel A. Fletcher. "Force microscopy of nonadherent cells: a comparison of leukemia cell deformability." Biophysical journal 90.8 (2006): 2994-3003.
46. Dulińska, Ida, et al. "Stiffness of normal and pathological erythrocytes studied by means of atomic force microscopy." Journal of biochemical and biophysical methods 66.1-3 (2006): 1-11.
47. Blewett, Jenny, Kathleen Burrows, and Colin Thomas. "A micromanipulation method to measure the mechanical properties of single tomato suspension cells." Biotechnology letters 22.23 (2000): 1877-1883.
48. Lekka, Małgorzata, et al. "Cancer cell recognition–mechanical phenotype." Micron 43.12 (2012): 1259-1266.
49. Ren, Juan, et al. "An atomic force microscope study revealed two mechanisms in the effect of anticancer drugs on rate-dependent Young's modulus of human prostate cancer cells." PloS one 10.5 (2015): e0126107.
50. Gindl, W., and H. S. Gupta. "Cell-wall hardness and Young's modulus of melamine-modified spruce wood by nano-indentation." Composites Part A: Applied Science and Manufacturing 33.8 (2002): 1141-1145.

51. Wang, Kui, et al. "Elastic modulus and migration capability of drug treated leukemia cells K562." Biochemical and biophysical research communications 516.1 (2019): 177-182.
52. Kaplan, Robert C., et al. "T cell activation predicts carotid artery stiffness among HIV-infected women." Atherosclerosis 217.1 (2011): 207-213.
53. Calò, Annalisa, et al. "Force measurements on natural membrane nanovesicles reveal a composition-independent, high Young's modulus." Nanoscale 6.4 (2014): 2275-2285.
54. Bui, V. C., Y. U. Kim, and S. S. Choi. "Physical characteristics of Saccharomyces cerevisiae." Surface and Interface Analysis: An International Journal devoted to the development and application of techniques for the analysis of surfaces, interfaces and thin films 40.10 (2008): 1323-1327.
55. Liu, Xinyu, et al. "Elastic and viscoelastic characterization of mouse oocytes using micropipette indentation." Annals of biomedical engineering 40.10 (2012): 2122-2130.
56. Sun, Yu, et al. "A bulk microfabricated multi-axis capacitive cellular force sensor using transverse comb drives." Journal of Micromechanics and Microengineering 12.6 (2002): 832.
57. Sun, Yu, et al. "Mechanical property characterization of mouse zona pellucida." IEEE transactions on nanobioscience 2.4 (2003): 279-286.
58. Jones, Wendy R., et al. "Alterations in the Young's modulus and volumetric properties of chondrocytes isolated from normal and osteoarthritic human cartilage." Journal of biomechanics 32.2 (1999): 119-127.

59. Hochmuth, Robert M. "Micropipette aspiration of living cells." Journal of biomechanics 33.1 (2000): 15-22.
60. Kee, Yee-Seir, and Douglas N. Robinson. "Micropipette aspiration for studying cellular mechanosensory responses and mechanics." Dictyostelium discoideum Protocols. Humana Press, Totowa, NJ, 2013. 367-382.
61. Esteban-Manzanares, Gustavo, et al. "Improved measurement of elastic properties of cells by micropipette aspiration and its application to lymphocytes." Annals of biomedical engineering 45.5 (2017): 1375-1385.
62. Vaziri, Ashkan, and Mohammad R. Kaazempur Mofrad. "Mechanics and deformation of the nucleus in micropipette aspiration experiment." Journal of biomechanics 40.9 (2007): 2053-2062.
63. Discher, Dennis E., David H. Boal, and Seng K. Boey. "Simulations of the erythrocyte cytoskeleton at large deformation. II. Micropipette aspiration." Biophysical Journal 75.3 (1998): 1584-1597.
64. Baaijens, Frank PT, et al. "Large deformation finite element analysis of micropipette aspiration to determine the mechanical properties of the chondrocyte." Annals of biomedical engineering 33.4 (2005): 494-501.
65. Wang, C. X., L. Wang, and C. R. Thomas. "Modelling the mechanical properties of single suspension‐cultured tomato cells." Annals of Botany 93.4 (2004): 443-453.
66. Ashkin, Arthur. "Acceleration and trapping of particles by radiation pressure." Physical review letters 24.4 (1970): 156.
67. Ashkin, Arthur, et al. "Observation of a single-beam gradient force optical trap for dielectric particles." Optics letters 11.5 (1986): 288-290.

68. Seeger, S., et al. "Application of laser optical tweezers in immunology and molecular genetics." Cytometry: The Journal of the International Society for Analytical Cytology 12.6 (1991): 497-504.
69. Choudhary, Dhawal, et al. "Bio-molecular applications of recent developments in optical tweezers." Biomolecules 9.1 (2019): 23.
70. Polimeno, Paolo, et al. "Optical tweezers and their applications." Journal of Quantitative Spectroscopy and Radiative Transfer 218 (2018): 131-150.
71. Moffitt, Jeffrey R., et al. "Recent advances in optical tweezers." Annual review of biochemistry 77 (2008).
72. Dao, Ming, Chwee Teck Lim, and Subra Suresh. "Mechanics of the human red blood cell deformed by optical tweezers." Journal of the Mechanics and Physics of Solids 51.11-12 (2003): 2259-2280.
73. Yousafzai, Muhammad Sulaiman, et al. "Investigating the effect of cell substrate on cancer cell stiffness by optical tweezers." Journal of Biomechanics 60 (2017): 266-269.
74. Yousafzai, Muhammad S., et al. "Substrate-dependent cell elasticity measured by optical tweezers indentation." Optics and Lasers in Engineering 76 (2016): 27-33.
75. Andersson, Helene, and Albert Van den Berg. "Microfluidic devices for cellomics: a review." Sensors and actuators B: Chemical 92.3 (2003): 315-325.
76. Lee, Chia-Yen, et al. "Microfluidic mixing: a review." International journal of molecular sciences 12.5 (2011): 3263-3287.
77. Kjeang, Erik, Ned Djilali, and David Sinton. "Microfluidic fuel cells: A review." Journal of Power Sources 186.2 (2009): 353-369.

78. Grass, B., et al. "Micro-structured analytical instrumentation for the analysis of liquids." Spectrochimica Acta Part B: Atomic Spectroscopy 57.10 (2002): 1575-1583.
79. Sajeesh, P., and Ashis Kumar Sen. "Particle separation and sorting in microfluidic devices: a review." Microfluidics and nanofluidics 17.1 (2014): 1-52.
80. Wang, Lin, and Paul CH Li. "Microfluidic DNA microarray analysis: A review." Analytica chimica acta 687.1 (2011): 12-27.
81. Choi, Jong-ryul, et al. "Microfluidic assay-based optical measurement techniques for cell analysis: A review of recent progress." Biosensors and Bioelectronics 77 (2016): 227-236.
82. Lecault, Véronique, et al. "Microfluidic single cell analysis: from promise to practice." Current opinion in chemical biology 16.3-4 (2012): 381-390.
83. Wheeler, Aaron R., et al. "Microfluidic device for single-cell analysis." Analytical chemistry 75.14 (2003): 3581-3586.
84. Tang, Minghui, et al. "A review of biomedical centrifugal microfluidic platforms." Micromachines 7.2 (2016): 26.
85. Giordano, Braden C., et al. "On-line sample pre-concentration in microfluidic devices: A review." Analytica chimica acta 718 (2012): 11-24.
86. Miralles, Vincent, et al. "A review of heating and temperature control in microfluidic systems: techniques and applications." Diagnostics 3.1 (2013): 33-67.
87. Abgrall, P., and A. M. Gue. "Lab-on-chip technologies: making a microfluidic network and coupling it into a complete microsystem—a review." Journal of micromechanics and microengineering 17.5 (2007): R15.

88. Xue, Chengcheng, et al. "Constriction channel based single-cell mechanical property characterization." Micromachines 6.11 (2015): 1794-1804.
89. Shelby, J. Patrick, et al. "A microfluidic model for single-cell capillary obstruction by Plasmodium falciparum-infected erythrocytes." Proceedings of the National Academy of Sciences 100.25 (2003): 14618-14622.
90. Rosenbluth, Michael J., Wilbur A. Lam, and Daniel A. Fletcher. "Analyzing cell mechanics in hematologic diseases with microfluidic biophysical flow cytometry." Lab on a Chip 8.7 (2008): 1062-1070.
91. Hou, Han Wei, et al. "Deformability study of breast cancer cells using microfluidics." Biomedical microdevices 11.3 (2009): 557-564.
92. Abkarian, Manouk, Magalie Faivre, and Howard A. Stone. "High-speed microfluidic differential manometer for cellular-scale hydrodynamics." Proceedings of the National Academy of Sciences 103.3 (2006): 538-542.
93. Gabriele, Sylvain, et al. "Microfluidic investigation reveals distinct roles for actin cytoskeleton and myosin II activity in capillary leukocyte trafficking." Biophysical journal 96.10 (2009): 4308-4318.
94. Sharei, Armon, et al. "A vector-free microfluidic platform for intracellular delivery." Proceedings of the National Academy of Sciences 110.6 (2013): 2082-2087.
95. Khan, Z. S., and S. A. Vanapalli. "Probing the mechanical properties of brain cancer cells using a microfluidic cell squeezer device." Biomicrofluidics 7.1 (2013): 011806.

96. Mak, Michael, and David Erickson. "A serial micropipette microfluidic device with applications to cancer cell repeated deformation studies." Integrative Biology 5.11 (2013): 1374-1384.
97. Lee, Lap Man, and Allen P. Liu. "A microfluidic pipette array for mechanophenotyping of cancer cells and mechanical gating of mechanosensitive channels." Lab on a Chip 15.1 (2015): 264-273.
98. Gossett, Daniel R., et al. "Hydrodynamic stretching of single cells for large population mechanical phenotyping." Proceedings of the National Academy of Sciences 109.20 (2012): 7630-7635.
99. Dudani, Jaideep S., et al. "Pinched-flow hydrodynamic stretching of single-cells." Lab on a Chip 13.18 (2013): 3728-3734.
100. Mietke, Alexander, et al. "Extracting cell stiffness from real-time deformability cytometry: theory and experiment." Biophysical Journal 109.10 (2015): 2023-2036.
101. Sakuma, Shinya, and Fumihito Arai. "Cellular force measurement using a nanometric-probe-integrated microfluidic chip with a displacement reduction mechanism." Journal of Robotics and Mechatronics 25.2 (2013): 277-284.
102. Warnat, S., et al. "PolyMUMPs MEMS device to measure mechanical stiffness of single cells in aqueous media." Journal of Micromechanics and Microengineering 25.2 (2015): 025011.
103. Gnerlich, Markus, Susan F. Perry, and Svetlana Tatic-Lucic. "A submersible piezoresistive MEMS lateral force sensor for a diagnostic biomechanics platform." Sensors and Actuators A: Physical 188 (2012): 111-119.

104. Liu, Shaoyang, and Yifen Wang. "Application of AFM in microbiology: a review." Scanning 32.2 (2010): 61-73.

105. Ohnesorge, F. M., et al. "AFM review study on pox viruses and living cells." Biophysical journal 73.4 (1997): 2183-2194.

106. Hughes, Megan L., and Lorna Dougan. "The physics of pulling polyproteins: a review of single molecule force spectroscopy using the AFM to study protein unfolding." Reports on Progress in Physics 79.7 (2016): 076601.

107. Puchner, Elias M., and Hermann E. Gaub. "Force and function: probing proteins with AFM-based force spectroscopy." Current opinion in structural biology 19.5 (2009): 605-614.

108. Radmacher, Manfred. "Studying the mechanics of cellular processes by atomic force microscopy." Methods in cell biology 83 (2007): 347-372.

109. Thomas, Gawain, et al. "Measuring the mechanical properties of living cells using atomic force microscopy." JoVE (Journal of Visualized Experiments) 76 (2013): e50497.

110. Kuznetsova, Tatyana G., et al. "Atomic force microscopy probing of cell elasticity." Micron 38.8 (2007): 824-833.

111. Sen, Shamik, Shyamsundar Subramanian, and Dennis E. Discher. "Indentation and adhesive probing of a cell membrane with AFM: theoretical model and experiments." Biophysical journal 89.5 (2005): 3203-3213.Costa, K. D., and F. C. P. Yin. Costa, K. D., and F. C. P. Yin. "Analysis of indentation: implications for measuring mechanical properties with atomic force microscopy." (1999): 462-471.

112. Radotić, Ksenija, et al. "Atomic force microscopy stiffness tomography on living Arabidopsis thaliana cells reveals the mechanical properties of surface and deep cell-wall layers during growth." Biophysical journal 103.3 (2012): 386-394.
113. Li, Mi, et al. "Atomic force microscopy imaging and mechanical properties measurement of red blood cells and aggressive cancer cells." Science China Life Sciences 55.11 (2012): 968-973.
114. Kaneko, Takakazu, et al. "Sequence analysis of the genome of the unicellular cyanobacterium *Synechocystis* sp. strain PCC6803. II. Sequence determination of the entire genome and assignment of potential protein-coding regions." DNA research 3.3 (1996): 109-136.
115. Gao, Hong, and Xudong Xu. "Depletion of Vipp1 in *Synechocystis* sp. PCC 6803 affects photosynthetic activity before the loss of thylakoid membranes." FEMS microbiology letters 292.1 (2009): 63-70.
116. Nakasugi, Kenlee, Charles J. Svenson, and Brett A. Neilan. "The competence gene, comF, from *Synechocystis* sp. strain PCC 6803 is involved in natural transformation, phototactic motility and piliation." Microbiology 152.12 (2006): 3623-3631.
117. Nakahara, Kou, et al. "On-chip transportation and measurement of mechanical characteristics of oocytes in an open environment." Micromachines 6.5 (2015): 648-659.
118. Ito, Keitaro, et al. "Temporal transition of mechanical characteristics of HUVEC/MSC spheroids using a microfluidic chip with force sensor probes." Micromachines 7.12 (2016): 221.

119. Sugiura, Hirotaka, et al. "On-chip method to measure mechanical characteristics of a single cell by using moiré fringe." Micromachines 6.6 (2015): 660-673.
120. Sugiura, Hirotaka, et al. "Large indentation method to measure elasticity of cell in robot-integrated microfluidic chip." IEEE Robotics and Automation Letters 2.4 (2017): 2002-2007.
121. Millet, Olivier, et al. "Electrostatic actuated micro gripper using an amplification mechanism." Sensors and Actuators A: Physical 114.2-3 (2004): 371-378.
122. Dague, Etienne, et al. "An atomic force microscopy analysis of yeast mutants defective in cell wall architecture." Yeast 27.8 (2010): 673-684.
123. Dague, Etienne, et al. "Assembly of live micro-organisms on microstructured PDMS stamps by convective/capillary deposition for AFM bio-experiments." Nanotechnology 22.39 (2011): 395102.
124. Alsteens, David, et al. "Structure, cell wall elasticity and polysaccharide properties of living yeast cells, as probed by AFM." Nanotechnology 19.38 (2008): 384005.
125. Goldenbogen, Björn, et al. "Dynamics of cell wall elasticity pattern shapes the cell during yeast mating morphogenesis." Open biology 6.9 (2016): 160136.
126. Overbeck, Achim, et al. "Compression Testing and Modeling of Spherical Cells–Comparison of Yeast and Algae." Chemical Engineering & Technology 40.6 (2017): 1158-1164.
127. Chaudhari, R. D., et al. "Effect of bud scars on the mechanical properties of Saccharomyces cerevisiae cell walls." Chemical engineering science 84 (2012): 188-196.

128. Barazani, B., et al. "MEMS squeezer for the measurement of single cell rupture force, stiffness change, and hysteresis." Journal of Micromechanics and Microengineering 27.2 (2016): 025002.
129. Chang, Di, et al. "Measurement of the mechanical properties of single *Synechocystis* sp. strain PCC6803 cells in different osmotic concentrations using a robot-integrated microfluidic chip." Lab on a Chip 18.8 (2018): 1241-1249.5
130. Baker Brachmann, Carrie, et al. "Designer deletion strains derived from Saccharomyces cerevisiae S288C: a useful set of strains and plasmids for PCR‐mediated gene disruption and other applications." Yeast 14.2 (1998): 115-132.
131. Scariot, F. J., et al. "The fungicide Mancozeb induces metacaspase-dependent apoptotic cell death in Saccharomyces cerevisiae BY4741." Apoptosis 21.7 (2016): 866-872.
132. Hertz, Heinrich. "Ueber die Berührung fester elastischer Körper." Journal für die reine und angewandte Mathematik 1882.92 (1882): 156-171.
133. Yi, Taechung, Lu Li, and Chang-Jin Kim. "Microscale material testing of single crystalline silicon: process effects on surface morphology and tensile strength." Sensors and Actuators A: Physical 83.1-3 (2000): 172-178.
134. Onda, Kazuhisa, and Fumihito Arai. "Multi-beam bilateral teleoperation of holographic optical tweezers." Optics express 20.4 (2012): 3633-3641.
135. Schneckenburger, Herbert, et al. "Cell viability in optical tweezers: high power red laser diode versus Nd: YAG laser." Journal of biomedical optics 5.1 (2000): 40-45.

136. Legtenberg, Rob, A. W. Groeneveld, and M. Elwenspoek. "Comb-drive actuators for large displacements." Journal of Micromechanics and microengineering 6.3 (1996): 320.
137. Gustafsson, Mats GL. "Surpassing the lateral resolution limit by a factor of two using structured illumination microscopy." Journal of microscopy 198.2 (2000): 82-87.
138. Ri, S., M. Fujigaki, and Y. Morimoto. "Sampling moiré method for accurate small deformation distribution measurement." Experimental mechanics 50.4 (2010): 501-508.
139. Guelpa, Valérian, et al. "Subpixelic measurement of large 1D displacements: Principle, processing algorithms, performances and software." Sensors 14.3 (2014): 5056-5073.
140. Legtenberg, Rob, A. W. Groeneveld, and M. Elwenspoek. "Comb-drive actuators for large displacements." Journal of Micromechanics and microengineering 6.3 (1996): 320.
141. https://en.wikipedia.org/wiki/Osmosis
142. Sleator, Roy D., and Colin Hill. "Bacterial osmoadaptation: the role of osmolytes in bacterial stress and virulence." FEMS microbiology reviews 26.1 (2002): 49-71.
143. Ajouz, Bassam, et al. "Release of thioredoxin via the mechanosensitive channel MscL during osmotic downshock of Escherichia coli cells." Journal of Biological Chemistry 273.41 (1998): 26670-26674.
144. Nanatani, Kei, et al. "Characterization of the role of a mechanosensitive channel in osmotic down shock adaptation in *Synechocystis* sp PCC 6803." Channels 7.4 (2013): 238-242.

145. Tatara, Yoichi. "Extensive theory of force-approach relations of elastic spheres in compression and in impact." (1989): 163-168.
146. Liu, K. K., D. R. Williams, and B. J. Briscoe. "The large deformation of a single micro-elastomeric sphere." Journal of Physics D: Applied Physics 31.3 (1998): 294.
147. Moeendarbary, Emad, et al. "The cytoplasm of living cells behaves as a poroelastic material." Nature materials 12.3 (2013): 253-261.
148. Rebelo, Luciana Magalhaes, et al. "Comparison of the viscoelastic properties of cells from different kidney cancer phenotypes measured with atomic force microscopy." Nanotechnology 24.5 (2013): 055102.
149. Hu, Jiliang, et al. "Size-and speed-dependent mechanical behavior in living mammalian cytoplasm." Proceedings of the National Academy of Sciences 114.36 (2017): 9529-9534.
150. Lang, Ingeborg, et al. "Plasmolysis: loss of turgor and beyond." Plants 3.4 (2014): 583-593.
151. Haswell, Elizabeth S., Rob Phillips, and Douglas C. Rees. "Mechanosensitive channels: what can they do and how do they do it?." Structure 19.10 (2011): 1356-1369.
152. Perozo, Eduardo, et al. "Open channel structure of MscL and the gating mechanism of mechanosensitive channels." Nature 418.6901 (2002): 942-948.
153. Buijs, Nicolaas A., Verena Siewers, and Jens Nielsen. "Advanced biofuel production by the yeast Saccharomyces cerevisiae." Current opinion in chemical biology 17.3 (2013): 480-488.

154. Sneddon, Ian N. "The relation between load and penetration in the axisymmetric Boussinesq problem for a punch of arbitrary profile." International journal of engineering science 3.1 (1965): 47-57.
155. Bolshakova, A. V., et al. "Comparative studies of bacteria with an atomic force microscopy operating in different modes." Ultramicroscopy 86.1-2 (2001): 121-128.
156. Shen, Yajing, et al. "Effect of ambient humidity on the strength of the adhesion force of single yeast cell inside environmental-SEM." Ultramicroscopy 111.8 (2011): 1176-1183.
157. Pelling, Andrew E., et al. "Local nanomechanical motion of the cell wall of Saccharomyces cerevisiae." Science 305.5687 (2004): 1147-1150.
158. Kopycinska-Müller, Malgorzata, Roy H. Geiss, and Donna C. Hurley. "Contact mechanics and tip shape in AFM-based nanomechanical measurements." Ultramicroscopy 106.6 (2006): 466-474.
159. Suchodolskis, Arturas, et al. "Elastic properties of chemically modified baker's yeast cells studied by AFM." Surface and interface analysis 43.13 (2011): 1636-1640.
160. Velegol, Stephanie B., and Bruce E. Logan. "Contributions of bacterial surface polymers, electrostatics, and cell elasticity to the shape of AFM force curves." Langmuir 18.13 (2002): 5256-5262.
161. Kasas, S., and A. Ikai. "A method for anchoring round shaped cells for atomic force microscope imaging." Biophysical Journal 68.5 (1995): 1678-1680.
162. Touhami, Ahmed, Bernard Nysten, and Yves F. Dufrêne. "Nanoscale mapping of the elasticity of microbial cells by atomic force microscopy." Langmuir 19.11 (2003): 4539-4543.

163. Lanero, Tiziana Svaldo, et al. "Mechanical properties of single living cells encapsulated in polyelectrolyte matrixes." Journal of biotechnology 124.4 (2006): 723-731.
164. Schiavone, M., Déjean, S., Sieczkowski, N., Castex, M., Dague, E., & François, J. M. (2017). Integration of biochemical, biophysical and transcriptomics data for investigating the structural and nanomechanical properties of the yeast cell wall. Frontiers in Microbiology, 8, 1806.
165. Nayyar, Ashima, et al. "Influence of cell surface and nanomechanical properties on the flocculation ability of industrial Saccharomyces cerevisiae Strains." Journal of Food Research 6.5 (2017).
166. Toyota, Kazuya, Ryosuke Tanaka, and Takaharu Okajima. "Stiffness of brewers' yeast under ethanol stress investigated by atomic force microscopy." Japanese Journal of Applied Physics 59.SN (2020): SN1005.
167. Arfsten, J., et al. "Compressive testing of single yeast cells in liquid environment using a nanoindentation system." Journal of Materials Research 23.12 (2008): 3153-3160.
168. Lulevich, Valentin V., Denis Andrienko, and Olga I. Vinogradova. "Elasticity of polyelectrolyte multilayer microcapsules." The Journal of chemical physics 120.8 (2004): 3822-3826.

Accomplishments

I. Journal Articles

1. **Chang, D.**, Sakuma, S., Kera, K., Uozumi, N., & Arai, F. (2018). Measurement of the mechanical properties of single Synechocystis sp. strain PCC6803 cells in different osmotic concentrations using a robot-integrated microfluidic chip. Lab on a Chip, 18(8), 1241-1249.
2. **Chang, D.**, Hirate, T., Uehara, C., Maruyama, H., Uozumi, N., & Arai, F. (2021). Evaluating Young's Modulus of Single Yeast Cells Based on Compression Using an Atomic Force Microscope with a Flat Tip. Microscopy and Microanalysis, 1-8. doi:10.1017/S1431927620024903

II. International conferences

1. Sahuma, S., **Chang, D.**, Arai, F., Kera, K., & Uozumi, N. (2017, January). Mechanical characterization of cyanobacteria under osmotic stress. In 2017 IEEE 30th International Conference on Micro Electro Mechanical Systems (MEMS) (pp. 1248-1251). IEEE.
2. **Chang, D.**, Sakuma, S., Kera, K., Uozumi, N., & Arai, F. (2017, December). Mechanical characterization of a single synechocystis sp. PCC 6803 cell in different osmolarity solutions. In 2017 International Symposium on Micro-NanoMechatronics and Human Science (MHS) (pp. 1-3). IEEE.

3. **Chang, D.**, Sakuma, S., Uehara, C., Uozumi, N., & Arai, F. (2018, December). Mechanical Characterization of a Single Yeast Cell Using a Robot Integrated Microfluidic Chip. In 2018 International Symposium on Micro-NanoMechatronics and Human Science (MHS) (pp. 1-3). IEEE.
4. **Chang, D.**, Hirate, T., Uehara, C., Uozumi, N., & Arai, F. (2019, December). Calibration process for the Young's modulus of a mechanically trapped microbead measured by atomic force microscopy. In 2019 International Symposium on Micro-NanoMechatronics and Human Science (MHS) (pp. 1-2). IEEE.